N. B. WILLIAMS

Technical Manager, Chamberlin & Hill Ltd.,

Walsall, Staffordshire.

SOLIDIFICATION AND COOLING OF GREY CAST IRON IN SHELL MOULDS WITH PARTICULAR REFERENCE TO THE SUB-SURFACE STRUCTURE

THESIS
669.13
WIL
-9.NOV72 156114

Work carried out at University of Aston in Birmingham and submitted for degree of M.Sc. in July 1972.

ACKNOWLEDGEMENTS

Thanks are due to the Board of Directors of Chamberlin and Hill Ltd., who gave me the opportunity of carrying out this work and furthering my career. In particular I would like to thank the Managing Director, Mr. M. M. Hallett, for his help in selecting the topic for this research and his helpful discussions as the work has progressed. I thank Professor Alexander for the use of the facilities of the Metallurgy Department. I greatly thank Mr. K. A. Reynolds and Dr. J. Billington who, as supervisors, have helped me in every possible way, and who by useful discussions have contributed to the outcome of this research. I would like also to record thanks to Mr. D. Webb for his help in the foundry; Mr. N. Shirley for photographic services and my wife for her help in typing this work.

I must thank Chamberlin and Hill Ltd., for providing the necessary cast iron for the experiments, shell moulding and pattern shop facilities; British Industrial Sands for supplying shell moulding material; Foseco International and particularly Mr. C. Hall for the use of the Amitec laboratories, and the British Cast Iron Research Association for the use of library facilities. Finally, I would like to thank Schnectady Midland and particularly Mr. B.J. Alexander for his help and information regarding shell moulding resins.

SUMMARY

Shell moulded grey iron castings exhibit excessive amounts of ferrite and 'D' type graphite in the surface structure when compared to conventional green sand castings. A review of the literature does not reveal any satisfactory explanation for the structures which arise, although this gives some indication of the undesirability of the phenomenon and some means of overcoming it. For this reason, to enable a better assessment of the structures arising, the solidification of grey cast iron in shell moulds for sections up to 2.5 cm in thickness is studied and discussed in detail.

The thermal properties of various moulds, in terms of chilling power, were measured. It was found that the chilling power of silica shell moulds was 10% less than for a green sand mould with a nominal wall thickness of 5cm. The rate of heat extraction $\frac{dQ}{dt}$ for times less than 3 minutes, however, is marginally higher for silica shell moulds. It was found that resin content has no effect on chilling power value and it is suggested that the principal reason for the difference in chilling power between clay bonded and silica shell moulds is the difference in mould thickness.

It was found that the generally accepted longer solidification times for shell moulds opposed to green sand moulds do not exist at depths of 1 mm and 3 mm from the surface of 0.5 cm section plate castings. The solidification times were found to be the same although 'D' type graphite was formed only in the shell casting. The existence of

ferrite in the structure arises due to the graphite form being 'D' type, although the rate of cooling after solidification was shown to be very slow for shell moulds, when castings are left in the mould.

The depth of chill measured by wedge testing was the same for silica shell and clay bonded moulds. It is illustrated, however, that the mode of solidification is different and that a casting skin occurred on shell moulded specimens.

Experiments showed that the eutectic temperature was not influenced by the type of mould material, although a greater degree or undercooling occurs with shell moulds. It is suggested that the occurrence of D' type graphite in shell mould castings is due to the mode of solidification modifying the graphite form, other than increasing the rate of solidification or reducing the eutectic temperature.

Zircon and Olivine shell moulds are shown to behave in an identical manner to similar silica moulds.

Solidification and cooling of grey cast iron in shell moulds with particular reference to the sub-surface structure

CHAPTER 1

INTRODUCTION

Differences occur in the structure and properties of iron castings produced in shell moulds as opposed to conventional green sand moulds. Pronounced effects occur in the outermost skin of the castings where the section thickness is great enough to prevent the effect from showing throughout the section.

The anomalies which arise may be summarised briefly as shown below.

1. There is a greater tendency, all other influencing factors being equal, for shell moulded castings to exhibit carbides in the surface microstructure.
2. The type of graphite formation found in the surface structure of shell moulded castings has a greater tendency to be 'D' type than for similarly produced green sand castings.
3. Castings produced by shell moulding have a strong tendency for the austenite phase near the surface to transform to ferrite rather than pearlite.

The above factors give rise to considerable problems in industry preventing in some instances the engineering

potential of shell moulded castings from being realised. The industrial aspect of the problem may be seen from the examples set out below.

EXAMPLE 1

Fig. 1.1 shows a typical range of thin section ($< \frac{1}{4}$") shell moulded castings with which difficulties of machining have arisen due to the presence of free carbides.

A micro examination of this type of casting, after machining difficulties had first come to light, produced the result shown in Fig. 1.2.

The existence of such carbide areas is highly detrimental to tool life on any machining operation, if this is still possible with the carbide present. This can mean that on small shell moulded components which should show reduced amounts of total machining due to greater dimensional accuracy, machining costs are offset due to higher degrees of tool wear.

It can be seen that the graphite structure is of the 'D' type in a ferrite matrix. Large areas of carbide Fe_3C can also be seen.

EXAMPLE 2

The occurence of excessive 'D' type graphite in the surface structure of castings causes problems due to the ferritic matrix which is usually associated with it. Fig. 1.3 illustrates two such castings and the component produced from them. These components are in an automatic gear mechanism for a motor car.

Fig. 1.1 Typical thin section grey iron castings produced by the shell moulding technique.

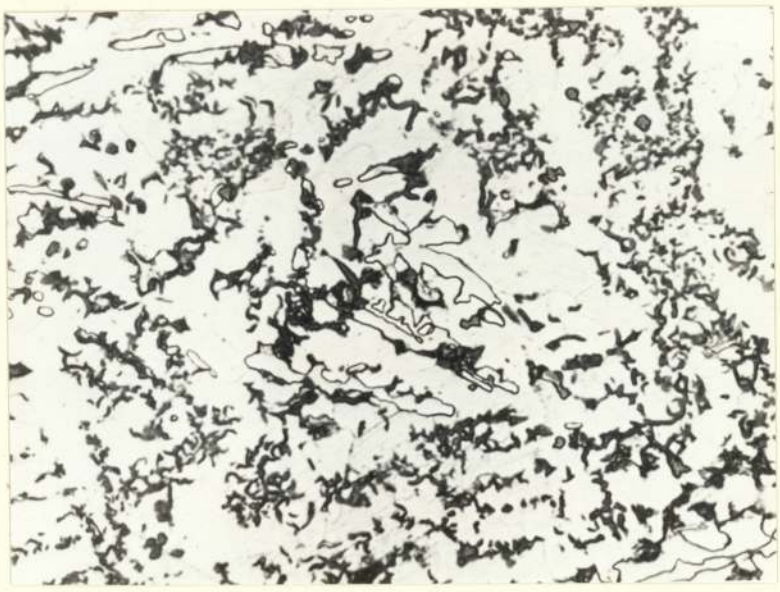

Fig. 1.2. Microstructure of thin section grey iron, shell moulded casting illustrating 'D' type graphite and Fe_3C in ferrite matrix (X250). Etched 2% Nital.

This particular problem manifests itself in two distinct ways. Firstly, ferrite at the surface is highly undesirable due to the risk of pick up by moving parts in the event of any lubricant break down. This aspect is fundamental to the use of the castings shown in Fig. 1.3. Secondly, it was found that the presence of ferrite gave rise to "splitting" when the two component parts were riveted together. This does not occur when the matrix structure of the castings is pearlitic.

The surface microstructure and the structure at the centre of the components is shown in Fig. 1.4.

With the surface microstructure containing excessive amounts of ferrite, the surface is not ideal for the application shown in Fig. 1.3. In order to overcome this the casting would require a machining operation to remove the ferrite skin. This defeats the object of purchasing a shell moulded casting for the component since the aim is to obtain a casting of good dimensional tolerance, hence limiting the degree of machining that would have to be done. Other techniques may be used to remove the ferrite which occurs but are not found necessary with similarly produced green sand castings.

EXAMPLE 3

The existence of large amounts of ferrite associated with 'A' and 'D' type graphite causes problems with low tensile strengths. The inability to carry out quality control by hardness testing, where only the surface exhibits ferrite, is also a major problem. Fig. 1.5 illustrates the

Fig. 1.3 Shell moulded automobile transmission castings and subsequent component part.

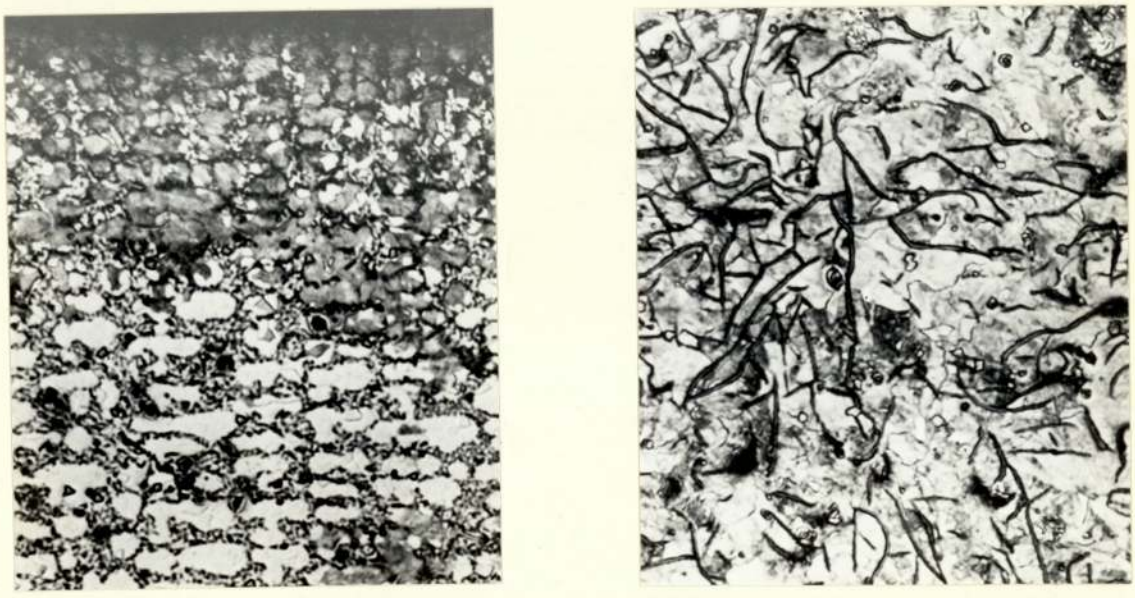

(a) At the surface (b) At the centre of section

Fig. 1.4 Microstructure (X100) of the above castings. Etched 2% Nital.

difference in graphite and matrix structure at the surface and centre of a medium section ($1\frac{1}{2}$") shell moulded casting.

Engineering users of grey cast iron shell moulded castings commonly adopt Brinell hardness testing as a means of batch inspection quality control for incoming parts. The existence of ferrite near the surface at depths of $\frac{1}{8}$" causes failure to determine the matrix structure throughout a casting, which is the aim of the operation.

Such surface effects have been noted by Angus (1) for green sand castings but to a far less degree. The structures are thought to be associated with the mode of solidification of the casting and hence the heat flow between the metal and mould. Little work has been carried out in the field of shell moulded castings despite its developing engineering importance as a production technique.

The aim of the present work was to study the solidification of castings produced in shell moulds and compare this with solidification of similarly shaped green sand moulded castings. The resulting graphite structures were examined and compared to the solidification characteristics that were associated with them. Particular attention was given to the mode of solidification and the resulting graphite structures in the surface layers of castings. The subsequent rate of cooling in the solid state was also examined, together with the matrix structures which arose. Some consideration of the influence of the graphite form and solidification rate on the subsequent matrix structures to which the cast iron

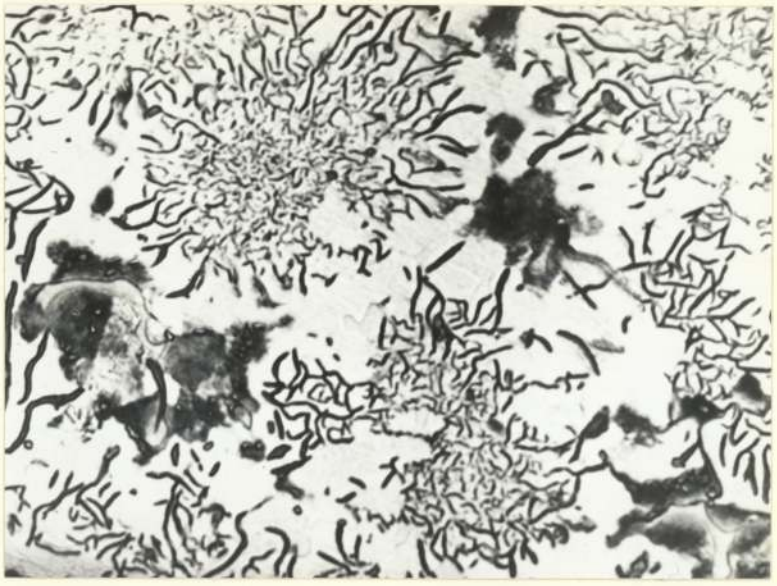

(a) At the surface

(b) At the centre of the section

Fig. 1.5 Microstructure (X100) of medium section shell moulded grey iron casting. Etched 2% Nital.

transformed was thought to be necessary in view of the structures illustrated in Figs. 1.4 and 1.5.

An initial study of the comparative thermal properties of various shell moulding materials and of green sand moulding material was also considered necessary in order to provide data for the analysis of heat flow and subsequently an explanation of the structures produced.

This technique was also required to examine the effects of other influencing mould factors which included the variation in mould thickness, and its composition. In this manner any suggested influence of mould variants would be determined by examining actual solidification patterns.

CHAPTER 2

2.1 THE SHELL MOULDING PROCESS

Before discussing the factors influencing the cooling and structure formation of shell moulded grey cast iron it is appropriate to deal with some more general aspects of the shell moulding process.

The Croning process (2) was introduced into this country in 1947 and at once received considerable attention by the Foundry industry due to its potential for producing castings of excellent dimensional accuracy and surface finish.

The principle of the shell moulding process was originally outlined by Croning who described the process as a moulding technique using a mixture of fine grained silica sand and approximately 4 to 7 per cent of a powdered resin as a bonding agent. The moulding material was placed on a heated metal pattern plate when the resin first liquified for a depth of 4 - 8 mm, in contact with the pattern plate. The surplus moulding material could then be discarded by inverting. With subsequent heating the resin hardened, bonding the sand grains together into a non-fusible insoluble state.

The process indicated that the synthetic resins used as bonding agents required special properties without which the moulding process would not be possible. Furthermore, the silica sands suitable for such a bonding process would also require certain properties.

Büchen (3) carried out a comprehensive survey of resins suitable for the shell process. The production of resin

materials due to the effect of formaldehyde on phenol had been shown by Van Boyer. Two main groups of resins were produced.

i. Resoles produced by the reaction of phenol with an excess of formaldehyde and an alkaline catalyst.

These resins formed three possible states:-

(a) Resole - soluble, fusible and self hardening resin.

(b) Resitol - self hardening but retaining plastic properties.

(c) Resite - insoluble , non-fusible and hardened.

ii. Novalaks produced from phenol plus a molar deficiency of formaldehyde with an acid catalyst, i.e.

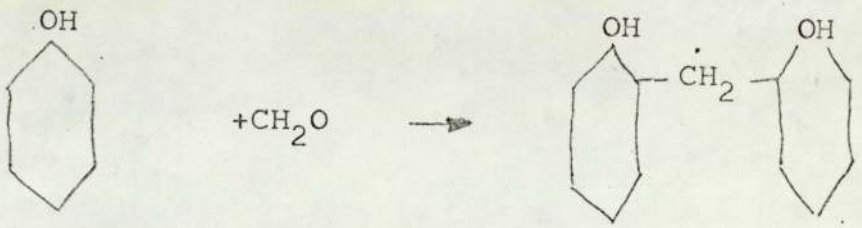

Büchen stated that these resins which were soluble were fusible but can be hardened indirectly by the addition of a hardening agent of the methylene group.

It was pointed out, therefore, that two types of resin could possibly be used, i.e. the resole (type i(a)) or Novalak types since any suitable resin must be fusible and hardenable but not expandable after hardening.

Resoles which are self hardening present greater process difficulties than the Novalak resins. Alexander (4) showed that the Novalak resins undergo second stage hardening by the

combined action of heat and hexamethylene tetramine. The latter substance decomposes on heating to act as both catalyst and formaldehyde donor.

The use of Novalak type resins was generally adopted but it was shown that the use of powdered resin and sand mixtures was inefficient. The quantity of resin used could be reduced and better distribution achieved by coating the sand grains with the Novalak resin by a different technique from powdered resin. Resin wasted in coating the surface in some cases represented 20 - 30 per cent of the total used. In order to achieve the better efficiency of coating, it was shown (5) that sand grains could be coated using preheated sand and warm air blown through the sand mill in which the sand was being coated by resin. The temperature used was 130°C, at which temperature limited melting of the resin occurs, making a plastic form which enabled it to be coated on to the sand grains very efficiently. After coating, sand was passed through a disintegrator and cooler. The quantity of resin required was proportional to the total surface area of the sand, but using the hot coating technique resin contents of 3 - 5 per cent have been found to be very suitable. Rounded sand particles have been shown to give better properties for a constant resin content, angular sand grains resulting in a higher resin consumption for efficient coating. Similarly, resin consumption for efficient bonding was increased as the fineness of the sand was increased. However, since the principal advantage of the shell process is the accurate dimensional tolerances which can be achieved, a high quality surface is desirable together with sharp

definition, hence fine grain size sands are used in the process. A measure of the sand grain size and shape with reference to the amount of resin required in the coating process, can be obtained by the specific surface of sand measured by means of air permeability. An example of typical values is shown below, (from Morgan (6)).

Types of Sand	Specific Surface
Lynn SS	200 cm^2/gm
Buckland	204 cm^2/gm
Congleton	123 cm^2/gm

The Congleton sand would thus be regarded as a poor shell moulding material due to the reduced area of contact which would be obtained on bonding; higher resin contents would be required to achieve efficient bonding.

The shell process developed along two lines for the production of moulds - (a) allowing the sand to free fall on to the heated pattern plates in the so called dump box process, (b) blowing the sand between heated pattern plates.

The dump box technique was developed for mould making and remains the principal method of production. The resin coated sand is brought into contact with the pattern plate heated to 240°C, the resin first melts allowing the layer in contact with the pattern to adhere to the form of the pattern, the surplus sand is then dumped. The action of further heat is upon the hexamethylene tetramine to produce hardening. The hardened shell can then be ejected from the heated pattern plate. The effect of grain size distribution upon the packing density was shown (5) to be small when the dumping method of production was used.

Morgan (6) showed that the density of shell moulds was normally very little different from the density of the loose material, i.e.

Material	Loose Material	Cured Shell
4% Resin		
Silica Sand	1.53	1.46 - 1.55
Zircon	2.90	3.0

On casting a shell mould the only substance influenced by heat is the resin. Phenolic resins undergo pyrolysis under the action of heating, the final products depending upon the formation of the resin. It has been shown (7) that the gaseous products that are produced by the pyrolysis of phenol formaldehyde resins at 700 - 800°C and 950 - 1250°C include methane, carbon monoxide and carbon dioxide. However, since the resins may break down into three possible methyl and sixteen possible polymethyl phenols, subsequent decomposition may result in the production of hydrogen, ethylene and other gaseous products.

2.2. STRUCTURE OF SHELL MOULDED CASTINGS

The introduction of shell moulding, a new technique for the production of castings having good dimensional accuracy, obviously necessitated a large amount of energy being devoted to its development. It was probably this process development that resulted in the metallurgical aspects of castings produced in shell moulds lagging behind. There is very little literature on the subject, the first paper of any significance being by Ames, Donner and Kahn (8). In that paper and a second by Ames (9)

several materials including cast iron were cast into shell moulds and their micro-structure examined. The structures obtained were compared with a control specimen produced in a green sand mould. It was shown, particularly for bronze and aluminium, that the grain size of shell cast materials was larger than that in conventionally cast material. Furthermore, it was shown that bronze cast into green sand moulds exhibited surface chill while similar material cast into shell moulds did not. All shell moulds were backed up in some way, a variety of materials being used including steel shot, copper shot and rammed green sand, apparently without any significant influence on the structure of the castings. The influence of shell thickness was also investigated and it was stated that there was a definite trend towards larger grain sizes as the thickness of the shell was increased. The above fact was quoted as being an example of the insulating effect of shell moulds. It was also shown by Ames[9] that the use of zircon sand, as opposed to silica sand for shell moulds, produced a much finer grain size which was comparable with that produced in conventional green sand moulds.

As a result of the work of Ames et al. it was generally thought that the cooling time of castings in shell moulds was greater than that of castings in green sand moulds as a result of the observed differences in grain size and since chill crystals were absent in bronze castings, it would be usual to assume solidification time was also longer. The

early work, however, did not attempt to give any quantitative assessment of cooling or suggest what was the effect of a shell mould without the use of a back-up material. Moray, Bishop and Pellini (10) measured solidification times and produced cooling curves for various plate castings made in shell moulds. The effects of the thickness of the mould and of the type of backing up material were examined for a number of materials including nodular cast iron.

By measurement of solidification times for a green sand mould, a table was produced showing solidification times for shell moulds compared with sand moulds. It was shown in direct contrast to the work of Ames that the solidification times for shell moulds, with either steel shot or gravel as a back up material, was less than for green sand moulded castings. The extent of the decrease in solidification time depended upon the type of backing material, i.e. steel shot gave a greater decrease than gravel, and on the shell to plate thickness ratio, i.e. the higher the ratio the smaller was the decrease in solidification time. This is illustrated for nodular iron in Fig. 2.1. For shell moulds without back up material, it was found that solidification time was significantly increased, both for those castings produced in air and in an argon atmosphere. This is shown for aluminium plates in Fig. 2.2.

Moray et al. measured the solidification time at the centre of a plate casting, but no attempt was made to determine the start and end of freezing for the progression of freezing through the thickness of castings. Furthermore, no comments were made on the influence that subsequent cooling rates of castings in shell moulds might have on that structure, i.e. due to solid state transformations being accelerated or suppressed.

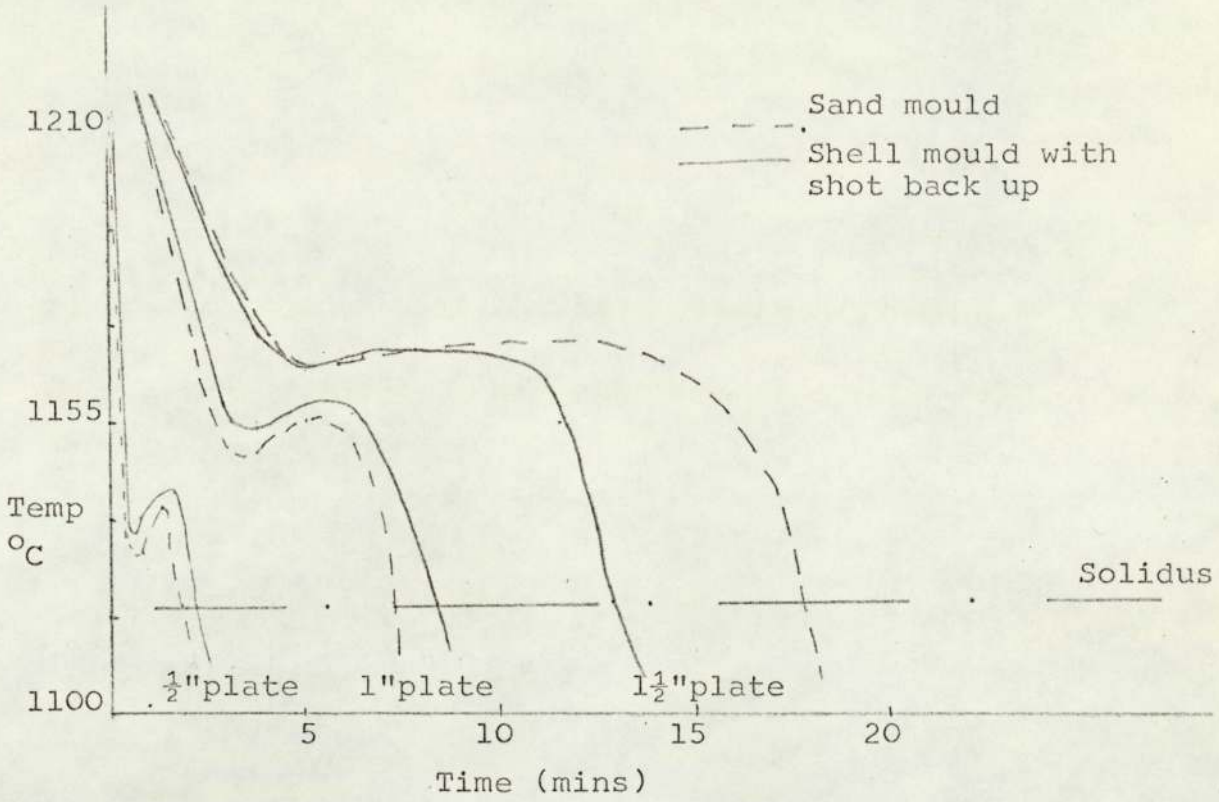

Fig. 2.1 Cooling curves for nodular cast iron

(After Moray et al.)

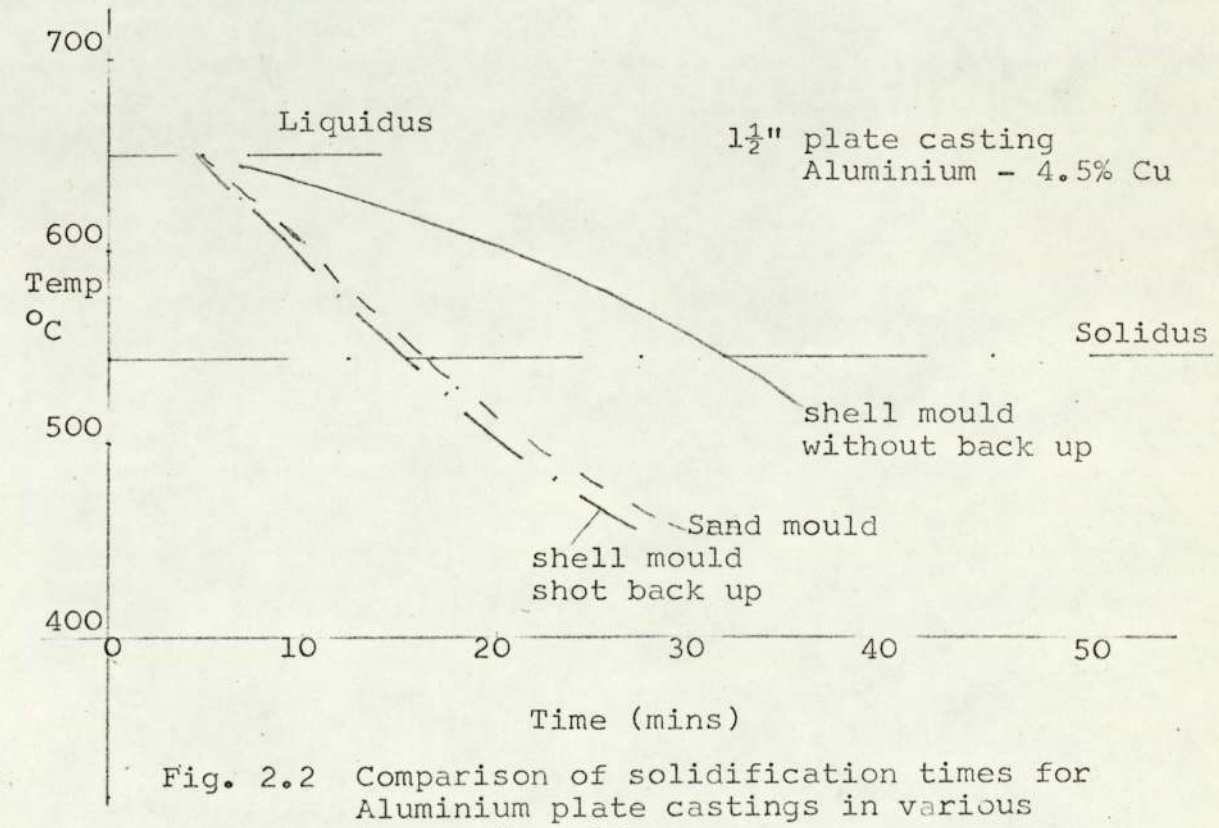

Fig. 2.2 Comparison of solidification times for Aluminium plate castings in various types of mould

(After Moray et al.)

Flinn (11) et al. looked at the surface structure of various shell cast metals compared with similar materials cast in green sand moulds, both nodular and grey iron were included in the materials examined. The work on the surface structure was carried out due to suggestions that shell moulds had a chilling effect on cast iron and a surface carburising effect for cast steel. The results were confusing but for grey iron some slight decarburisation was reported on heavy sections, i.e. 2" casting, at the surface exending to 0.010". For light sections, i.e. $\frac{1}{8}$", it was stated that there was a greater tendency for surface carbides to be present than in conventionally made castings. For nodular iron and steel it also suggested that slight decarburisation had occurred. The decarburisation was not measured quantitatively but assumed due to the presence of ferrite at the surface of the ferrous materials rather than pearlite which was present in the remainder of the structure.

The same authors showed that for leaded bronze (85-5-5-5) cast into shell moulds, lead was dispersed evenly and up to the as cast surface, whereas for green sand moulds the lead did not persist to the surface.

Glick (12) examined both solidification time, (at the centre of the section) and the structure of shell moulded castings in aluminium and copper alloys. The effect of sand mix, type of resin and back up material were all considered. It was shown that for aluminium bronze the solidification time, and the structure, were similar to those obtained in conventionally cast material. For an Al-Cu-Si alloy the structure of a shell moulded plate was similar to the green sand moulded plate, although the

solidification time was recorded as more than 25% shorter. For gun metal castings it was shown that the solidification time in shell moulds was 15 - 20 per cent longer than in green sand and that, whereas green sand castings had some columnar crystals in the structure, the shell castings had fine equi-axed grain structures.

For a constant plate thickness, Glick determined that as shell thickness increased the time for solidification decreased. The solidification time also decreased with different types of backing material and with zircon based sand, compared with silica sand. These results are illustrated in Table 2.1.

Glick concluded that the chilling power of zircon, silica shell and green sand moulds for gun metal and Al-Cu-Si castings were in the ratio of 0.8:1.2:1 respectively. The chilling power of silica sand moulds being raised by increasing the shell thickness (up to 1") or by using a backing material with high conductivity, e.g. steel shot.

This work confirmed the earlier findings that showed cooling curves for aluminium 4.5% copper alloys cast into various moulds as shown in Fig. 2.3.

Pollard (13) has commented that for aluminium alloys cast into shell moulds, lower mechanical properties are obtained than in conventional green sand alloys. He stated that studies of solidification have shown that shell moulds exhibit lower chilling power and hence freezing rates than green sand moulds.

As a result of this shell cast tensile test bars gave low tensile strengths due to unsoundness. The cooling rate was measured at the centre of the casting and at a position

Table 2.1

Comparison of solidification times for clay bonded moulds and shell moulds for various alloys

(After Glick (12))

Metal	Solidification time in green sand mould (secs)	Solidification time in silica shell mould (secs)	Solidification time in zircon shell mould (secs)
Al-Cu-Si (LM4)	420	285	270
Leaded-gunmetal	213	260	162
Aluminium bronze	114	120	105

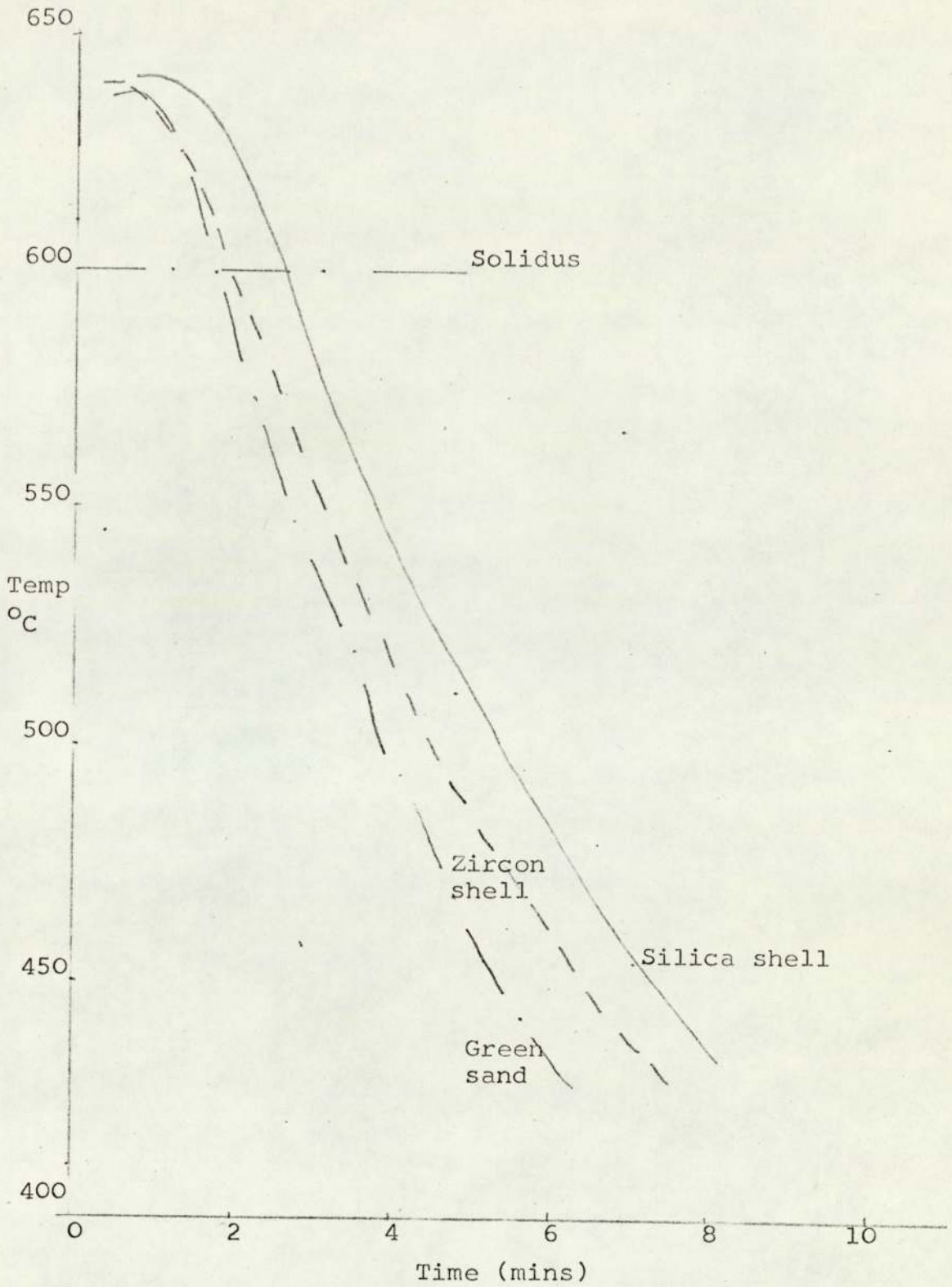

Fig. 2.3 Comparative cooling curves of aluminium - 4.5% Cu casting in various moulds

intermediate to the centre and surface. In their work the casting temperature of the alloys was 250°C above the eutectic temperature of approximately 450°C. The plate thickness was one inch, hence the time for solidification was considerable. It was indicated diagrammatically as being in excess of 16 minutes. The time for the commencement of solidification after casting was not made clear.

Jamuszewicz and Harpulan (14) carried out extensive work on the ability of shell moulds to remove heat and measure solidification times by means of cooling curves. The specimens used were plates of 100 mm x 60 mm and thickness of 3, 15 and 20 mm. The influence of the shell mould wall thickness and the percentage of resin added were also measured. They concluded that the intensity of the cooling of the iron castings was slightly increased by a decrease in the mould thickness and by increasing the resin content. It was also stated that the cooling of castings was slower in shell moulds than in green sand moulds.

Indirect references to the cooling rate of grey iron castings produced by shell moulding have been made in the literature together with a description of the structures produced with particular reference to the use of pearlite stabilising elements. Thwaites (15) described problems encountered in the production of zircon shell moulded castings due to ferritic skins associated with surface layers of fine undercooled graphite resulting from the 'special' cooling conditions pertaining to shell moulds. The use of tin as a technique to stabilise pearlite because of the presence of ferrite on the internal bores of castings for hydraulic applications was advocated.

Klaban (16), in a paper discussing the use of antimony as a pearlite stabiliser, said that at high rates of cooling, which were not sufficient for an iron to solidify white, favourable conditions were created for the formation of a structure consisting predominantly of a graphite/ferrite eutectic. Such a structure, he stated, was normally encountered in thin walled castings poured into shell or metal moulds. Photomicrographs of an 8 mm thick shell moulded cylinder liner casting were shown exhibiting the existence of 'D' type graphite and ferrite.

2.2.1 Discussion

The work on solidification of various alloys in shell moulds covers a wide range of materials. While there are some minor disagreements the workers are generally agreed that the solidification time for all types of shell moulded castings is slower than for corresponding sections in green sand moulds. It is also generally agreed that zircon shell moulds give a faster rate of solidification than silica sand moulds. However, all the workers used casting section thickness in excess of $\frac{1}{2}$" and none of them attempted to measure the progression of freezing from the surface or solidification times at the surface. Moray, Bishop and Pellini (10) did comment on the progression of freezing as a function of the solidification times at the centre of the casting.

In contrast, the observations made on the structure of grey iron castings by Klaban (16), Thwaites (15) were related specifically to either the surface of a casting or to thin walled section castings, i.e. less than $\frac{1}{2}$". The two results were, therefore, in no way complementary. Hence, while the

general solidification of castings of ½" or more in section may be slower in shell moulds there is no factual evidence to show that it is true for thin section castings. Solidification at the surface of thicker castings may also be equally as fast as in green sand moulds, if the subsequent rate after initial solidification is very much slower, i.e. giving an overall slower rate to the centre of the section. The work of Flinn (11) et al , in demonstrating a uniform dispersion of lead in leaded bronze up to the surface in all sections cast into shell moulds but never in green sand moulds, is interesting in this context.

Further indirect evidence of an initial nigh rate of cooling in a shell mould was suggested by Jackson (17) who commented that a chill zone of 7.5 mm was first formed in steel castings followed by a very slow cooling rate. Photomicrographs showing chill crystals were shown.

2.3 FACTORS INFLUENCING GRAPHITE STRUCTURE IN HYPO-EUTECTIC GREY CAST IRON

2.3.1 Solidification Rate

Cast iron may solidify, depending on the composition and cooling rate, either with all the carbon in the combined form, i.e. white iron, or with the carbon in the form of graphite, i.e. grey iron. In grey iron, flakes of graphite are dispersed throughout the metallic matrix in an apparently random pattern. The actual size, shape, pattern and amount of the graphite flakes may vary very considerably depending upon the conditions under which the iron solidified. Thus many factors (e.g. casting temperature, degree of superheat, composition) influence the type of graphite structure obtained.

However, how any cast iron solidifies is a major function of the rate of solidification.

The principles of solidification of hypo-eutectic cast iron have been outlined by Fuller and Hughes (18) and by Loper and Heine (19) amongst many others. The work has illustrated, as a direct result of observations of the solidification pattern, that austenite dendrites form at the liquidus, these grow into the liquid until the eutectic arrest temperature is reached. Eutectic solidification occurs from the edge towards the centre of the casting, although it was shown by Fuller and Hughes that some eutectic was formed simultaneously throughout the interior of the casting. Dawson and Oldfield (20) described the eutectic as spheroidal aggregates of austenite and graphite termed eutectic cells. They pointed out that the number of cells gave an excellent indication of the number of nuclei available for solidification in a given volume of liquid metal. Since the degree of nucleation is a function of the rate of solidification, then all other influencing factors being constant, the eutectic cell count gives an indication of the solidification rate.

This is illustrated in Fig. 2.4.

It can be seen that as the eutectic cell count increases then the cooling rate, expressed in terms of bar size, also increases. It could be expected that the rate of solidification increases, therefore, as the eutectic cell count of an iron increases. Oldfield (21) has shown that the higher the eutectic cell count the greater the degree of undercooling below the equilibrium eutectic temperature. This is illustrated

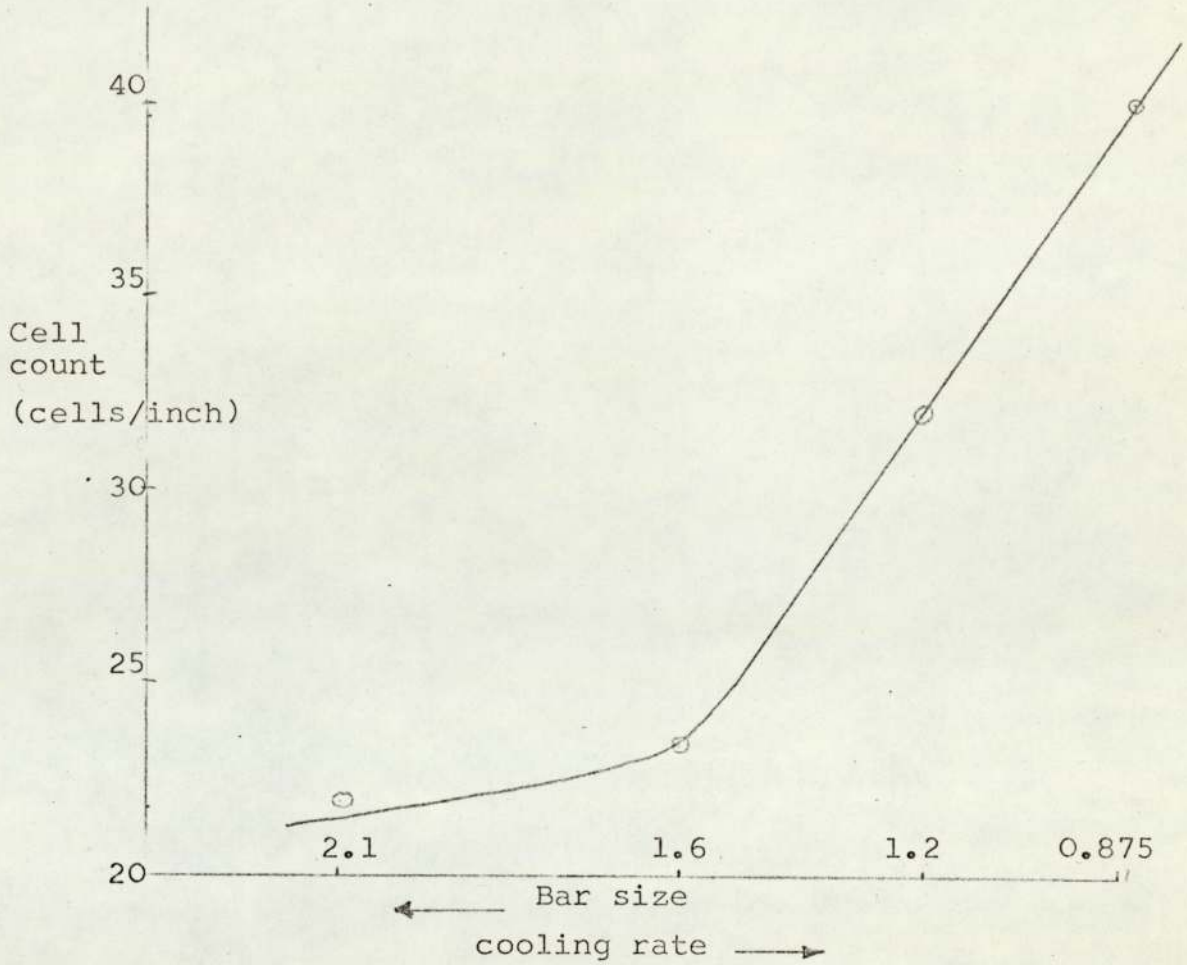

Fig. 2.4 The effect of cooling rate on eutectic cell number

below in Table 2.2

Cell Count Cells/inch	Undercooling	Cooling Rate
15	11.2°C	0.625
22	15.0°C	0.833
33	18.8°C	1.15

$$\text{Cooling rate} = \frac{1}{\text{bar diameter}}$$

The above facts take into account that the form of the graphite within the eutectic cell did not alter. The dispersion within the cell depends upon rate of solidification also (22). As the rate of solidification increases, the graphite form becomes very fine, i.e. the amount of branching by the graphite within a eutectic cell greatly increases. Typical graphite structures for a hypo-eutectic iron for high and low rates of solidification are shown in Fig. 2.5.

As can be seen from Fig. 2.5, in slowly cooled cast iron the dendrites cannot be distinguished from the matrix. However, when the graphite is finer, the dendritic pattern is clearly seen.

Work by Hillert (23) has further demonstrated the influence of solidification on the dispersion of graphite within the eutectic cell. Using undirectional solidification techniques it was shown that by varying the cooling rate from 1.2×10^{-4} cm/sec to 60×10^{-4} cm/sec, the structure was altered as in Fig. 2.6.

Variations in the rate of solidification may give varying growth rates within a eutectic cell so that it is possible for the centres of the cells to have either coarser (24) or finer (25) graphite forms than their peripheries. An example of the latter is shown in Fig. 2.7.

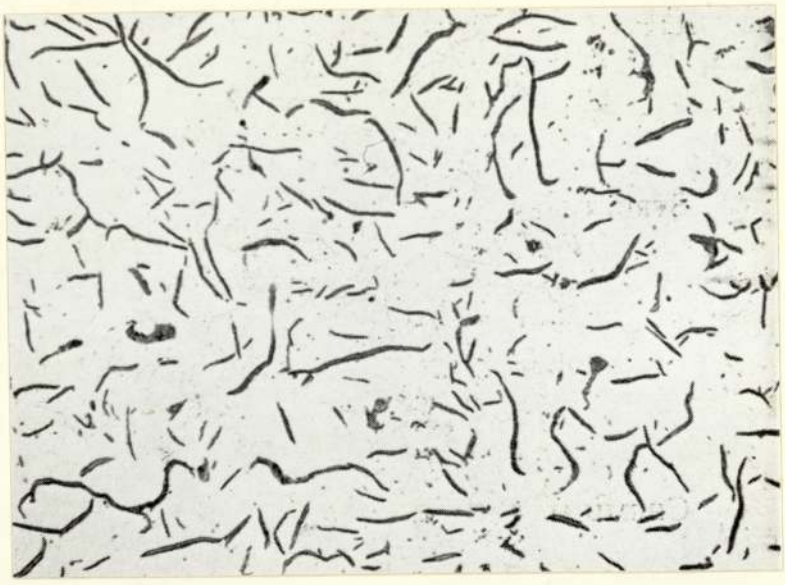

(a) Low rate of cooling

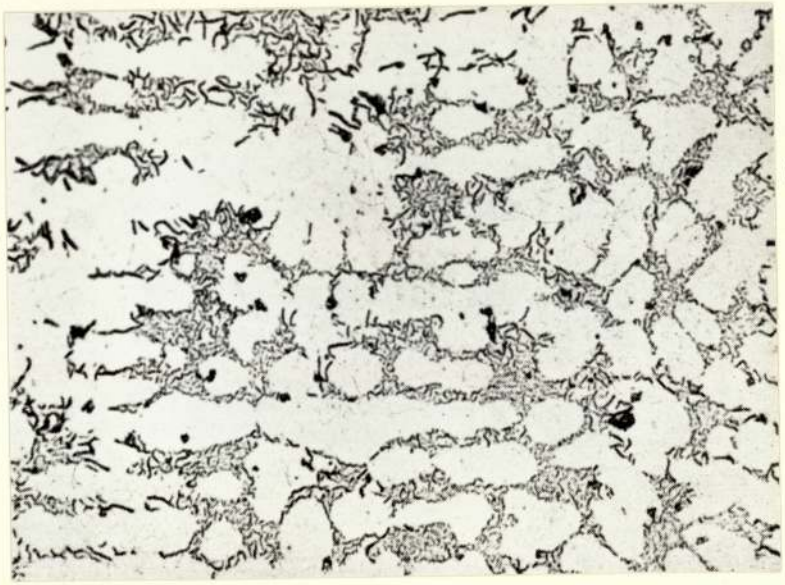

(b) High rate of cooling

Fig. 2.5 Photomicrographs illustrating typical graphite structures arising in hypoeutectic grey iron at high and low rates of cooling

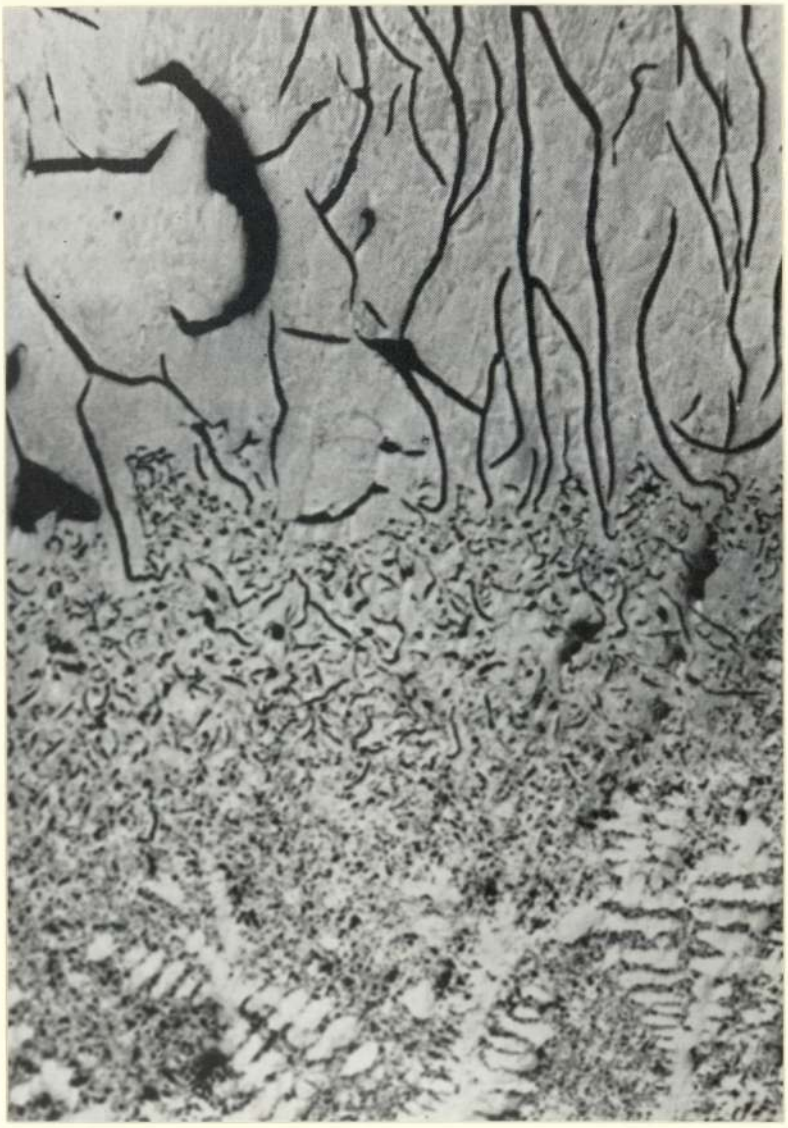

Fig. 2.6 Influence on graphite form of undirectionally solidified grey iron upon changing the cooling rate from 1.2×10^{-4} to 60×10^{-4} cm.sec.$^{-1}$

(After Hillert)

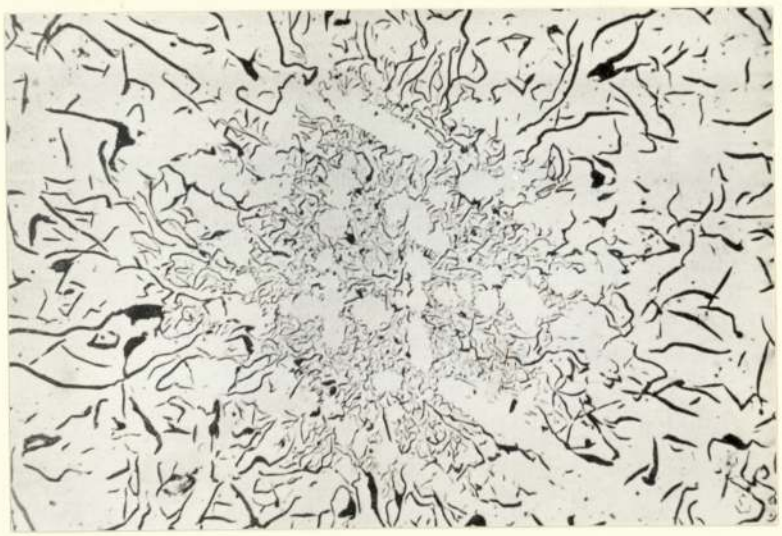

(a) Cooling rate progressively becoming slower. Unetched

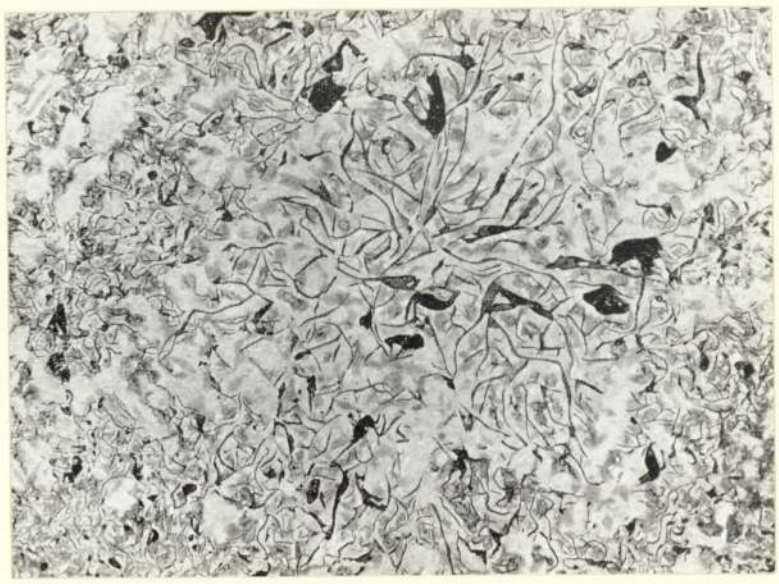

(b) Cooling rate becoming progressively faster. Etched in 2% Nital

Fig. 2.7 Influence of changes in cooling rate on the graphite form

Various sizes of graphite flakes within different cells may exist within the same casting, as the eutectic cell count may vary considerably from one part of the casting to another if the cooling rate varies.

2.3.2 Other influencing factors

2.3.2.1 Number of eutectic nuclei As described above, the degree of nucleation, and hence the graphite shape and size, is primarily a function of the rate of solidification. However, the addition, just prior to pouring of very small amounts of certain substances termed inoculants to molten iron, can alter the relationship between cooling rate, cell count and distribution within the cells. Dawson (26) showed for a number of substances, including ferro-silicon, that the number of eutectic cells is increased as the silicon content in the iron increases up to a certain limiting level. This is shown in Fig. 2.8.

Low nucleation rates lead to high growth rates of the eutectic cells (27) and hence frequent branching of the graphite occurs producing the type of structure shown in Fig. 2.6. Thus, the influence of inoculants in increasing the eutectic cell count is to oppose this type of structure.

2.3.2.2 Influence of superheating As the temperature to which molten iron is heated is increased the degree of undercooling which occurs subsequently is increased (28). This is shown in Table 2.3.

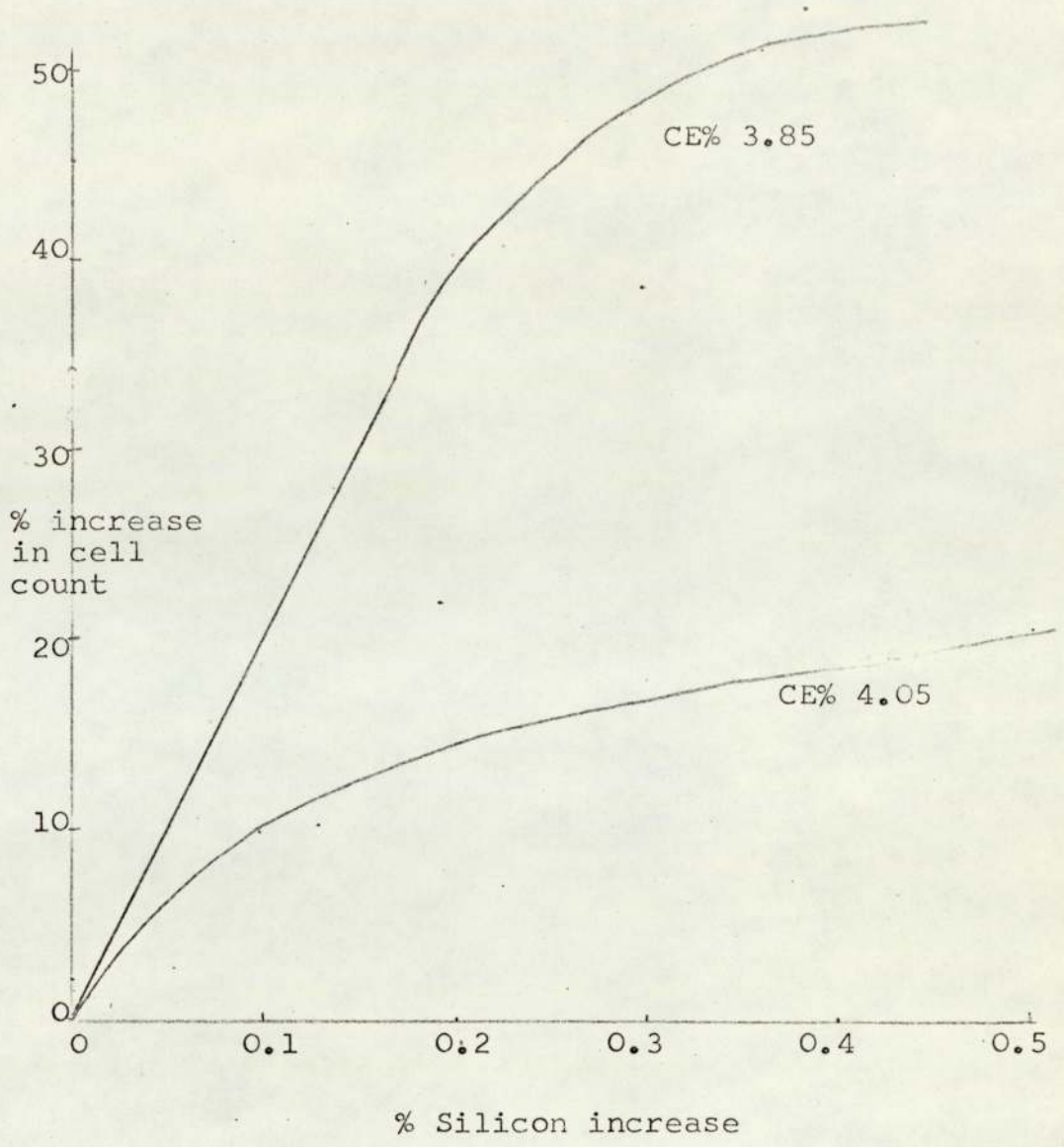

Fig. 2.8 Influence of increasing addition of ferro-silicon to a melt on cell count

Table 2.3. Influence of Superheating

Superheating Temperature °C	Pouring Temperature °C	Temperature for Eutectic Solidification °C
1450	1370	1140
1470	1380	1140
1510	1380	1139
1575	1370	1137
1630	1380	1135

As undercooling increases, the cell count should also increase. However, it has been shown by Fuller (29) that superheating to a higher temperature, or maintaining the superheating temperature for a longer time, reduces the number of eutectic cells due to possible elimination of nucleation sites.

2.3.2.3 Influence of compositions Commercial cast irons usually contain certain amounts of silicon, manganese, sulphur and phosphorus as well as minor quantities of many other elements. These elements can influence the process of nucleation and growth and hence the form that flake graphite takes in cast iron.

Of these elements the influence of sulphur has received the greatest attention. Boyles (30) first showed that it was this element which was principally responsible for the flake graphite structures observed in cast iron. Many workers (20) (29) have shown the difference in graphite form resulting from the presence of sulphur. Low sulphur or sulphur free irons show structures that consist mainly of fine undercooled graphite whereas sulphur bearing materials show coarse flake graphite structures.

The nucleation and growth of graphite is influenced by titanium (31) since it is now understood that it neutralises the influence of sulphur described above when it is present. Similarly, manganese (32) has a counter balancing effect on sulphur and hence reduces nucleation. Hughes (22) also refers to the fact that phosphorus increases the eutectic cellnumber probably due to increased nucleation.

The formation of 'D' type graphite

The formation of 'D' type graphite structures has received extensive examination. Hughes (22) says that most workers agree that this type of graphite forms directly on solidification from the melt. Kondic et al (33) have suggested that under certain circumstances this type of graphite may be produced by the decomposition of iron carbide eutectic at temperatures just below the solidus temperature. Oldfield (34) carried out a series of experiments by heating the ledeburite eutectic just below its melting point (1124°C) in the temperature range 1117-1122°C. The graphite obtained as a result of heat treatment was all of the quasi-flake compact type. The experiments did not produce any fine or undercooled graphite, either below the melting point of ledeburite or between the two melting points, i.e. ledeburite and the point where graphite is formed directly from the liquid. Oldfield concluded that very fine 'D' type graphite only occurred in the grey cast iron used when the liquid was undercooled considerably.

Boyles and Long (35) showed very effectively that the form of graphite obtained in a microstructure could be related to the

degree of undercooling obtained. In a number of grey cast irons they showed that the formation of 'D' type or fine rosette graphite corresponded with an increased degree of undercooling. Lower degrees of undercooling resulted in the formation of 'A' type graphite structures.

Hillert (23), using undirectional solidification techniques, has shown that the graphite form changes from 'A' type to the fine undercooled form when the solidification rate of the melt is rapidly increased. Extensive work on the formation of undercooled graphite, its relationship to austenite dendrite size and cooling rate has been done by Heine and associates (36,37,38). Using a number of commercial cast irons they showed that the formation of this form of graphite was a function of cooling conditions, carbon equivalent value and the solidification range over which the dendrites grow. Figs. 2.9 and 2.10 show a summary of the three factors and illustrate clearly the importance of the eutectic solidification temperature in determining the form of the graphite produced.

Heine has also shown that under certain conditions 'D' type graphite may be produced by very slow rates of cooling. This can occur in heavy section castings where 'A' type graphite grows slowly through the eutectic solidifcation range from a limited number of nucleation sites. This can result in a carbon concentration being set up in the remaining liquid which eventually results in interdendritic type 'D' graphite forming in the lower temperature range of eutectic solidification. Hence, the formation of fine 'D' type graphite can occur in thin section castings, at the surface of rapidly cooled castings or

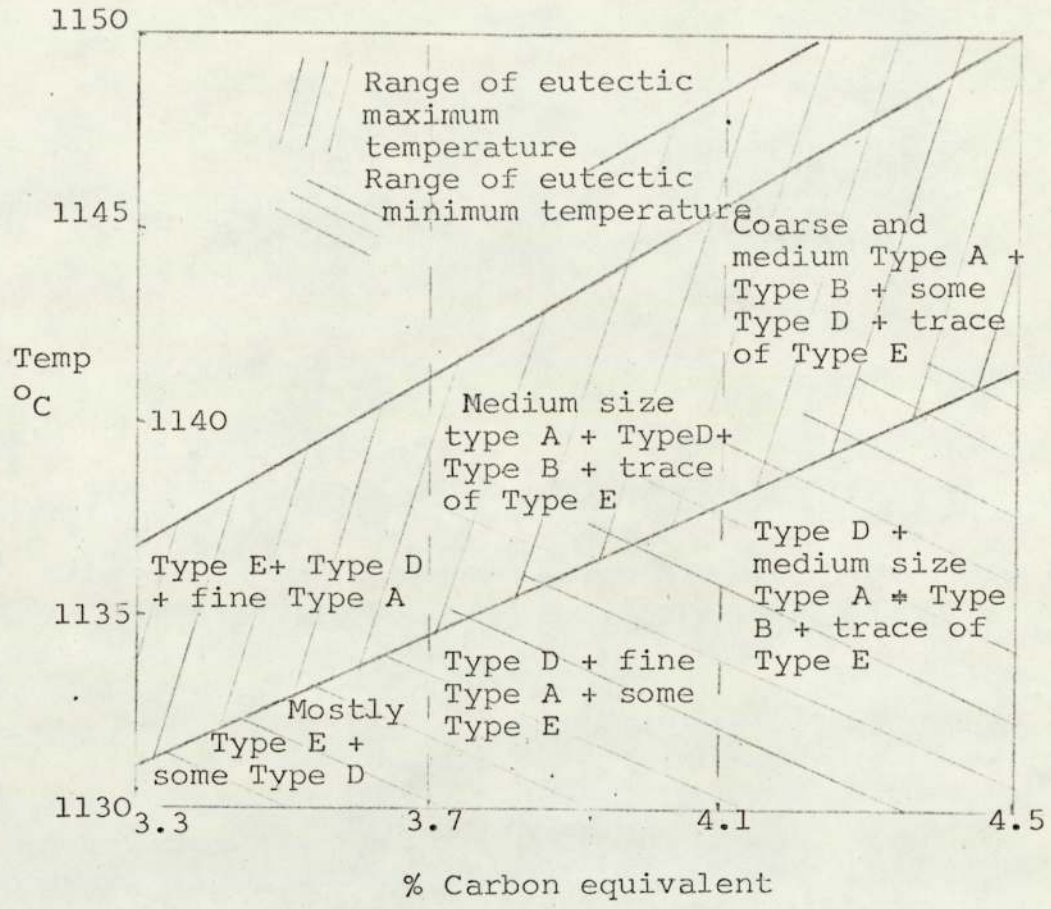

Fig. 2.9 Influence of eutectic temperature on the graphite form of grey cast iron with differing C.E. values

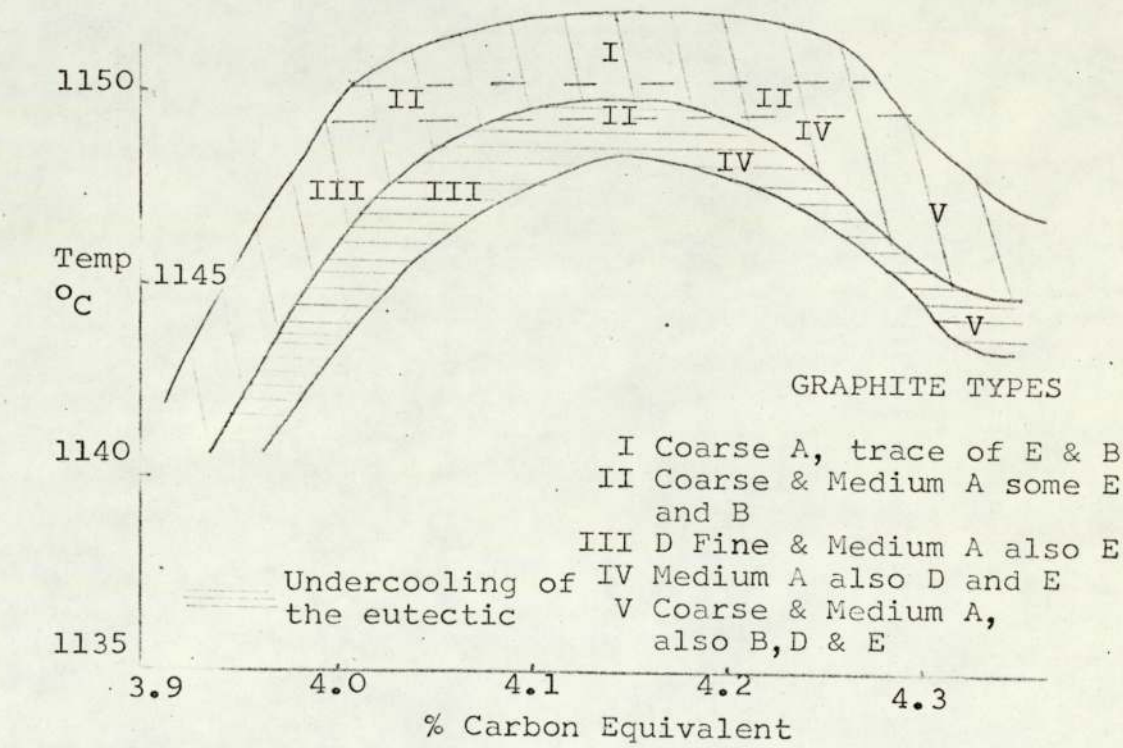

Fig. 2.10 Influence of undercooling on graphite form

throughout the section of heavier section castings co-existing with 'A' type graphite.

2.4 SOLIDIFICATION RATES

Solidification of a liquid metal occurs by the nucleation and growth of crystals. The shape and distribution of the crystals are subject to considerable variation (39) depending on the constitution of the alloy being cast, the melt history and prior treatment, the thermal conditions in the mould and in some instances the mould material.

Cooling of the liquid metal first involves removing the superheat and then evolution of latent heat at constant temperature, followed by cooling of the solid casting. Solidification in a mould, therefore, involves non-steady state heat flow. Ruddle (40) outlined the basic concept of the start of solidification in castings with crystallisation at the mould walls providing a thin layer of solid metal. The width of the solidification front is primarily dependent upon the type of metal or alloy that has been cast, this affects many factors in the resulting structure of a casting. Brandt, Bishop and Pellini (41) measured the rate of growth of the solid layer for many various metals, including pure metals, e.g. lead, long freezing range alloys e.g. bronze, and of alloys of near eutectic composition. It was shown that the band between the start and end of solidifcation could vary very considerably in width. The band was exceptionally narrow for pure metals, the solidification front being a line more than a zone, whereas for long freezing range alloys the solidification front was a zone which could stretch from the edge

almost to the centre of some castings. The solidification mode of grey cast iron in sand moulds was determined by Dunphy and Pellini (42) and is shown in the two diagrams, Figs. 2.11 and 2.12.

It can be seen that solidification takes the form of two separate fronts and bands, i.e. one for the start of dendrite solidification, the second for the eutectic phase. In a semi-infinite size plate casting, the fronts would move inwards towards the centre of the casting parallel to the mould face. The rate of advancement of the solidification front was first shown by Briggs and Gezeling (40) carrying out a pour out technique and measuring the wall thickness of the shell remaining after various intervals of time. The technique was extended considerably and it was shown that the theoretical relationship

(1) $D = q\sqrt{t}$

D = thickness of solidified metal

t = time

q = solidification constant

was true for a semi-infinite body. Chvorinov continued investigation of solidification rate of steel by the temperature measurement technique at various distances from the mould face. Chvorinov demonstrated that the solidification constant for the solidification of steel might be expressed as

(2) $q = 1.158 \frac{(\Theta i - \Theta o)b}{L.p^r}$

L = Latent heat

p^r = Density of metal

Θ_i = metal temperature Θ_o = mould temperature

b = heat diffusivity of the mould

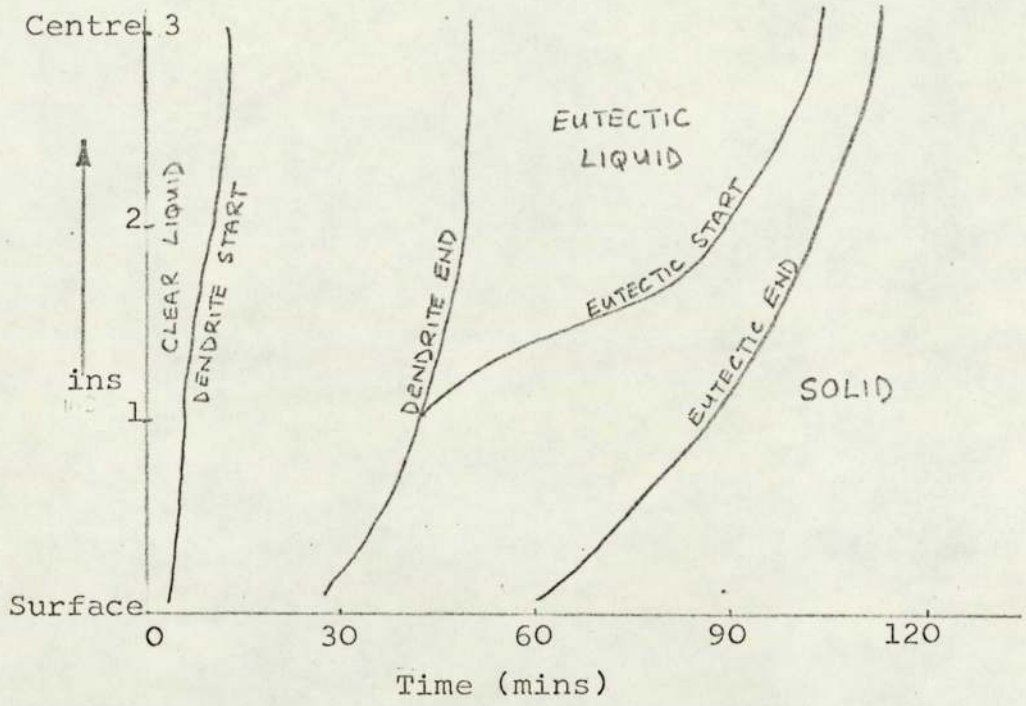

Fig. 2.11 Movement of start and end of solidification waves in a hypoeutectic grey iron casting

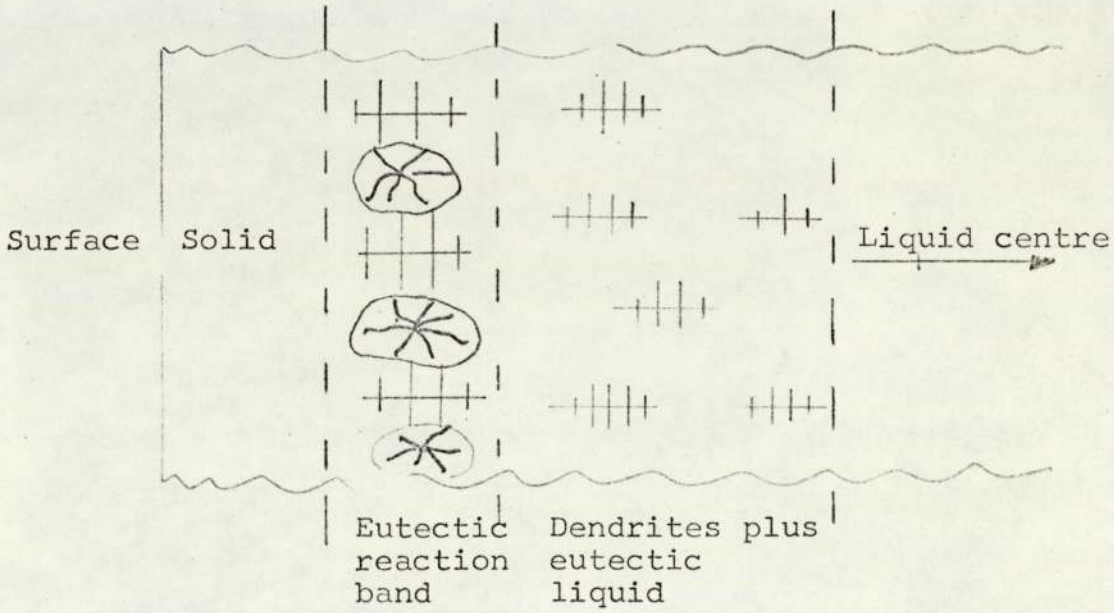

Fig. 2.12 Freezing mechanism of hypo-eutectic grey iron casting

Ruddle and Mincher also showed that skin formation followed a parabolic law $D = q\sqrt{t} - C$ where C represented the induction period before freezing began and during which superheat is dissipated.

In the mathematical assessment of the solidification rate by Carslaw and Jagar, it was shown that the parabolic law was to be expected and that the solidification constant might be expressed as

$$(3)\quad q = \frac{1.128\ b\ (\theta i - \theta o)}{L\ p^{r}}$$

where $b = \sqrt{kcp}$

where k = mould thermal conductivity
c = mould specific heat
p = mould density

The assumptions made are that there is a semi-infinite mould wall, a skin forming alloy, e.g. near eutectic composition alloy, and a constant temperature at the interface. For any mould material the relationship

$$(4)\quad \mathcal{E} = 1.128\ \sqrt{kcp}\ (\theta i - \theta o)$$

$\mathcal{E}$ = chilling power

gives a measure of the mould chilling power over a range of temperature. Typical values for chilling power for a selection of various silica moulding materials and two other materials are shown in the table 2.4.

Hence, it can be seen that chilling power may be influenced by the interface temperature and by the density of the mould.

It has been shown that as the moisture content of green sand moulds increased so did the conductivity. Ruddle and Mincher showed that the heat absorbed by the mould increased as the moisture content increased.

Table 2.4

Typical values for mould constant at various temperatures

(After Ruddle and Mincher (40))

Mould material	Interface Temperature ^{o}C	Calculated mould constant $cal.cm^{-2}min^{-\frac{1}{2}}$
Green Mansfield sand	548	105
	1083	237
Dry Synthetic sand	548	89.4
	798	151
	1083	244
Cement bonded sand	1083	330
Bonded Magnesite	548	230
	1083	354

The influence of ramming of green sand on solidification time was shown (43) for cast iron to be a reduction in solidification time as the degree of ramming increased. There was also an increase in the density of the mould where the harder ramming wasused.

The influence of ramming density, together with grain size of silica moulding sand, were shown by Berry, Kondic and Martin (44). The mean heat diffusivity and, therefore, chilling power was increased as the rammed density was increased. For two grades of the same sand the coarser grain size gave higher heat diffusivity values than the medium-fine sand for the same rammed density. These results are illustrated in Fig. 2.13.

In quantitatively defining the rate of solidification and wall thickness formation assumptions were made which may not be true in normal casting production. It is assumed firstly that the mould wall is semi-infinite and hence heat transfer from the mould face to the surroundings by convection and radiation is negligible. Where this conditiondoes not exist, allowances would have to be made for the subsequent loss of heat. Ruddle (40) states that in the case of sand castings the mould may usually be treated as if it were semi-infinite.

Berry et al (44) have shown that the second assumption of constant, instantaneously attained interface temperatures were not possible, an average temperature value being all that can be applied.

The third and most difficult assumption to meet in casting practice is that ofasemi-infinite mould wall. Finite

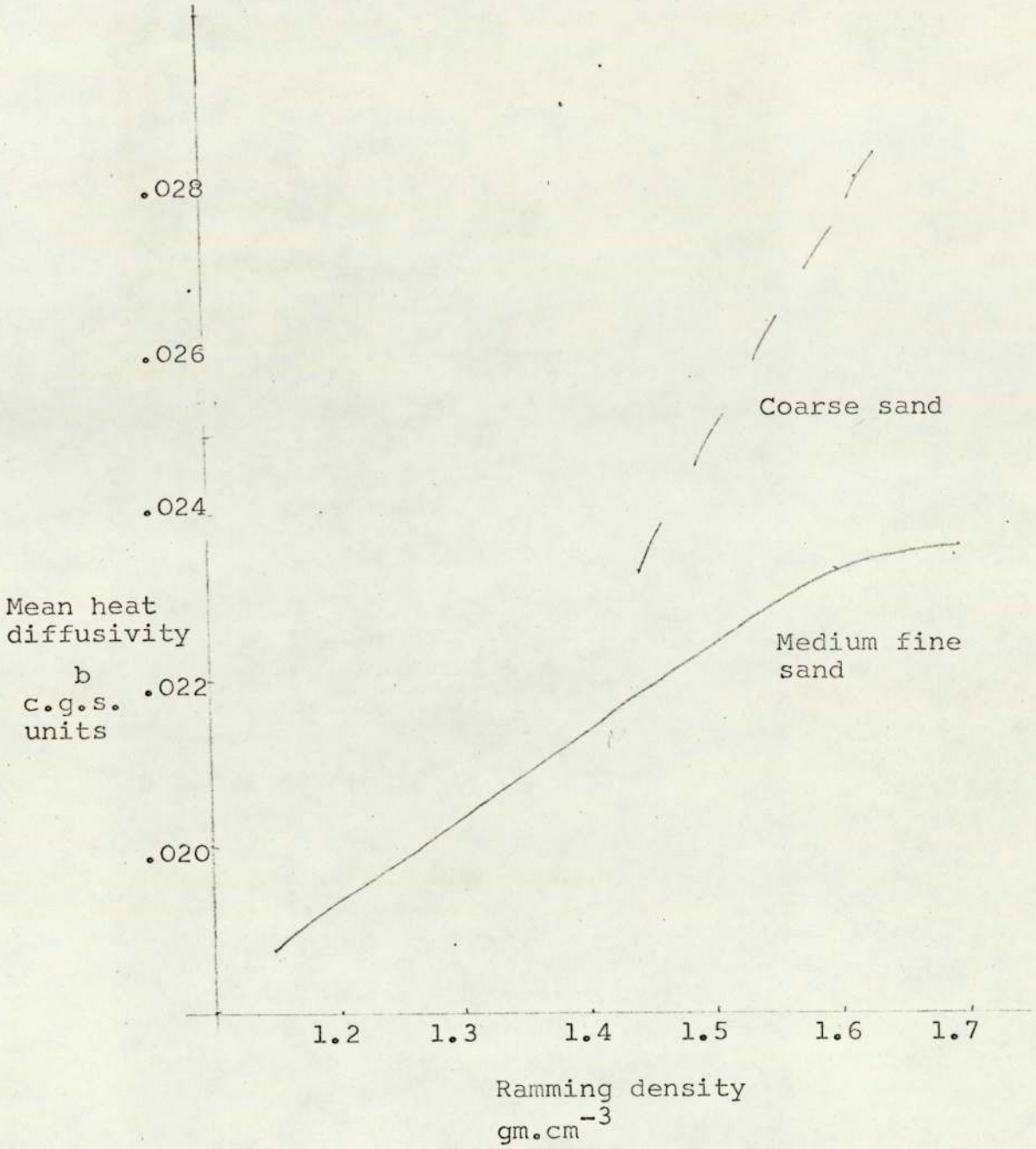

(AfterBerry et al)

Fig. 2.13 Influence of ramming density and sand grain size on the thermal properties of moulds

castings differ for two reasons -

(a) The rate of heat abstraction by mould corners and convex surfaces is much greater than that for plain mould walls. The influence of corners on the progress of the solidification front in areas well removed from them may well be marked.

(b) The area of the solidification front contracts continuously throughout freezing. Since the area over which heat is removed, i.e. surface of casting is fixed, the amount of heat generated by the solidification front is only balanced by the front accelerating as it moves towards the centre of the casting .

The application of the theoretical rate of solidification to the progress of freezing of finite castings is therefore difficult. However, it was shown by Chvorinov (40) that provided corner effects were ignored, the freezing time of a finite casting could be given by:

$$(5)\quad t = \frac{1}{q^2}\left(\frac{V}{A}\right)^2$$

q = solidification constant
V = volume of casting
A = Area of casting

Many workers have substantiated the equation for simple shapes. Ruddle (40) concluded that the rule was at least roughly true rather than highly accurate.

Discussion

The existence of extensive literature on the subject of solidification rates results in a wide diversification of results. The literature has been reviewed therefore with particular reference to short freezing range alloys and the near eutectic alloys typical of cast irons, together with particular attention to green sand and silica sand moulds

rather than chill moulds.

The relationship of the solidification time to the chilling power of moulds is reasonably well understood, hence for any casting in which semi-infinite conditions can be approached, the major factors which will control the rate of solidification for a given alloy poured at a given casting temperature, are fundamentally the mould thermal conductivity, mould specific heat and mould density. As has been shown, these may depend upon on a number of varying factors and therefore many different solidification rates can be achieved. Furthermore, the mould thickness may play a part in solidification time.

The need for the measurement of any solidification times or thermal gradients away from the influence of corners is shown to be essential.

CHAPTER 3

MEASUREMENT OF THERMAL PROPERTIES OF SHELL MOULDS

3.1 As has been seen from the previous chapter, in order to be able to analyse the rate of solidification of any casting it is necessary to be able to determine a value for the heat diffusivity of the mould and hence the solidification constant and chilling power. The total heat absorbed in time (t) by a unit area of the mould surface is given by equation (6).

$$Q = 1.128\ b\ (\theta i - \theta o)\ \sqrt{t}$$

$$Q = \mathcal{E}\ \sqrt{t}$$

Q = total heat removed
b = heat diffusivity
t = time
$\mathcal{E}$ = chilling power

This relationship is shown in Fig. 3.1 for castings produced in two moulding materials with different heat diffusivity values, cast from the same temperature.

Fig. 3.1

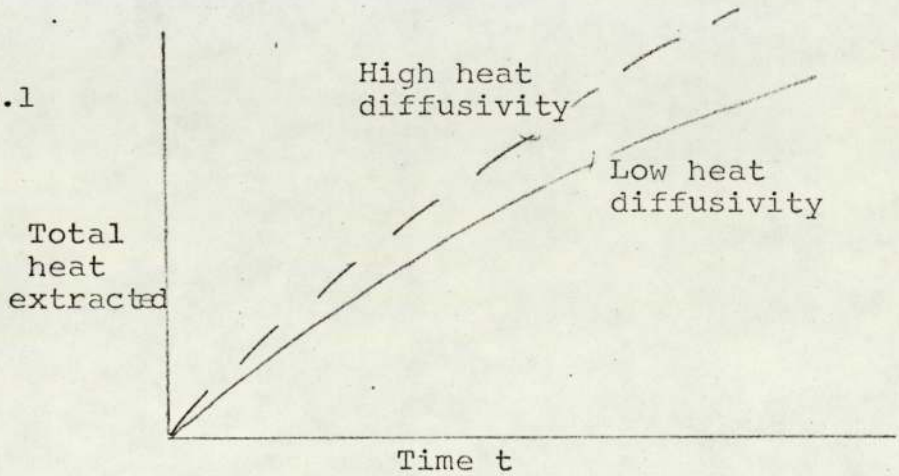

As shown in equation (3) $b = \sqrt{kc\rho}$ hence the determination of mould thermal conductivity, specific heat and density is essential in any consideration of difference in solidification rate.

Thermal conductivity and specific heat measurement

Thermal conductivity of any material is a property whichvaries with temperature and hence in analysing solidification, mould constants are calculated using mean values of thermal conductivity and specific heat since the temperature of the mould wall is continually varying. All moulding materials are composite materials and hence the determination of thermal conductivity on actual compacted moulds is desirable. Moulding materials based on silica sand, as normally used for green sand moulding and in shell moulding, are poor conductors of heat. The classic method for the determination of thermal conductivity is Lees method using a thin slab of the material to be tested. The temperature gradient through the specimen under steady state conditions and the rate of heat loss from a good conductor in contact with the specimen is measured and the conductivity calculated. Atterton (45) adopted another method for the determination of conductivity of moulding materials. In this technique a cylinder of the moulding sand was used with a resistance heating element through the centre. Two thermocouples were placed in the specimen at different distances from the centre of the specimen, (see Fig. 3.2, to measure the temperature gradient and rate of transfer of heat across the specimen.

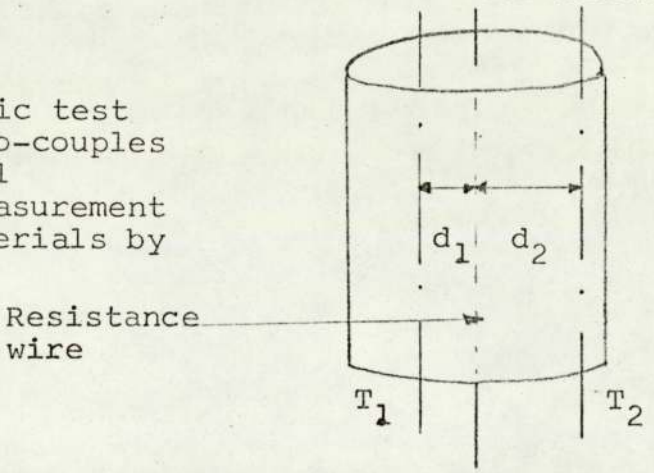

Fig. 3.2 Diagrammatic test piece and thermo-couples used for thermal conductivity measurement of moulding materials by Atterton (45)

In this technique the specimen could be placed in a vertical shaft furnace at any temperature and hence the conductivity at high temperatures measured. The criteria are to achieve steady state conditions as measured by T_1 and T_2 at the given temperature before heating the resistance wire.

With shell moulds difficulties arise due to the fact that resin binders undergo pyrolysis above 500°C which results in collapse of the mould. Thus the achievement of steady state conditions at any temperature approaching the casting temperature of grey cast iron (i.e. 1350°C) is impossible without mould collapse, and the values obtainable for loose silica sand are of no significance to solidification rates.

Similarly, in the determination of values for the specific heat of moulds it is necessary to measure the amount of heat required to raise the temperature of unit mass of the material by 1°C, but the material needs to be under perfectly steady conditions at the temperature at which the value is to be measured. This is impossible for shell moulds at all temperatures of relevance as the constitution of the mould is continually changing.

As extensive problems exist in the measurement of thermal conductivity and specific heat, due to the destruction of shell moulds before steady state conditions can become established, some special form of testing equipment was required which would allow the value of the heat diffusivity to be determined under non-steady state conditions, which approach the actual conditions during casting production.

This equipment could be based on equation (6) i.e.

$$Q = 1.128\ b\ (\theta i - \theta o)\ \sqrt{t}$$

Measurement of the total heat flow through a specimen of mould material from a known heat input and the manner in which this varies with time enables a measure of the mean heat diffusivity to be calculated at any instance of time.

3.2 TESTING EQUIPMENT, SPECIMENS AND MATERIAL USED

A piece of test equipment devised and built for the testing of liners for the hot tops of ingot moulds was ideally suited to the requirements outlined above for determining heat diffusivity.

The Amitec unit was designed as shown in Fig. 3.3. The principle is that a silicon carbide plate 23 cm square is heated to a specified temperature by means of silicon carbide resistance heating elements. The plate is completely enclosed by refractory materials at the top face and along all edges. The temperature of the plate is controlled by a fibrous light quide which measures accurately the plate temperature and is used for controlling power input to the heating elements, thus correcting any variation in the plate temperature to an accuracy of $\pm 5^{o}C$. The temperature of the plate is checked by means of a thermo-couple at the centre. On initial heating up of the silicon carbide plate, heat losses occur from the edges of the plate to the surrounding refractory material and hence a non-steady state input of power i.e. heat occurs. After a period of time, the non-steady losses are so small that, at the centre of the plate, steady state conditions are obtained where the current input to maintain a constant plate temperature is proportional to the heat being transferred through the refractory in contact with the top surface of the plate, i.e. the heat diffusivity of the refractory. Any changes in the conditions of the refractory in contact with the silicon carbide plate, which cause either a reduction or increase in heat diffusivity, is

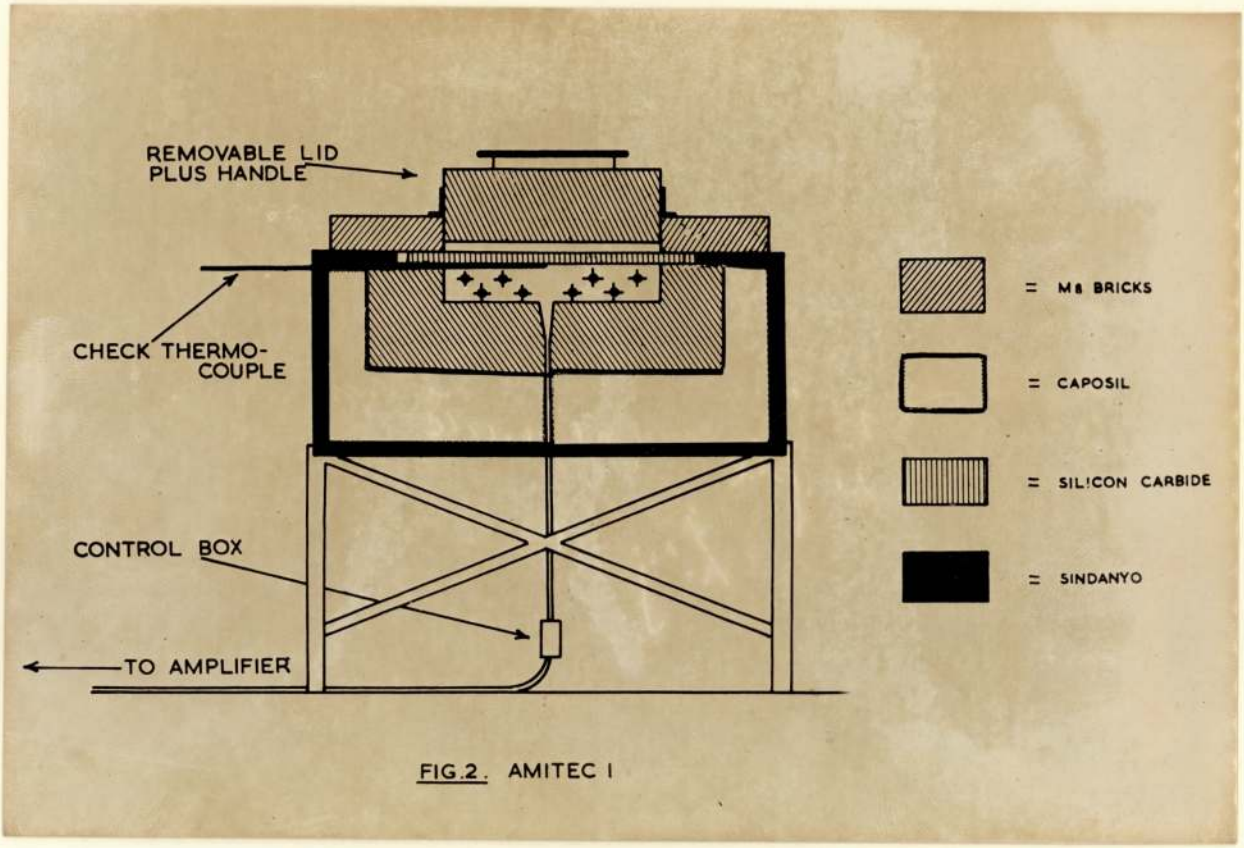

FIG.2. AMITEC I

Fig. 3.3 Diagrammatic layout of Amitec testing equipment.

immediately reflected in the power input to the heat source to maintain a constant plate temperature and, hence, in itself is a measure of the new heat diffusivity. In this manner, once the equipment has achieved steady state conditions at the centre of the plate, the refractory in contact with the top surface of the plate can be removed and a slab of mould material substituted for it. The exact conditions appertaining to a mould face coming into contact with liquid metal are simulated and the mould chilling power can be measured under conditions where the mould is undergoing variation in temperature gradient and where physical change, due to pyrolysis of the resin content, is taking place. Once steady state conditions are obtained, the power input to maintain the silicon carbide plate at temperature is a direct measure of the heat diffusivity of the material. With shell moulds this latter value is of little significance since solidification must take place before steady state conditions occur, since all bonding is lost upon completion of the pyrolysis process which in itself is a pre-requisite of steady state conditions for a shell mould. The equipment allows, therefore, two main factors to be determined -

i. The total quantity of heat extracted by a mould material in a given time, i.e. a measure of the mould constant, a loss factor correction being made which is determined for the equipment under steady state conditions.

ii. The rate of heat extraction expressed as $\frac{dQ}{dt}$ and its variation with time can be determined.

The Amitec unit used, illustrating the silicon carbide plate with light guide temperature recorder and the pulse count recorder, is shown in Fig. 3.4.

Fig. 3.4 (a) Amitec unit showing fibrous light guide temperature control

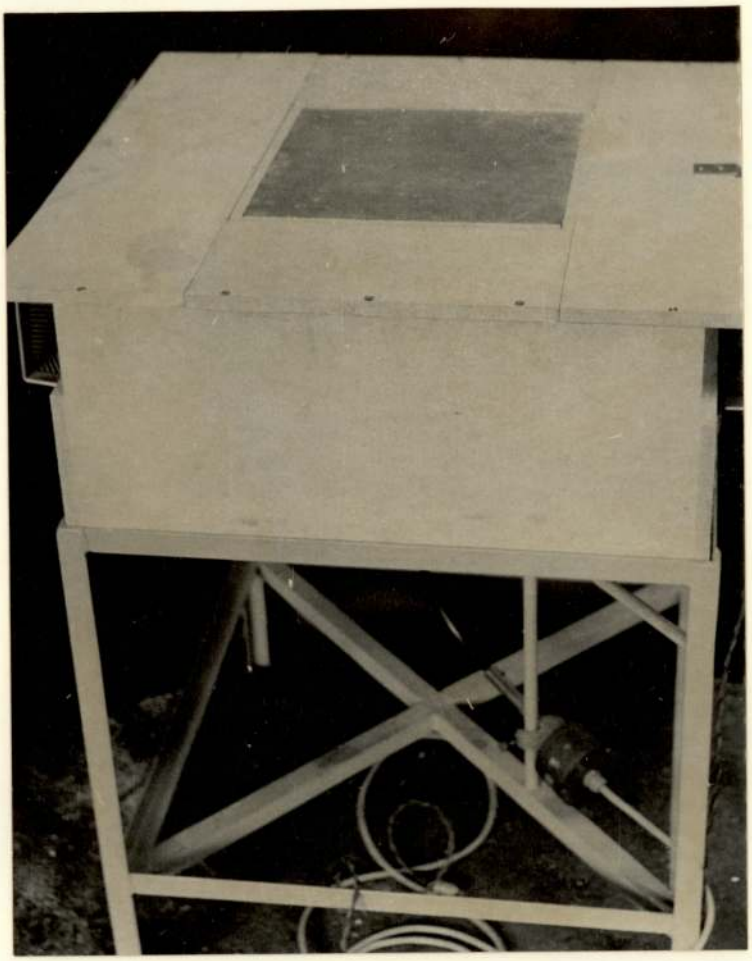

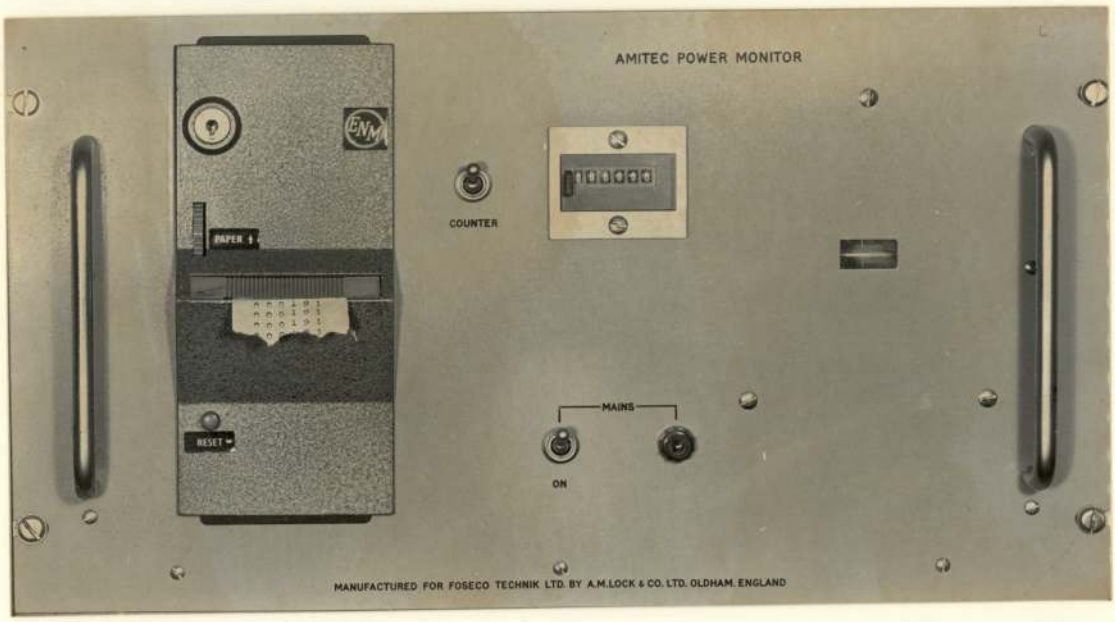

Fig. 3.4 (b) Power control unit of Amitec testing unit

The apparatus allows the plate temperature to be set at any selected value above 800°C up to 1500°C. The lower limit is necessitated by the use of a light cell temperature measurement technique only operational in the infra-red range; the upper limit is limited only by the physical properties of the heating elements. Hence, the plate temperature for the present study was set first at 1420°C and then a second test at 1350°C typical of cast iron pouring temperatures, by means of a thermostat controlled by the thermo-couple. When the plate is at temperature the light cell and power feed is used to control the plate temperature until a steady state has been reached. The power supply then required to maintain the temperature is then equal to the heat removed due to diffusivity through the material in contact with the top.

Correlation of power input to heat extraction

The amount of power fed into the heating elements can be measured in terms of kw/hrs, watt/secs or more conveniently as pulses. The latter is achieved by measuring the rotation of kw/hr disc using a series of holes and a photo-electric cell. This pulse count can then be printed out at intervals of time, e.g. 1 min. Hence:

Number of pulses x constant factor = watt/sec

Rate of supply of heat = $\frac{\text{Power}}{4.18}$ cal.sec^{-1}

Supply of heat in 1 min (cals) = $\frac{\text{Power} \times 60}{4.18}$ x No. of pulses recorded

Since the area of the plate is 520 cm^2 Rate of heat supply in cal/cm^2/ in one minute = $\frac{\text{number of pulses per min} \times Z}{2173}$

where Z is constant factor converting pulses into power units.

The system has a heat loss factor and power loss factor. These are constant and are determined experimentally so that allmeasurements made must have plate surface losses and background losses which are constant and known at a steady state condition. The mould slab is then placed on the plate at the temperature of testing, after first removing the refractory block. The physical change from the refractory block to the slab of mould material gives a period of some 5 seconds where the plate is exposed to air, heat losses occur which cannot be corrected. However, the rate of heat extraction during this period is constant for all tests carried out.

Specimens

The form of specimen used is constant in terms of surface area, with only the depth variable. This is shown if Fig. 3.5

Since the aim of the work was not concerned with the relative ability of different mould materials, i.e. clay bonded sand, compared with resin bonded sand, to extract heat but with the relative heat extraction ability of typical green sand moulds and shell moulds, thedimension d was varied extensively for the two types of mould. In normal green sand moulding practice minimum depth of mould above the surface of the casting being produced does not usually go below 5 cm. This depth would apply only to castings weighing up to 10 - 15 lbs and would be very much greater for heavier castings. Castings being compared in this work would vary in weight from a few ounces to 15 lbs and hence a mould wall thickness of 5 cm is quite typical of actual practice. The depth (d) of the clay bonded sand specimens was, therefore, set at a nominal value of 5 cm.

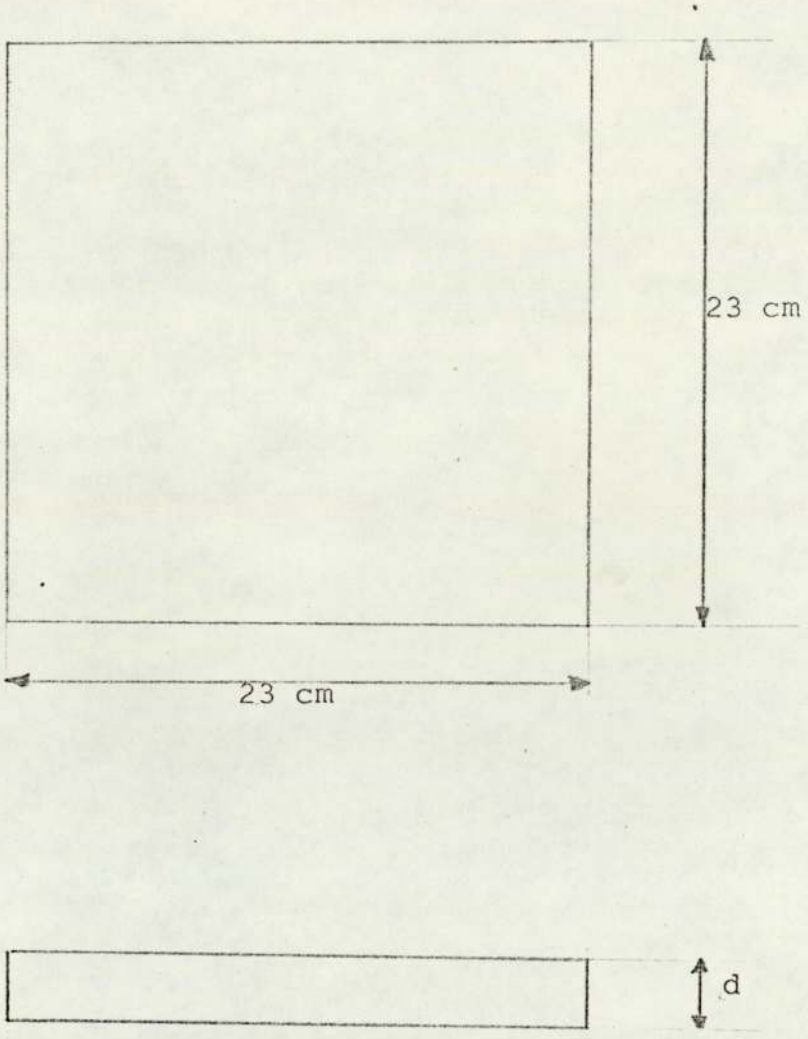

Fig. 3.5 Amitec test specimen

In normal shell moulding practice, the mould wall thickness is, by implication of the process, considerably less than 5 cm. Thickness values of 6 mm were quoted (3) in early work. In industrial practice, where the use of backing materials, e.g. steel shot, is not employed it is common for mould wall thickness values to vary in the range 0.8 - 1.8 cm. In view of variation in thickness which can be used specimen thickness (d) was nominally set at 9 mm, 12 mm, 18 mm and 24 mm.

Production of specimens

The shell mould specimens were produced by cutting them from moulds produced by the dump box technique described earlier. The pattern plate temperature used was 220°C and the mould thickness varied by varying the investment time.

It was found impracticable to use specimens of clay bonded sand in the green state due to break up on handling. The mould was produced, therefore, by hand ramming green moulding sand into an aluminium frame to a mould hardness value of 70, followed by drying at a temperature of 140°C for 2 hrs. Under these conditions the specimens produced had sufficient strength for the degree of handling that was required.

3.3 MATERIALS USED

In order to make comparisons, several variations of material were used. Material composition and sieve gradings are shown in Table 3.1 and Fig. 3.6

The actual dimensions of specimens used of the various materials and the plate temperature employed for each specimen are summarised in Table 3.2.

Table 3.1

The composition and physical properties of materials used for Amitec Testing (49)

Property	Shell Sand 3	Shell Sand 5	Clay bonded sand
Origin of Sand	Kings Lynn	Kings Lynn	Bromsgrove
BSS Grading 16	Nil	Nil	Nil
22	Nil	Nil	0.2
30	Nil	Nil	0.2
44	0.2	0.7	0.5
60	1.2	2.1	4.2
72	2.1	2.1	-
100	22.1	18.7	26.0
150	57.5	53.0	37.0
200	16.1	21.6	15.9
Pan	0.9	1.9	6.6
A.F.S. No.	99	102	-
Grain Shape	Sub-angular	Sub-angular	Sub-angular
Loss on ignition	4.16	4.99	4.1
Type of resin	Solid Novalak	Solid Novalak	-
Softening point	95°C	93°C	-
Clay content	-	-	8.5
Coal dust content	-	-	-
Moisture content	-	-	3.5
Tensile strength per 1% resin	20.2 lbs	22.4 lbs	-
Green strength	-	-	8.3
Dry strength	-	-	7.5

Fig. 3.6 Mechanical sieve analysis of sand used for Amitec testing

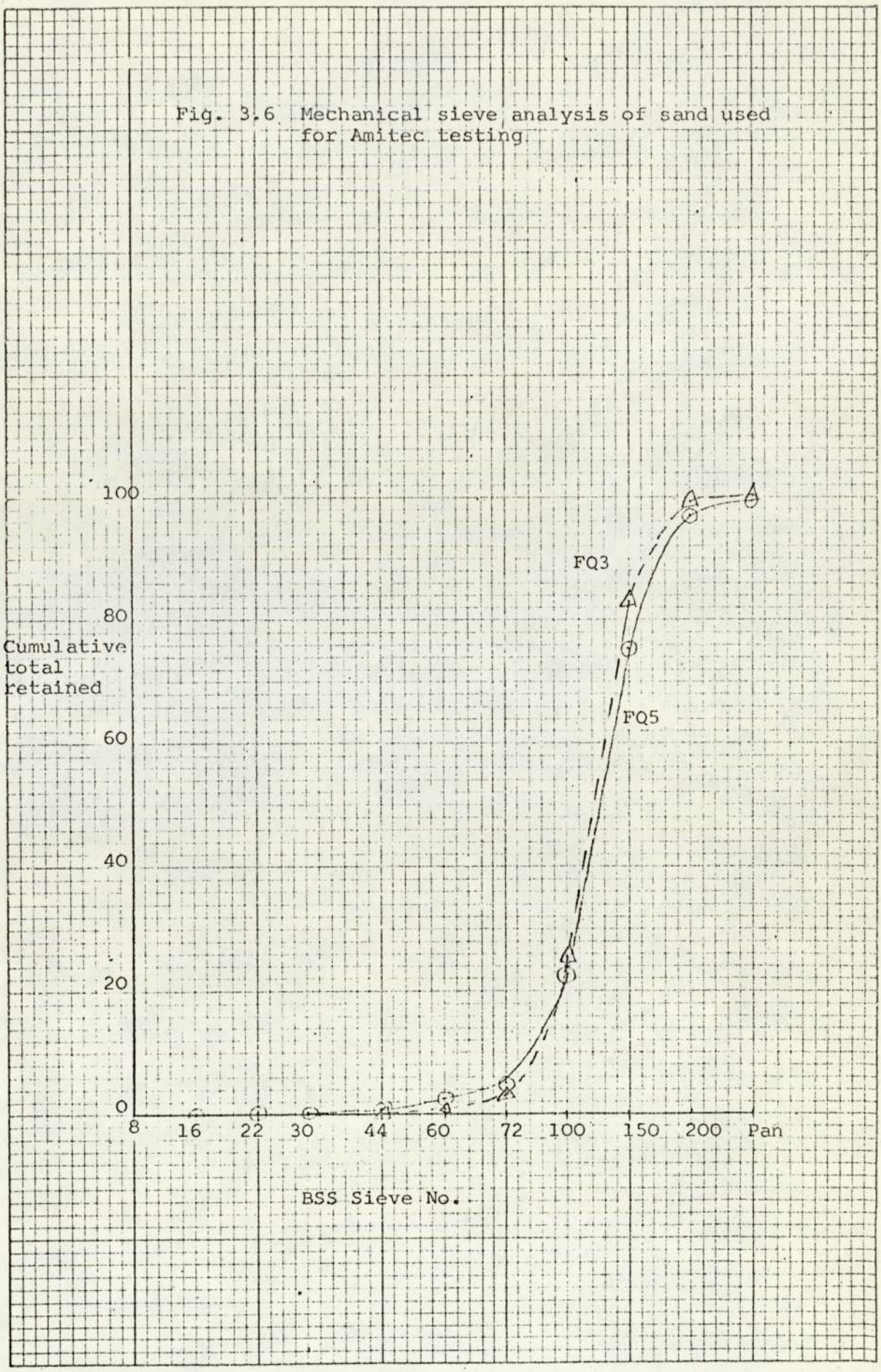

Table 3.2

Details of test specimens used

Specimen no.	Plate Temperature	Material	Depth d.	Density
1	1350°C	Clay bonded sand	49.2 mm	1.45
2	1350°C	FQ 3	15.9 mm	1.54
3	1420°C	FQ 3	8.0 mm	1.38
4	1420°C	FQ 5	8.0 mm	1.32
5	1420°C	FQ 5	9.5 mm	1.50
6	1420°C	FQ 5	11.1 mm	1.44
7	1420°C	FQ 5	17.5 mm	1.45
8	1420°C	FQ 5	24.6 mm	1.54
9	1420°C	Clay bonded	47.6 mm	1.54
10	1420°C	FQ 5	15.9 mm	1.51

3.4 RESULTS

(a) Comparison of heat extraction by shell mould and clay bonded sand mould

Specimens 1 and 2 were used with a plate temperature of 1350°C. The results obtained are shown in Figs. 3.7, 3.8 and 3.9. Fig. 3.7 shows a plot of the rate of heat extraction versus time and hence gives an indication of the chilling power of the mould material initially. Fig. 3.8 is a plot of the total heat loss through the mould versus time since $Q = \sqrt{t}$, the form is parabolic. Fig. 3.9 enables the value of ε to be determined as the slope of the plot of total heat loss versus $\sqrt{t}$. The values obtained are as follows:

Specimen 1. $\varepsilon = \frac{Q}{\sqrt{t}} = \frac{656}{2} = 328$ cal.cm^{-2}min$^{-\frac{1}{2}}$

Specimen 2. $\varepsilon = \frac{Q}{\sqrt{t}} = \frac{582}{2} = 291$ cal.cm^{-2}min$^{-\frac{1}{2}}$

(b) Influence of mould thickness on the heat extraction properties of shell moulds

In order to determine the influence of mould thickness onthe heat extraction properties, specimens 4, 5, 6 and 7 were used. The specimens were produced from the same batch material and were tested at 1420°C. The results are summarised in Fig. 3.10 which shows the maximum and minimum rate of heat extraction $\frac{dQ}{dt}$ and its variation with time.

The results showed that in each case the maximum value of $\frac{dQ}{dt}$ was attained after 1 minute, the values are shown in Table 3.3 for each specimen together with the value at steady state heat diffusivity and the time at which the latter was achieved.

Fig. 3.7 Rate of heat extraction versus time

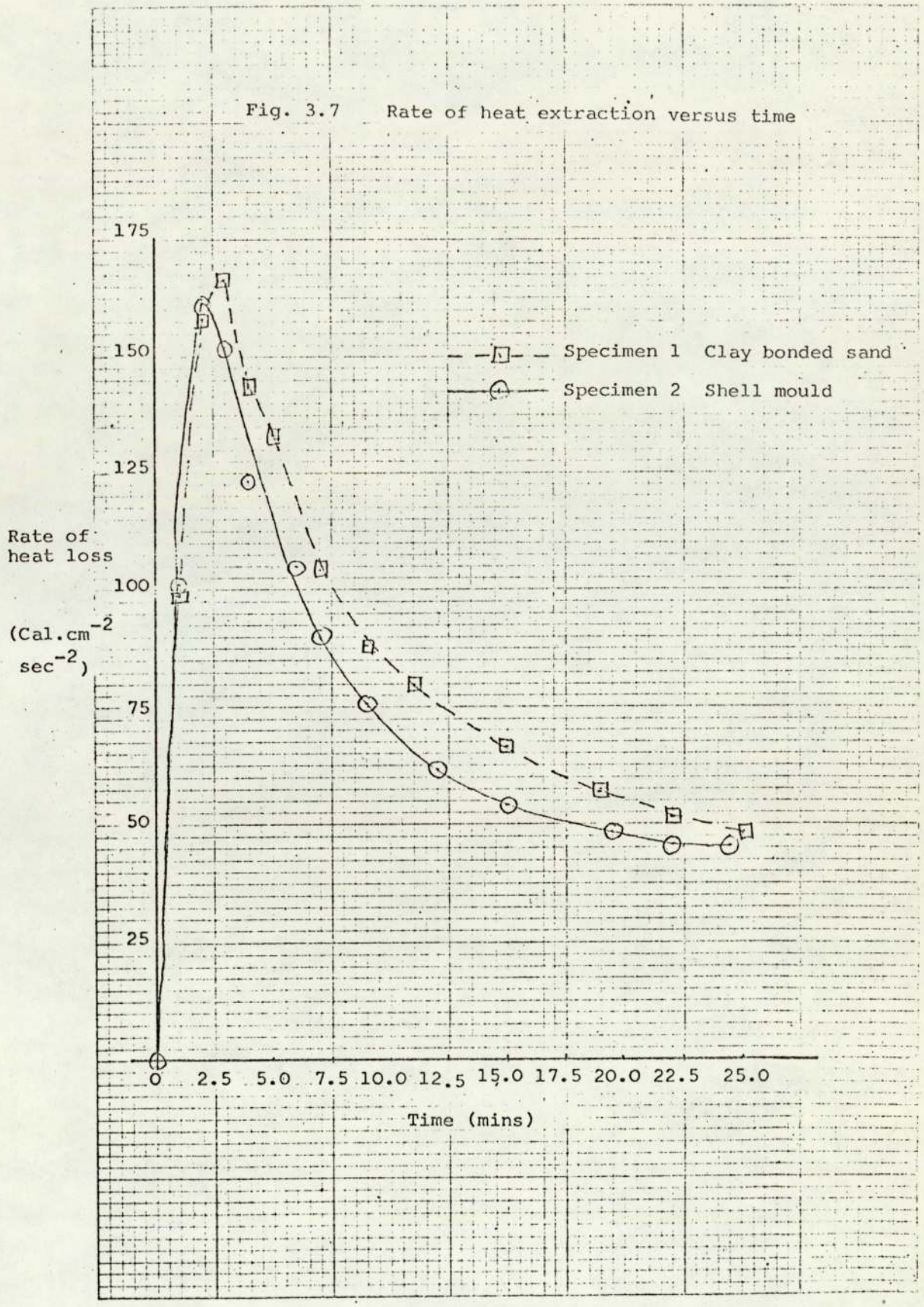

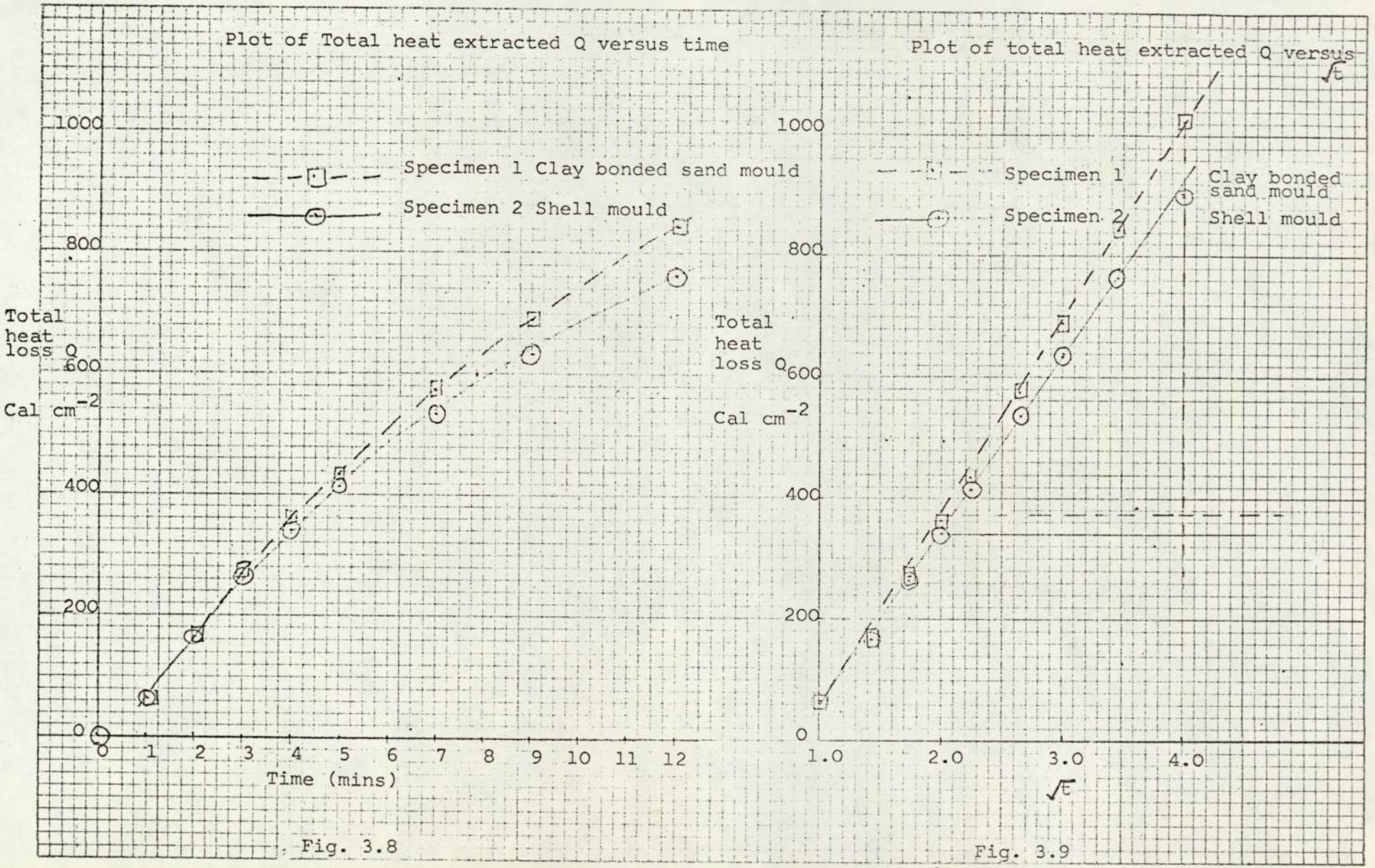
Plot of Total heat extracted Q versus time
Specimen 1 Clay bonded sand mould
Specimen 2 Shell mould
Total heat loss Q
Cal cm^{-2}
1000
800
600
400
200
0
0 1 2 3 4 5 6 7 8 9 10 11 12
Time (mins)
Plot of total heat extracted Q versus $\sqrt{t}$
Specimen 1
Clay bonded sand mould
Specimen 2
Shell mould
Total heat loss Q
Cal cm^{-2}
1000
800
600
400
200
0
1.0 2.0 3.0 4.0
$\sqrt{t}$

Fig. 3.8

Fig. 3.9

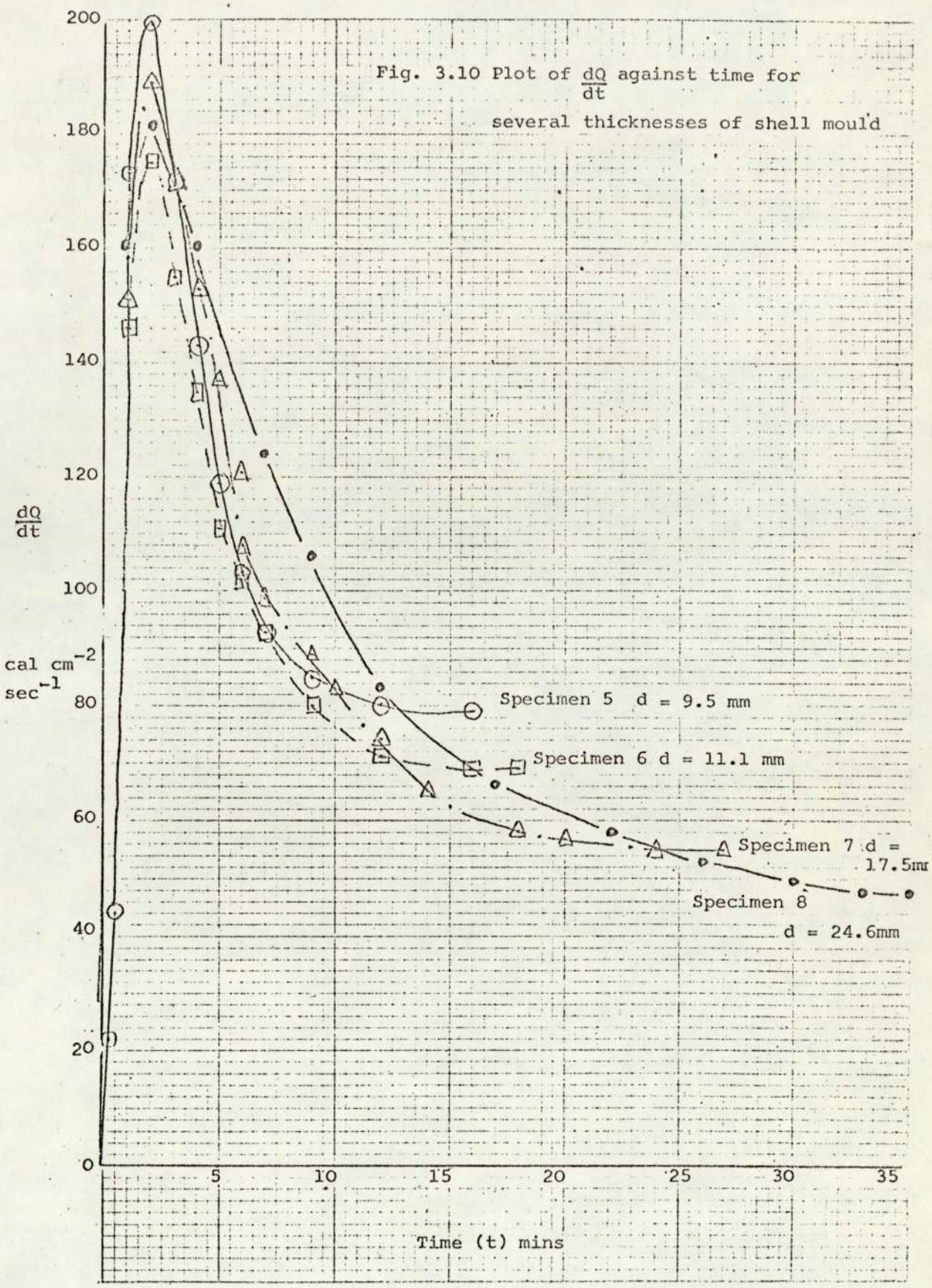
Fig. 3.10 Plot of dQ/dt against time for several thicknesses of shell mould
200
180
160
140
120
100
80
60
40
20
0
dQ/dt
cal cm⁻² sec⁻¹
5
10
15
20
25
30
35
Time (t) mins
Specimen 5 d = 9.5 mm
Specimen 6 d = 11.1 mm
Specimen 7 d = 17.5mm
Specimen 8
d = 24.6mm

Table 3.3

Maximum and steady state values of $\frac{dQ}{dt}$

Specimen No.	'D'	Maximum value $\frac{dQ}{dt}$ $cal.cm^{-2}sec^{-1}$	Steady state value $dQ/dt cal.cm^{-2}sec^{-1}$	Time for steady state - Mins.
5	9·5 mm	200	79	12
6	11.1mm	175	69	16
7	17.5mm	189	55	24
8	24.6mm	182	48	33

(c) Influence of resin content on the heat extraction properties of shell moulds

Specimens 3 and 4 were of the same thickness and were tested at 1420°C. The variable in these specimens was in the resin content, they were 4% and 5% respectively, as measured by the loss on ignition value. Fig. 3.11 summarises the results obtained for a plot the rate of heat loss against time.

(d) Influence of test plate temperature on heat extraction properties of moulds

The object of determining the influence of test temperature was to compare the mould properties, i e. mould constant, value that would be obtained and to simulate the influence of differing casting temperatures on the rate of heat extraction by the mould. The results are presented therefore, in Fig. 3.12 as a plot of Q (total heat extracted) against $\sqrt{t}$ for specimen numbers 7 and 10. These were produced from the same materials and were of approximately the same thickness, specimen 7 being tested at 1420°C and specimen 10 at 1350°C.

Specimens 1 and 9 show the influence of varying plate temperature on the rate of heat extraction of clay bonded sand moulds at 1420°C and 1350°C. The results are shown in Fig. 3.13.

The slope values for Fig. 3.12 are the value of the mould constant or chilling power and are as shown below for specimens 7 and 10.

Specimen No.	Test Temperature	Mould constant
7	1420°C	325
10	1350°C	280

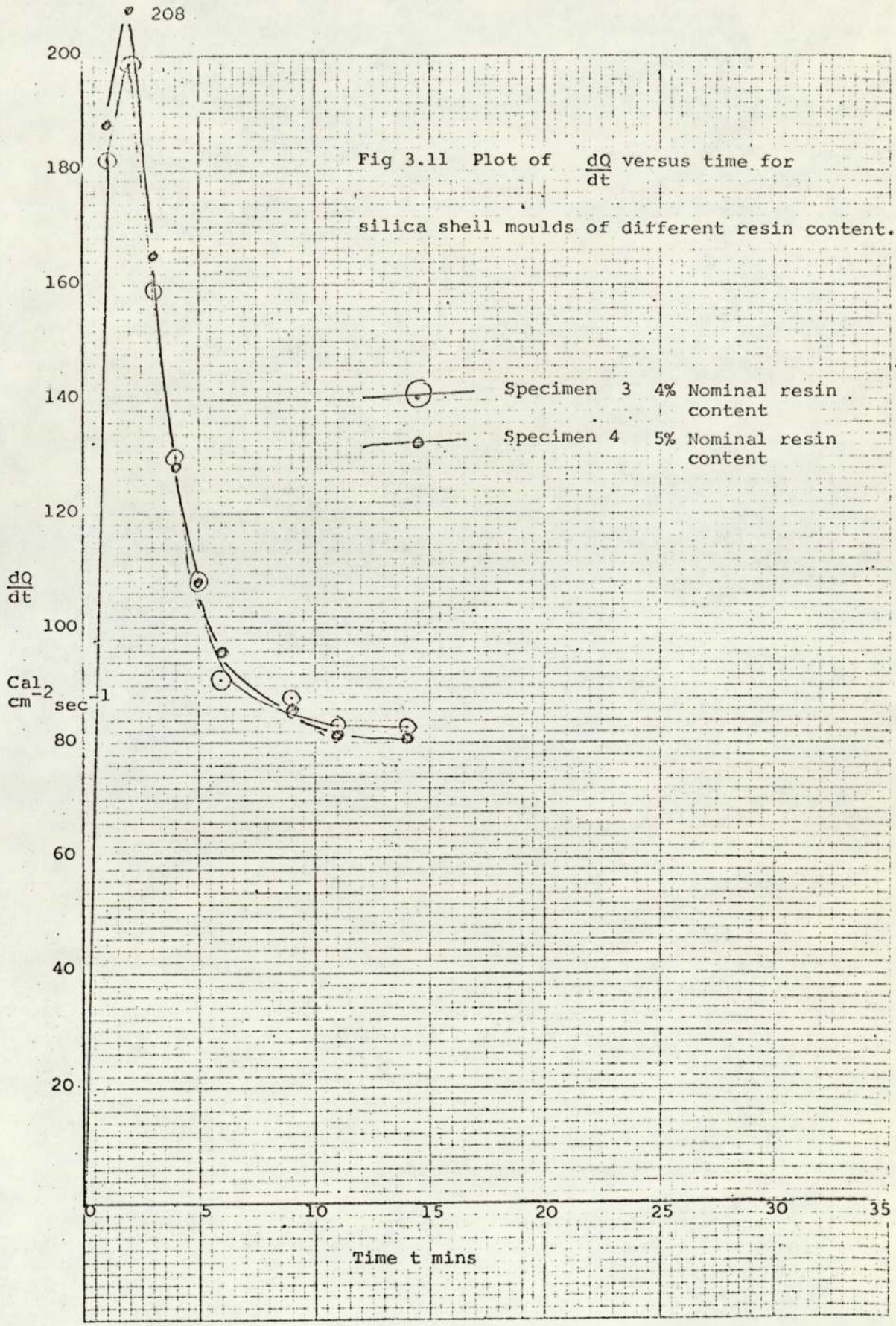

Fig 3.11 Plot of $\frac{dQ}{dt}$ versus time for silica shell moulds of different resin content.

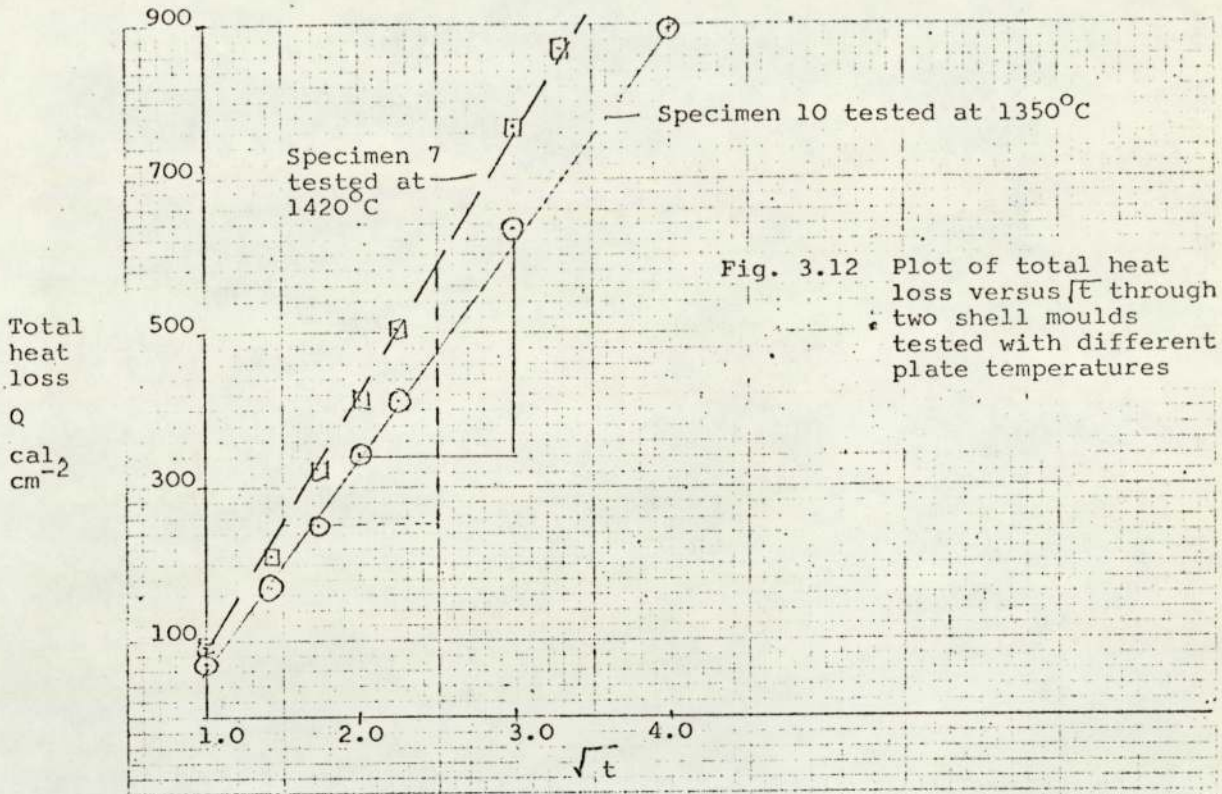

Fig. 3.12 Plot of total heat loss versus $\sqrt{t}$ through two shell moulds tested with different plate temperatures

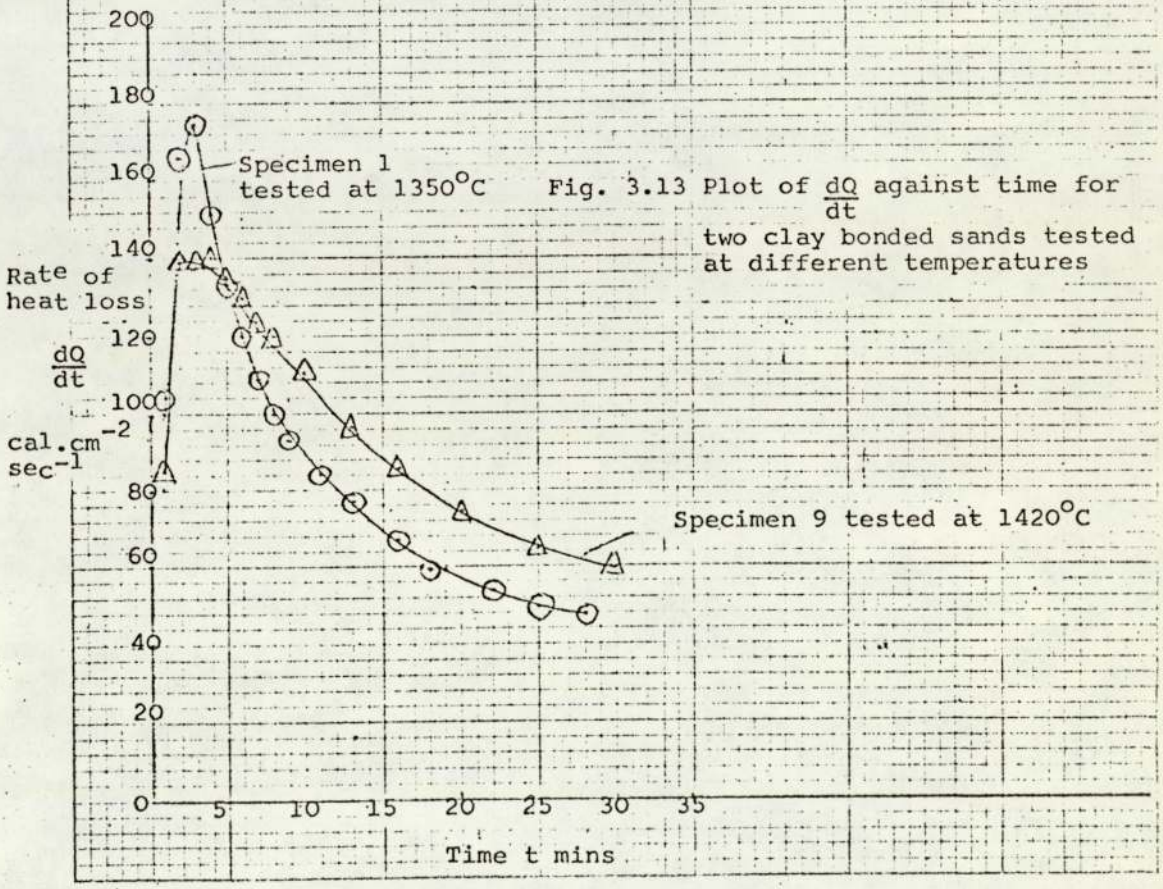

Fig. 3.13 Plot of $\frac{dQ}{dt}$ against time for two clay bonded sands tested at different temperatures

3.5 DISCUSSION OF RESULTS

The comparison of the rate of heat extraction for a normal shell mould 15.9 mm thick and a normal clay bonded sand mould 49.2 mm thick as shown in Fig. 3.7, illustrates that the rate of heat extraction $\frac{dQ}{dt}$ is similar for both types of mould for periods of time under 3 minutes. However, the rate of heat extraction was marginally higher for the shell mould in the first two minutes of testing, i.e. 102 $cal.cm^{-2}sec^{-1}$ and 161 $cal.cm^{-2}sec^{-1}$ compared with 99 $cal.cm^{-2}sec^{-1}$ and 158 $cal.cm^{-2}sec^{-1}$ for the clay bonded mould. After the initial period of 2 minutes the rate of heat extraction was always greater for the clay bonded mould. This is shown most clearly in Fig. 3.8 which illustrates that the total heat removed for the two moulds is very similar for the first two minutes, the clay bonded material increasing above the shell mould progressively for times longer than 2 minutes. The form of the curve in Fig. 3.8 is parabolic and hence obeys the basic heat loss equation.

$$Q \propto \sqrt{t}$$

A plot of Q against $\sqrt{t}$ (Fig. 3.9) verifies this, giving a straight line graph from which the values of the mould constant ξ are given. The values show that the clay bonded material has the higher value of mould constant 328 $cal.cm^{-2}min^{-\frac{1}{2}}$ compared with the value of 291 $cal.cm^{-2}min^{-\frac{1}{2}}$ for the shell mould. The values obtained compare very favourably with values obtained on clay bonded, dried moulding sand by Ruddle. A comparison of values obtained is shown in Table 3.4.

Table 3.4

Comparison of mould constant values

Source	Material	Density	Interface Temp °C	Mould Constant
Actual results	Bromsgrove Dry Moulding sand	1.45	1420	328
Ruddle & Mincher	Mansfield Dry Moulding sand	1.56	1083	228
Chvorinov	Steel Moulding sand	1.73	1500	370

From Figs. 3.8, 3.9 and Table 3.4 the method of determining the value of the mould constant using Amitec testing is substantiated.

Although the values obtained show a substantial difference in chilling power (a difference of 10%), between the two materials, these could be entirely due to the differences in mould thickness since ability to remove heat is influenced by the wall thickness where this cannot be regarded as semi-infinite. This would be so for the shell mould since it can be seen from Fig. 3.7 that the rate of heat extraction is constant after 22.5 minutes, implying that the mould is completely under steady state conditions and heat is being lost only from the top surface of the mould to the atmosphere. This is not the case with the clay bonded mould, as $\frac{dQ}{dt}$ does not reach a constant value.

While the clay bonded sand illustrates a higher chilling power, it is interesting to note that $\frac{dQ}{dt}$ and the value of Q for times less than 2 minutes are very similar for both types of mould, hence it is doubtful whether there could be any significant difference in either the solidification rate or solidification time for castings which solidify in times of less than two minutes. This could be expected for castings of the types illustrated in Fig. 1.1.

The influence of mould thickness upon heat absorption and upon the rate of solidification is of particular importance for shell moulds, since they automatically show greater percentage variances from mould to mould than any

clay bonded sand mould, if only due to the fact that the initial mould thickness is so much less. The influence of shell mould thickness on the rate of heat absorption with time is shown in Fig. 3.10. It can be seen that the initial rate of heat absorption was inconsistent within the range 173 - 200 cal. $cm^{-2}sec^{-1}$ after 2 minutes. However, after this period a pattern emerged which shows that the thicker the mould the quicker the value of $\frac{dQ}{dt}$ falls to a constant value. The constant value is taken to represent a condition of heat saturation of the mould. As seen in Table 3.3 the time for this condition to occur increases very substantially as the mould thickness increases. The time to reach a state where heat saturation occurs is almost linear as is shown in Fig. 3.14.

The total heat loss from the plate to the mould increases as the mould thickness increases, as shown in Table. 3.5, for times greater than 3 minutes.

This finding is similar to those by Bishop, Brandt and Pellini (46) where it was shown that an increase of 4 times in the mould thickness increased the heat absorbed by 20% for a 7" square ingot. The present results show that an increase in mould thickness of 123% increased the heat absorbed by 16.5% after 7 minutes and by 19% after 16 minutes.

The rate of heat extraction, the total heat absorbed and the mould constant are all increased as the mould thickness increases. However, $\frac{dQ}{dt}$ or the value of Q had a general trend in reverse of this for times less than 3 minutes. Fig. 3.10 shows that specimen 6 did not follow the trend in this respect.

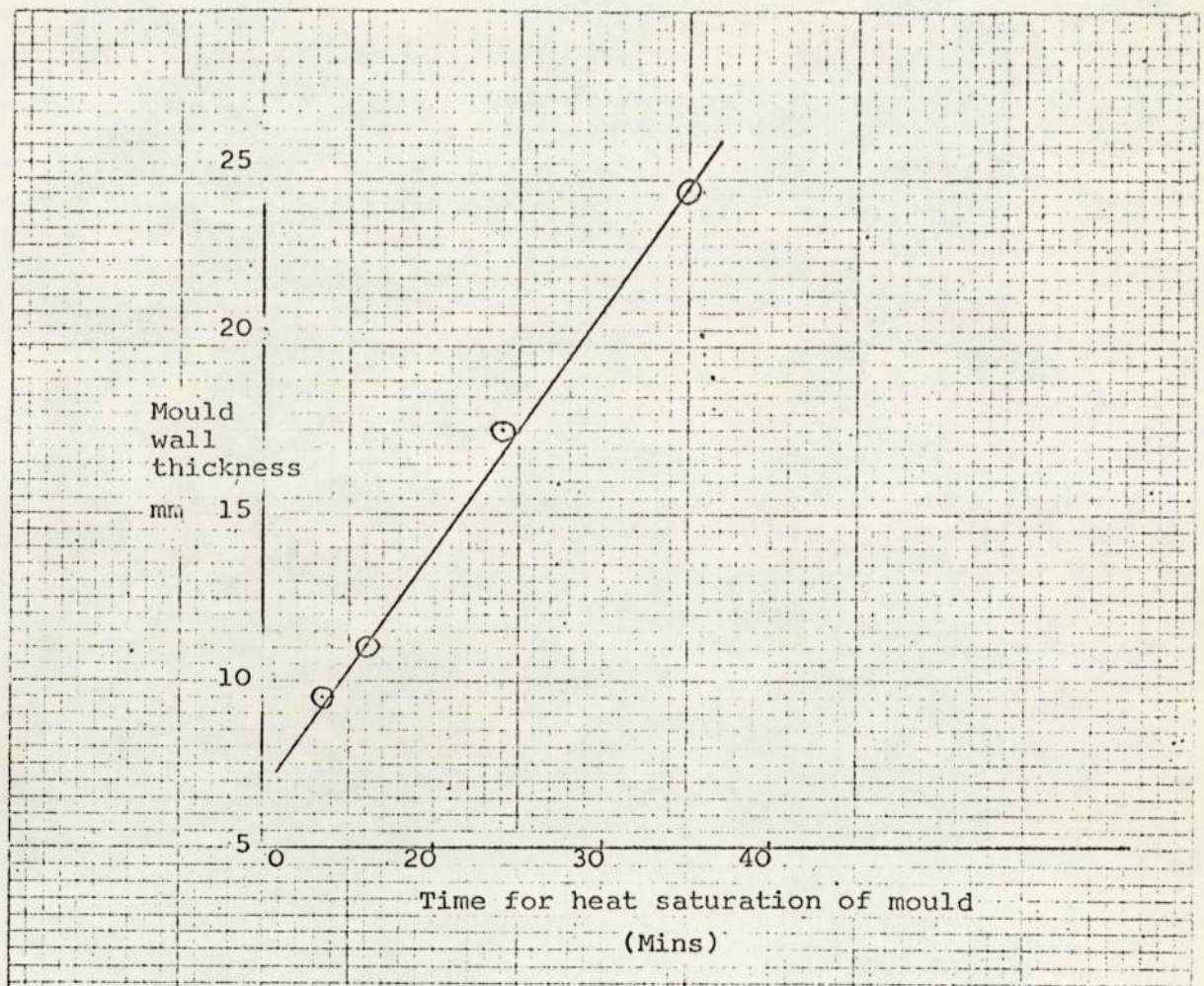

Fig. 3.14 Variation of time for heat saturation of mould with wall thickness

Table 3.5

Influence of shell mould thickness on heat absorption

Specimen No.	Mould Thickness	Net heat absorbed after 7 mins. cal. cm^{-2}	Net heat absorbed after 16 mins cal. cm^{-2}
6	11.1 mm	584	1000
7	17.5 mm	652	1082
8	24.6 mm	680	1190

These results agree with the results obtained on specimen 1 and 2, where the thinner shell mould showed a marginally higher value for $\frac{dQ}{dt}$ for 2 minutes, but had a lower overall heat absorption and mould constant than the clay bonded sand. The relationship between specimens 1 and 2 was exactly the same as for specimens 5 and 8, where the variable was the thickness of the mould. The results shown in Fig. 3.11 illustrate that variation in resin content within the range used for industrial shell mould production does not influence the heat, absorbtion characteristics of the mould after the initial period of interface heating has been exceeded. The values of $\frac{dQ}{dt}$ at times of 3 minutes and less show that the higher resin content gave higher rates of heat removal. An increase of 0.83% resin gave an increase of 5% in the values of $\frac{dQ}{dt}$ for times less than 3 minutes. This small difference could be attributed to the reduction in void space which might be expected due to the higher resin content, and the subsequent increase in mould density which was recorded, i.e. lower resin content mould density 1.32 gm. cm^{-3}, higher resin content 1.38 $gm.cm^{-3}$.

The results (Table 3.6) show that the mould constant or chilling power is influenced by the test plate temperature and hence casting temperature. This is to be expected since both specific heat and thermal conductivity are temperature dependent. Actual heat diffusivity values calculated from equation 6 are shown for temperatures of 1350°C and 1420°C.

Table 3.6

Calculated heat diffusivity values

Specimen No.	Test Temperature	Heat Diffusivity * $b = \sqrt{kcf}$ c.g.s. units
7	1420°C	0.0208
10	1350°C	0.0188

* For room temperature 30°C

These values compare with values for dry synthetic sand quoted by Ruddle of 0.026. However, lower values could be expected for shell moulds since the fine grain size materials used would be expected to result in lower values of thermal conductivity. Clay bonded samples tested at 1350°C and 1420°C showed a similar pattern (Fig. 3.13), the total quantity of heat being extracted being greater at 1420°C than at 1350°C and the mould constant also increased. An unusual feature in these tests, however, is that the maximum value of $\frac{dQ}{dt}$ was substantially lower for the higher test temperature of 1420°C than at 1350°C. This is the opposite of what would be expected, and contrasts with the results obtained for shell moulds, but no logical explanation for this anomaly can be advanced.

3.6 CONCLUSIONS

The following conclusions were deduced from the results of this part of the investigation:-

(a) The testing technique gave values for the mould constant and heat diffusivity for shell moulds and clay bonded moulds, which compare reasonably with previously published values for similar moulding materials. The values obtained are mean values for heat absorption over a relatively long period of time (25 mins.) and cannot be usefully determined for periods of time less than 8 minutes.

(b) Heat diffusivity and mould constant increase as the temperature of testing increases.

(c) Chilling power and total heat absorbed are increased by

increasing mould wall thicknesses. The rate of heat extraction is higher for thin moulds for times of up to 3 minutes but this is reversed for larger times.

(d) Clay bonded sand shows an increased chilling power over shell moulds, thought to be due to the difference in thickness. However, the rate of heat transfer by shell moulds is slightly greater than clay bonded moulds up to 3 minutes. For periods greater than 3 minutes heat transfer becomes greater for clay bonded moulds.

(e) Resin content within a limited range of 4 - 5% does not influence the chilling power of silica shell mouds.

CHAPTER 4

MEASUREMENT OF COOLING TIMES AND EXAMINATION OF MICRO-STRUCTURES FOR SHELL MOULDED AND CLAY BONDED, SAND CAST, GREY IRON CASTINGS

The results shown in Chapter 3 indicated that it was necessary to determine if ~~the~~ a difference in cooling time existed for castings which solidified in less than 3 minutes from the time of pouring, using shell moulded and clay bonded moulds. The previous results suggested that solidification times within this range were likely to be very similar, with a slight possibility of solidification times for the shell moulded castings being shorter. The measurement of cooling curves and comparison with the micro-structure of the specimens would enable any differences to be correlated.

4.1 EXPERIMENTAL TECHNIQUES

4.1.1 Determination of cooling times

Specimens In order to achieve solidification times of 3 minutes or less, the section thickness of the specimen used had to be small. However, it was necessary, in order to achieve a semi-infinite cooling condition, to have a casting with a large surface area in one plane, thus avoiding the influence of corners on the solidification time. The form of the pattern used, therefore, was a

square plate of the same dimensions as the Amitec specimen shown in Fig. 3.5 previously. In this manner, the cooling curves would correlate more accurately with the results obtained in Chapter 3. The thicknesses of the specimens used was 0.5 cm, 1.5 cm and 2.5 cm. These values were chosen in order to cover a wide range of solidification times, the 0.5 cm specimen being designed to give solidification times comparable with many of the castings illustrated earlier.

4.1.2 Production of Moulds

Pattern equipment was produced which was interchangeable between a dump box shell moulding machine and a jolt squeeze moulding machine. The shell moulds were produced at a temperature of 220°C for various investment times, depending upon the thickness of shell mould being produced and the material being invested. The clay bonded moulds were produced in steel boxes, 5 cm in depth, the moulds being jolted to produce a mould hardness of 70. The pattern equipment for both methods of production and the jolt squeeze moulding machine are shown in Fig. 4.1.

The running and gating system was integral with the top half of the pattern which was 0.5 cm thick. The bottom half of the pattern equipment was variable, depending upon the thickness of the specimen required. For a 0.5 cm specimen the bottom pattern plate was blank, while for a 2.5 cm specimen the bottom pattern plate had a pattern 2.0 cm thick mounted on it.

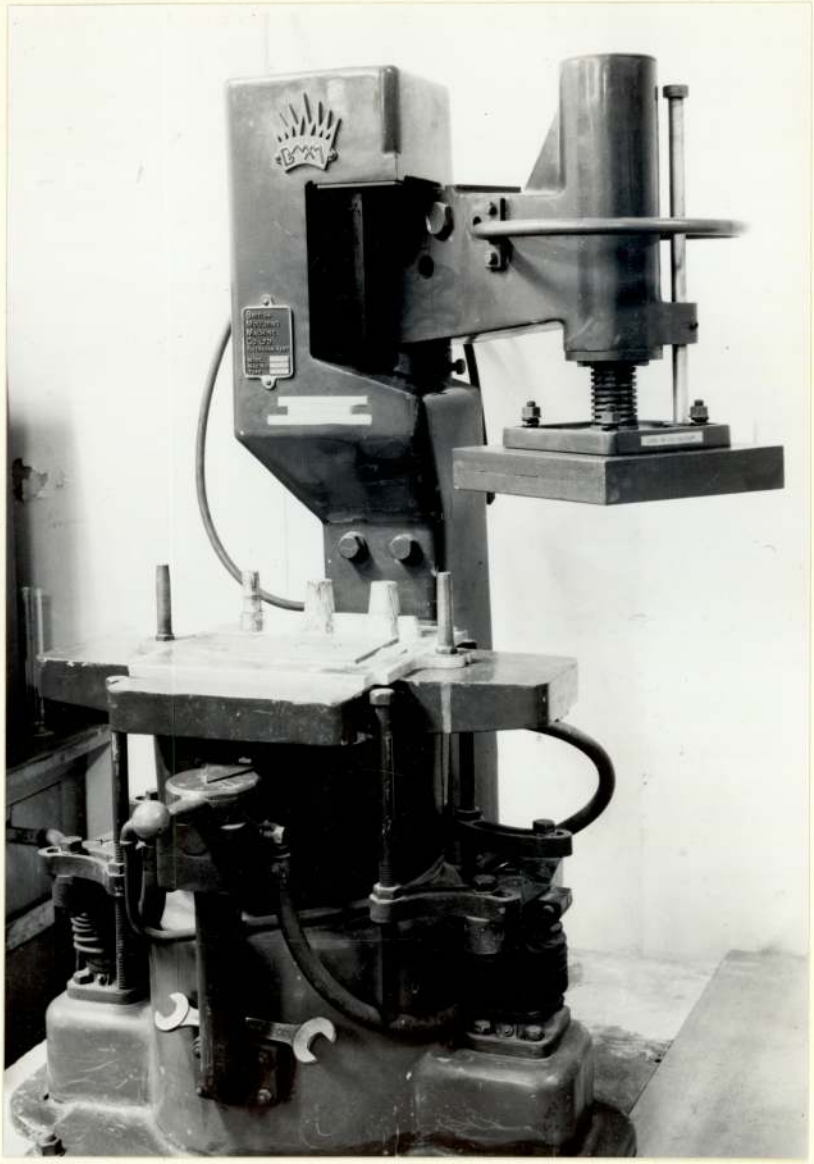

Fig. 4.1 Illustration of jolt squeeze moulding machine with test plate pattern in position.

4.1.3 Temperature Measurement

The metal temperatures were measured using platinum platinum-rhodium thermocouples and an ultra violet light recorder. The thermocouple wires were 0.25 mm in diameter, the hot junction being produced by butt welding. These were then enclosed in silica sheaths which were 0.75 mm in diameter. The U.V. recorder was used in order to achieve the best possible response time which, consequently, depended upon the thermocouples and not the recorder. Positioning of the thermocouples within the moulds was at distances of 1 mm and 3 mm from the top surface of the mould, and was in the horizontal plane in order to minimise the influence of temperature gradients on the hot junction. The arrangement of the mould cavity with the thermocouples in position for a 0.5 mm shell mould specimen is shown in Fig. 4.2.

The accurate positioning of the thermo couples was achieved by using two step prints at a depth of 1 mm and 3 mm from the top surface at the sides of the specimen on which the ends of the silica sheath could rest. Two small pads protruding from the top surface of the mould 1 mm and 3 mm deep respectively were found necessary in order to prevent bowing of the silica tube and thermocouple away from the ends of the plate due to the buoyancy of the liquid metal. The arrangement is shown diagrammatically in Fig. 4.3.

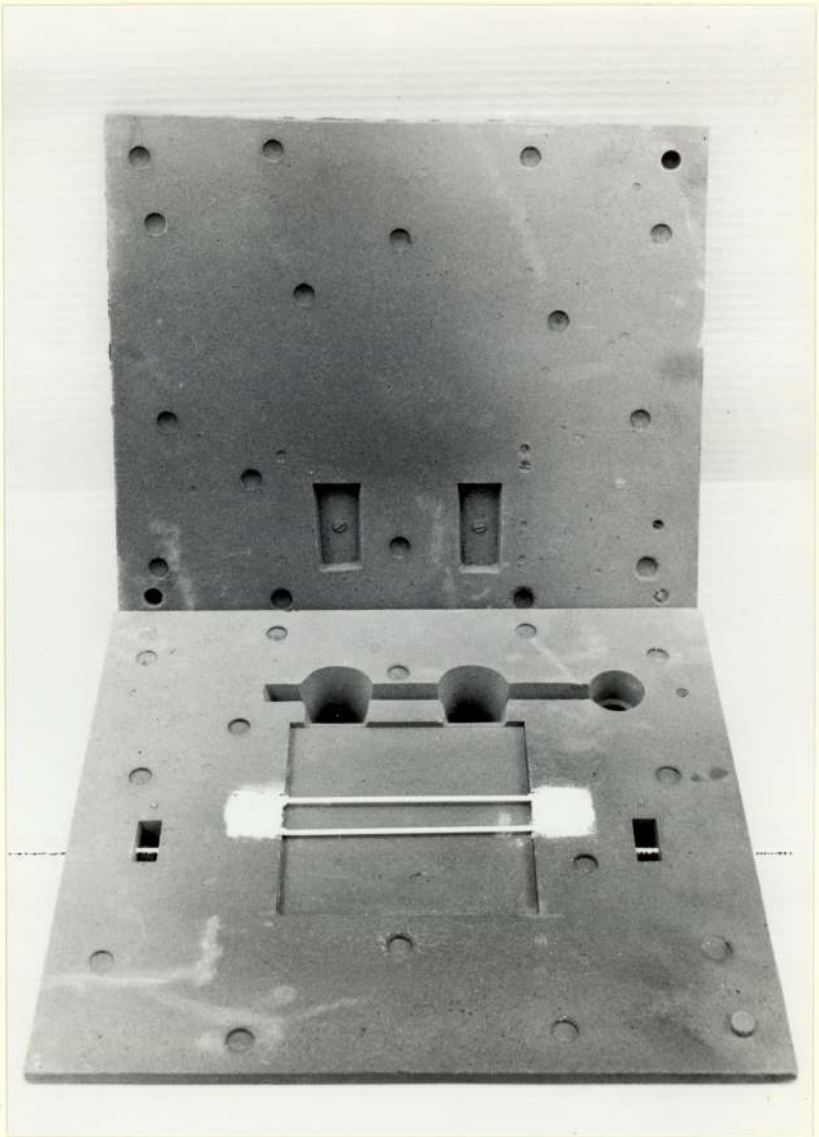

Fig. 4.2 Shell mould for 0.5 cm plate casting, showing thermo couple positioning in the mould cavity and mould wall.

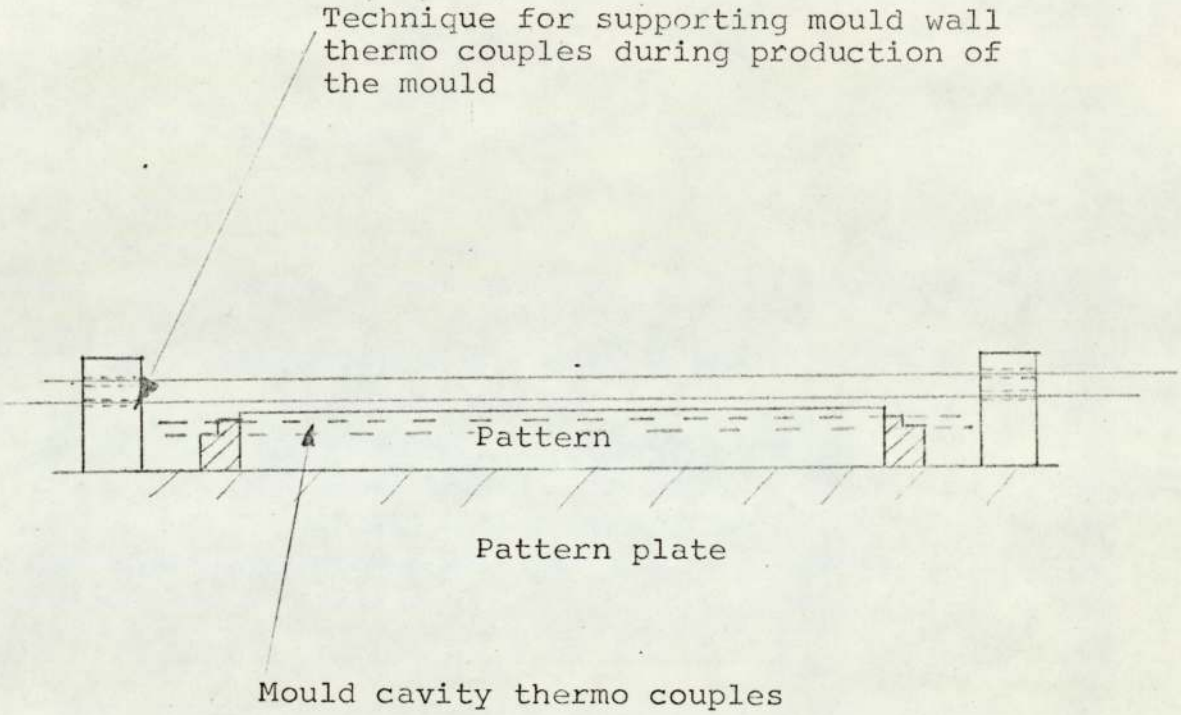

Fig. 4.3 Positioning of thermo couples in shell moulds

Thermocouples used for measuring the rate of heat up of the mould wall at distances of 1 mm, 2 mm and 5 mm from the interface were chromel-alumel. The positioning of these thermocouples was achieved by incorporating a wire into the shell moulding pattern equipment while producing the mould, the wire being held in two pads at the appropriate distances above the mould surface. This is shown in Fig. 4.3.

The specimen plates produced are shown in Fig. 4.4 for a shell mould and clay bonded mould.

The metal was melted in a coreless induction furnace of 7 kilograms capacity, and the casting temperature measured in the ladle prior to pouring. A general layout of a mould for casting and the recording technique is shown in Fig. 4.5.

4.1.4 Materials used

The cast iron used in the experiments had a nominal composition given in Table 4.1.

This represents a carbon equivalent value of 4.20 - 4.3, i.e. eutectic composition, and is typical of that produced to meet B.S.1452 Grade 12 for grey cast iron.

Mould materials were silica, zircon and olivine shell moulds and clay bonded moulding sand. The properties of the moulding materials used are listed in Table 4.2 and actual details for each experiment in Table 4.3.

4.2. OTHER EXPERIMENTAL TECHNIQUES

(a) Macro and micro-examination

Macro-examination entailed polishing and etching the

Fig. 4.4 Sand cast plate specimen (left) and shell cast plate specimen

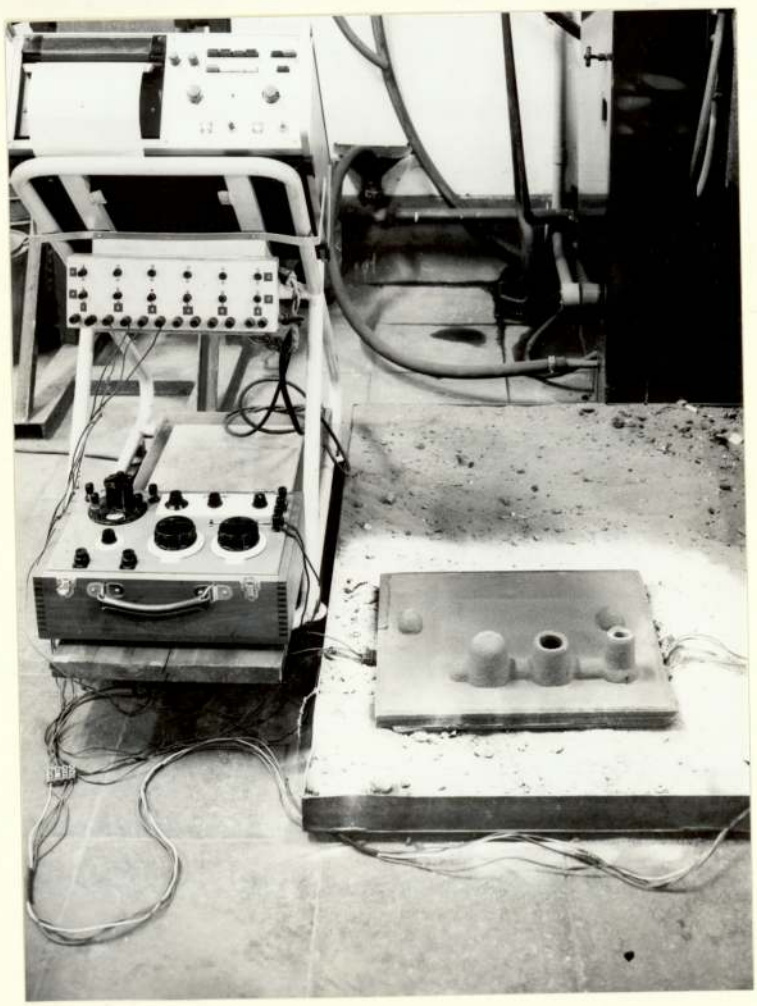

Fig. 4.5 Illustration of the general layout for casting and recording solidification time for a shell mould

Table 4.1

Nominal composition of hypo-eutectic grey cast iron used in experiments

Element	Composition Range
Carbon	3.30 - 3.45%
Silican	2.40 - 2.70%
Manganese	0.40 - 0.60%
Sulphur	0.10 - 0.15%
Phosphorus	0.40 - 0.60%
Chromium	0.15% Max.

Table 4.2

Properties of Moulding Materials Used

Shell Sands

Property	Silica FQ 5	Zircon	Olivine	Clay bonded Sand
Grain shape	Rounded Sub-angular	Rounded Sub-angular	Angular	-
Loss on ignition	4.99	2.20	3.81	4.5
Type of resin	Solid Novalak	Liquid Novalak	Resule Novalak	
Clay content	-	-	-	9.2
Coaldust content	-	-	-	-
Moisture content	-	-	-	-
Tensile strength	22.4	59.2	22.2	-
Per % resin				
Green strength	-	-	-	7.6
Dry strength	-	-	-	-
BSS Grading 16	NIL	NIL	NIL	NIL
22	NIL	NIL	0.3	0.42
30	NIL	NIL	0.6	0.2
44	0.7	0.3	0.9	0.5
60	2.1	0.6	10.4	3.5
72	2.1	0.2	15.7	-
100	18.7	6.2	38.7	24.5
150	53.0	53.7	22.7	37.6
200	21.6	37.5	7.9	16.4
Pan.	1.9	1.5	2.9	9.3

Table 4.3

Details of various moulds used in solidification experiments

Experiment No.	Mould Material	Casting Thickness	Mould Thickness	Density
1	Silica shell sand	0.5 cm	1.2 cm	1.46
2	Silica shell sand	1.5 cm	1.2 cm	1.41
3	Silica shell sand	2.5 cm	1.2 cm	1.45
4	Clay bonded sand	0.5 cm	5.0 cm nominal	1.51
5	Clay bonded sand	1.5 cm	5.0 cm nominal	1.46
6	Olivine shell sand	0.5 cm	1.2 cm	1.68
7	Zircon shell sand	0.5 cm	1.1 cm	2.55
8	Zircon shell sand	1.5 cm	1.1 cm	2.57

specimens in order to develop the cell structure. Etching was carried out in Steads reagent and structures normally examined at 15 x magnification. Micro-structures were taken from the edge and centre of a centre line section of the plate casting. Samples were etched with a solution of 2% nital.

(b) Chill testing technique

The comparative chilling abilities of a shell mould (silica sand 5% nominal resin content) and of a clay bonded green sand were examined using the wedge test technique. The dimensions of the standard wedge used are shown in Fig. 4.6. Both samples were cast together hence ensuring complete uniformity of material and casting temperature. The moulds used and the fractured test pieces are shown in Fig. 4.7.

(c) Influence of cooling rate on solid state transformation in cast iron containing 'D' type graphite structures

A thin section piece of grey iron containing a micro-structure where the graphite was predominantly 'D' type was cut, and subjected to different rates of cooling. The specimen is shown in Fig. 4.8.

The specimen was heated to 920^{o}C for 15 minutes and quenched in oil to a depth of 2" from the base. Thus half of the specimen was effectively air quended and half oil quenched. The specimen was sectioned longitudinally and

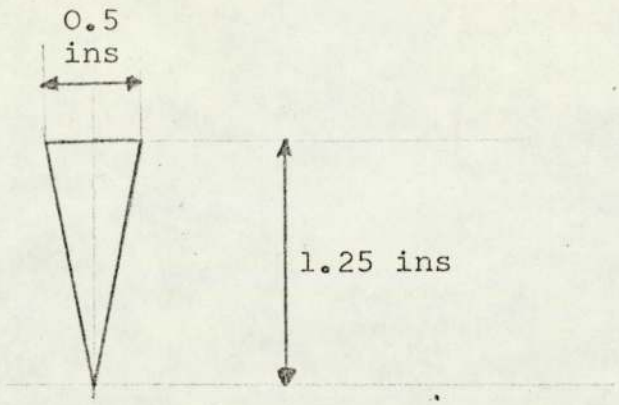

Fig. 4.6 Dimensions of wedge test piece

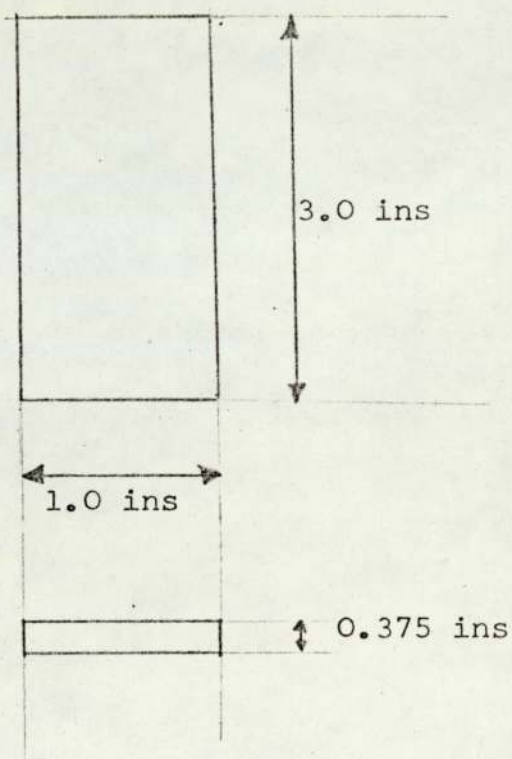

Fig. 4.8 Dimensionof oil quenched specimen

Fig. 4.7 Silica shell and green sand moulds used for wedge testing and the fractured test pieces produced

the variation in microstructure examined to determine the influence of varying cooling rate on the matrix structure, to determine whether any critical rate of cooling existed that could produce a completely ferritic matrix.

4.3 RESULTS

4.3.1 Comparison of solidification time and microstructures of 0.5 cm thick plate casting

Specimen numbers 1, 4, 6 and 7 were cast from a ladle temperature of 1475°C. The composition of the plates was as shown in Table 4.4.

The cooling curves obtained are shown in Fig. 4.9. The total time for solidification from the start of pouring at 1 mm from the surface was:-

Specimen No.	Type of Mould	Total solidification Time (secs)
1	Silica shell mould	60
4	Clay bonded mould	56
6	Olivine shell mould	56
7	Zircon shell mould	58

The microstructures of the silica shell and clay bonded mould specimens taken at the surface of the plates are illustrated in Fig. 4.10 and Fig. 4.11 respectively. The clay bonded specimen illustrated a microstructure up to the surface of 'A' type graphite in a matrix of pearlite. The silica shell moulded specimen, while exhibiting a similar structure to the clay bonded specimen at the centre of the

Table 4.4

Analysis of Specimens 1, 4, 6 and 7

Specimen No.	C	Si	Mn	S	P
1	3.32	2.40	0.54	0.132	0.54
4	3.31	2.45	0.52	0.130	0.54
6	3.34	2.42	0.52	0.125	0.54
7	3.32	2.45	0.51	0.130	0.52

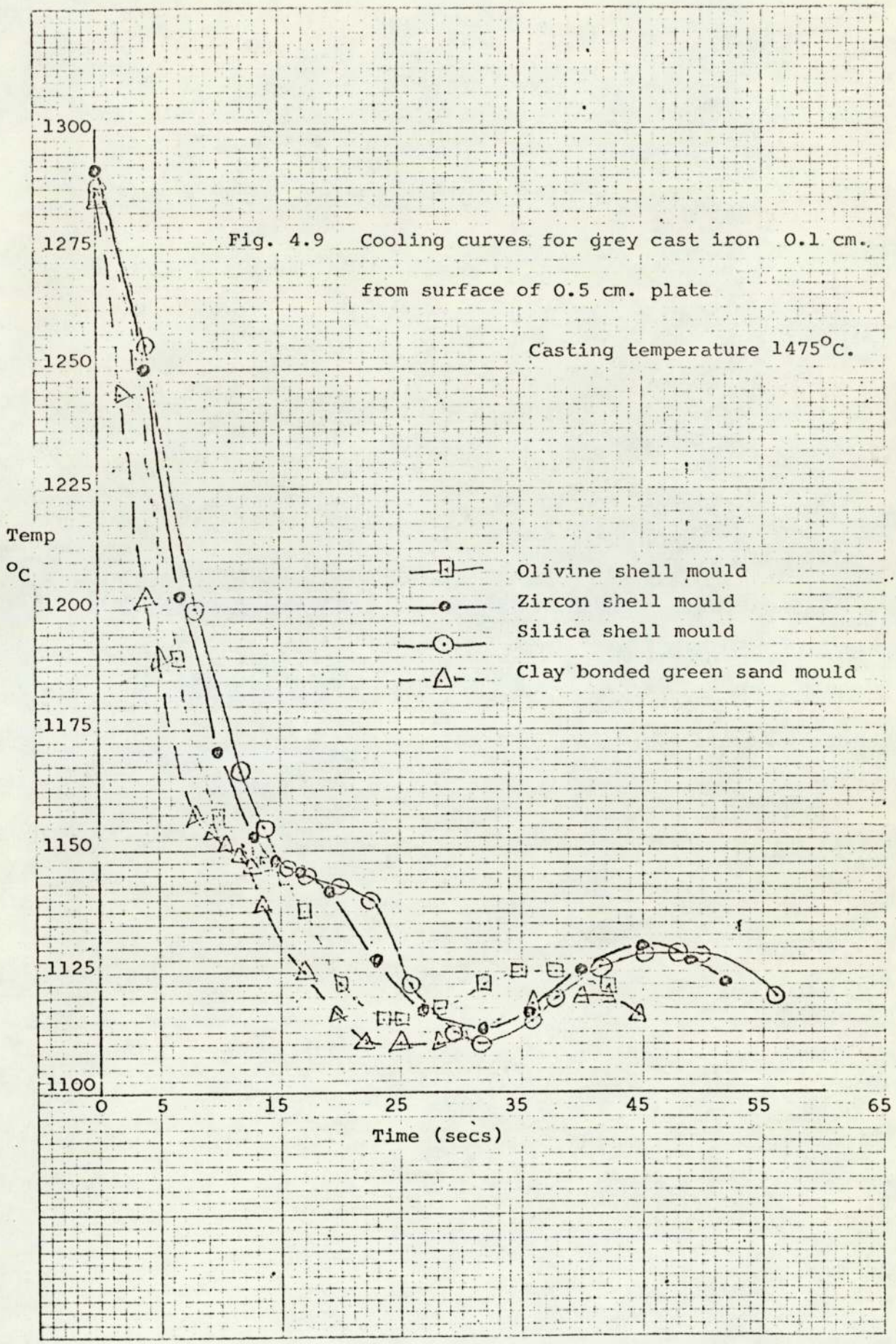

Fig. 4.9 Cooling curves for grey cast iron 0.1 cm. from surface of 0.5 cm. plate

Casting temperature 1475°C.

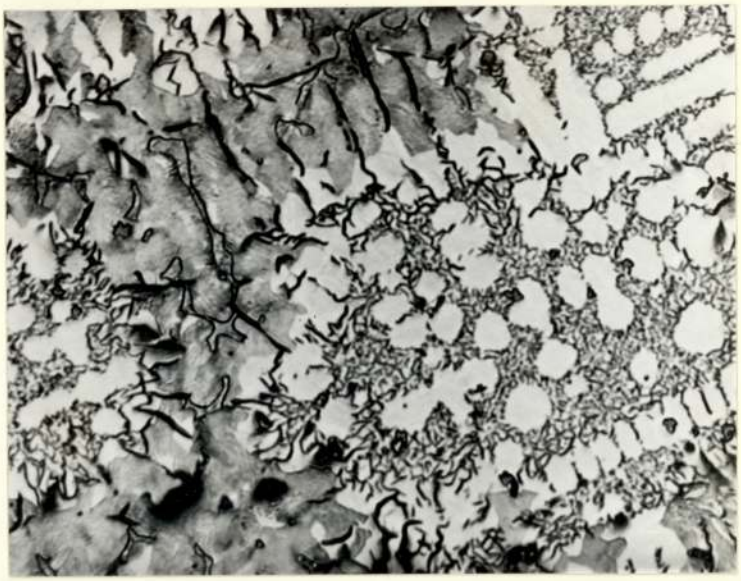

Fig. 4.10 Microstructure at the surface of silica shell 0.5cm plate casting. The structur illustrates extensive 'D' type graphite. Etched 2% nital. Magnification X250.

Fig. 4.11 Microstructure at the surface of clay bonded sand 0.5cm plate casting. Graphite form is 'A' type. Etched 2% nital. Magnification X250.

plate, exhibited areas of 'D' type graphite and ferrite at the surface, amounting to approximately 50% of the structure. The remainder of the structure at the surface was of 'A' type graphite in a pearlitic matrix.

Fracture of the plate castings revealed that the silica shell cast plate exhibited some chill on the free edge opposite the ingates. The fracture specimens are shown in Fig. 4.12.

Cell structures of the specimens revealed a difference in the nature of the cell structure at the surface of the shell cast specimens as illustrated in Fig. 4.13. The green sand clay bonded mould illustrates continuity of the cell boundaries to the surface of the casting. Some boundaries being at right angles to the surface. In the shell moulded plates the cell boundaries do not continue to the surface. A continuous boundary parallel to the surface existed at the interface.

4.3.2 Solidification times and microstructures of specimens with plate thickness greater than 0.5 cm

Cooling curves were obtained for specimens 2, 3, 5 and 8 to establish and compare the cooling times of the thicker plate castings. The results are summarised in Table 4.5. Casting temperature of all plate castings was 1475°C. It was found that for specimens of 1.5 and 2.5 cm thickness the difference in total solidification time at a distance of 1 mm and 3 mm from the top surface was insignificant.

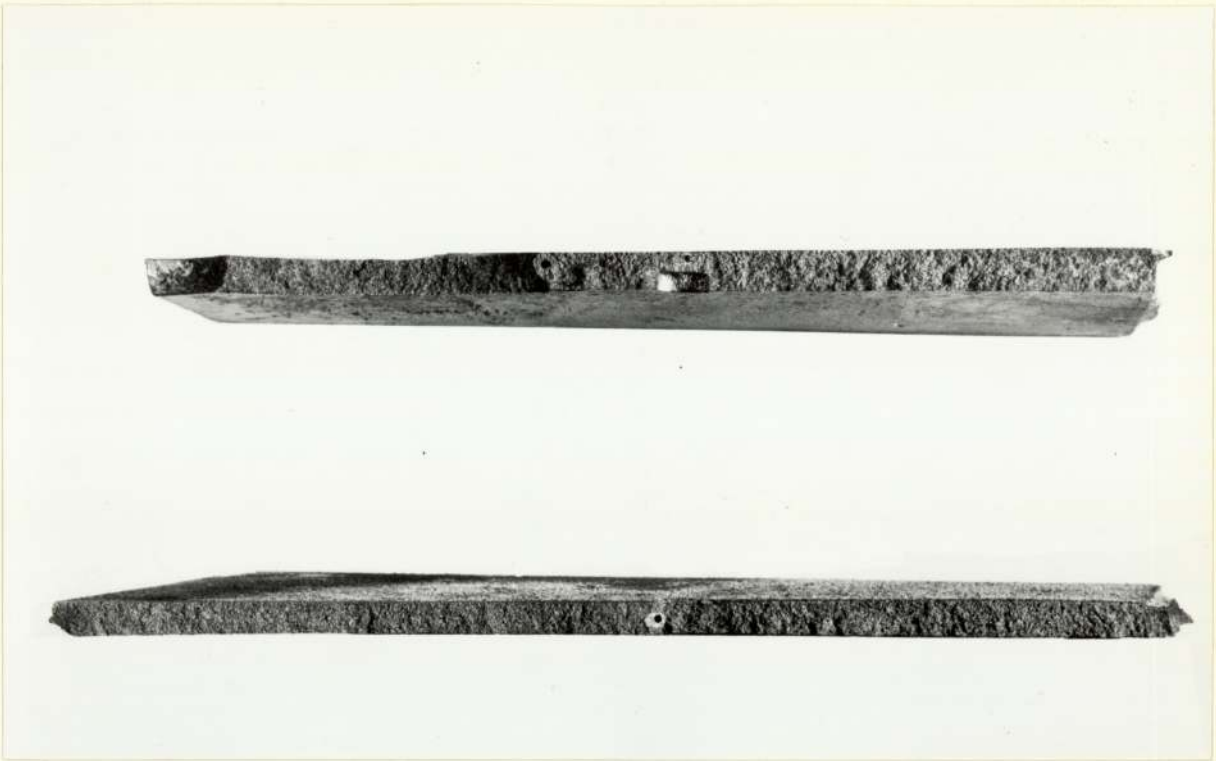

Fig. 4.12 Fractured 0.5 cm test plates for silica shell mould (top) and clay bonded green sand mould (bottom)

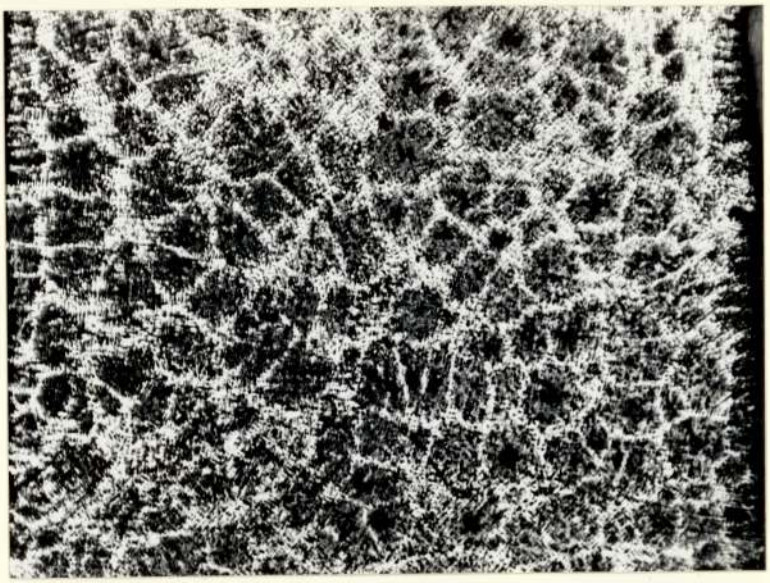

(a) Clay bonded green sand plate casting

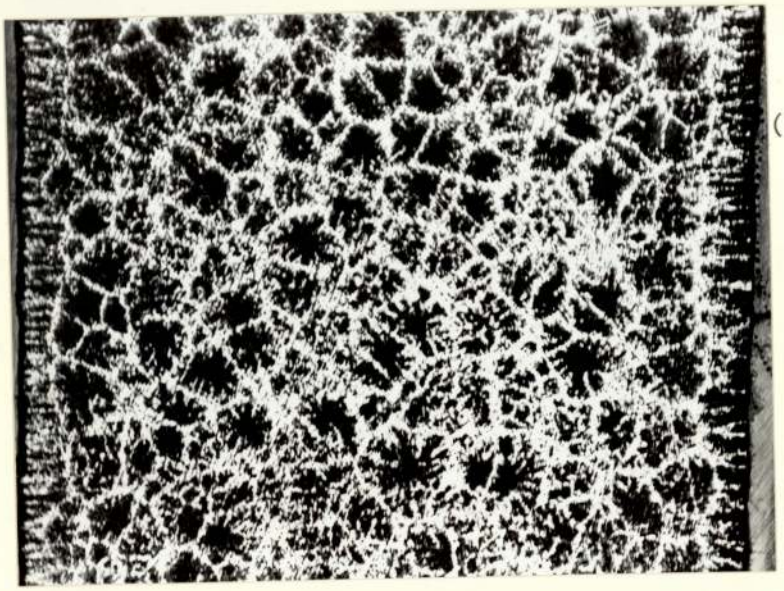

(b) Silica shell moulded test casting

Fig. 4.13 Cell structures of 0.5 cm plate castings. Etched in Steads reagent. Magnification X15.

Table 4.5

Solidification times for plate castings thicker than 0.5 cm

Specimen No.	Casting Thickness	Mould Material	Total solidification time
2	1.5 cm	Silica shell	123 secs
3	2.5 cm	Silica shell	184 secs
5	1.5 cm	Clay bonded green sand	106 secs
8	1.5 cm	Zircon shell	128 secs

The microstructure of the sand cast plate consisted of 'A' type graphite in a matrix of 100% pearlite at the surface and centre of the plate. The shell cast samples in all cases exhibited some 'D' type graphite with associated ferrite in the microstructure of the surface. The percentage of ferrite in the matrix varied from 40% to 85% approximately. The microstructure at the immediate surface (i.e. to a depth of 0.2 mm approximately) was of 'A' type graphite and pearlite. The microstructure at the centre of the shell cast specimens was of 'A' type graphite in a completely pearlitic matrix. Typical microstructures obtained on the 1.5 cm plate cast into the zircon shell mould is shown in Fig. 4.14. All of the above castings were knocked out of the mould after solidification and allowed to air cool.

4.3.3 Temperature gradients existing in shell moulds during and after solidification

The casting of grey iron into shell moulds results in pyrolysis of the resin binder. Since some reactions are exothermic, internal heating of the mould occurs as well as heat transfer from the metal in the mould. Fig. 4.15 shows two stages in the combustion of a shell mould after casting. Fig. 15(a) shows the combustion 30 seconds after pouring. Fig. 4.15(b) represents the stage that mould decomposition had reached 2 minutes after casting. The rate of heat up of the mould at a distance of 1 mm from the mould/metal interface was measured for specimens 1, 2 and 3, hence illustrating the effect of casting section size. The results are shown

(a) Surface structure illustrating 'D' type graphite and ferrite.

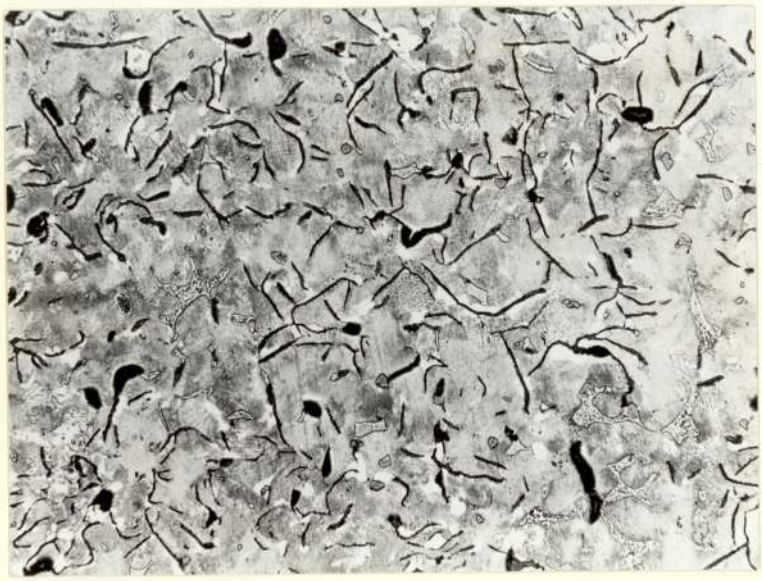

(b) Structure at the section centre. Graphite shown is 'A' type.

Fig. 4.14 Microstructure at the surface and section centre of 1.5 cm Zircon shell cast plate. Etched 2% nital. Magnification X100.

(a) 30 seconds after the end of pouring 0.5cm plate casting

(b) 2 minutes after the end of pouring 0.5cm plate

Fig. 4.15 Combustion stages of shellmould

graphically in Fig. 4.16.

Fig. 4.17 shows the temperature gradients which existed in a mould for specimen 3 and the time for the mould temperature to fall below the solid state transformation temperature of cast iron. The time required for the mould at 1 mm from the metal interface to fall to 720°C was approximately 118 minutes from the time of pouring.

4.3.4 Results of wedge chill tests

The wedges produced by this experiment are shown in Fig. 4.7. These were poured at a temperature of 1420°C and air cooled after solidification. The depth of chill was as shown below:

Silica shell mould nominal 5.0 per cent resin	Depth of chill on wedge 7.5mm.
Clay bonded green sand mould	7.5 mm.

The cell structures of the wedges produced are shown in Fig. 4.18. The cell boundaries of the green sand cast wedge extend to the surface, whereas they do not for the shell cast wedge. It can be seen that the average cell size is slightly larger for the shell cast wedge. The shell cast wedge exhibited a continuous band or casting skin at the surface. Microstructures of the wedges along the top edge were

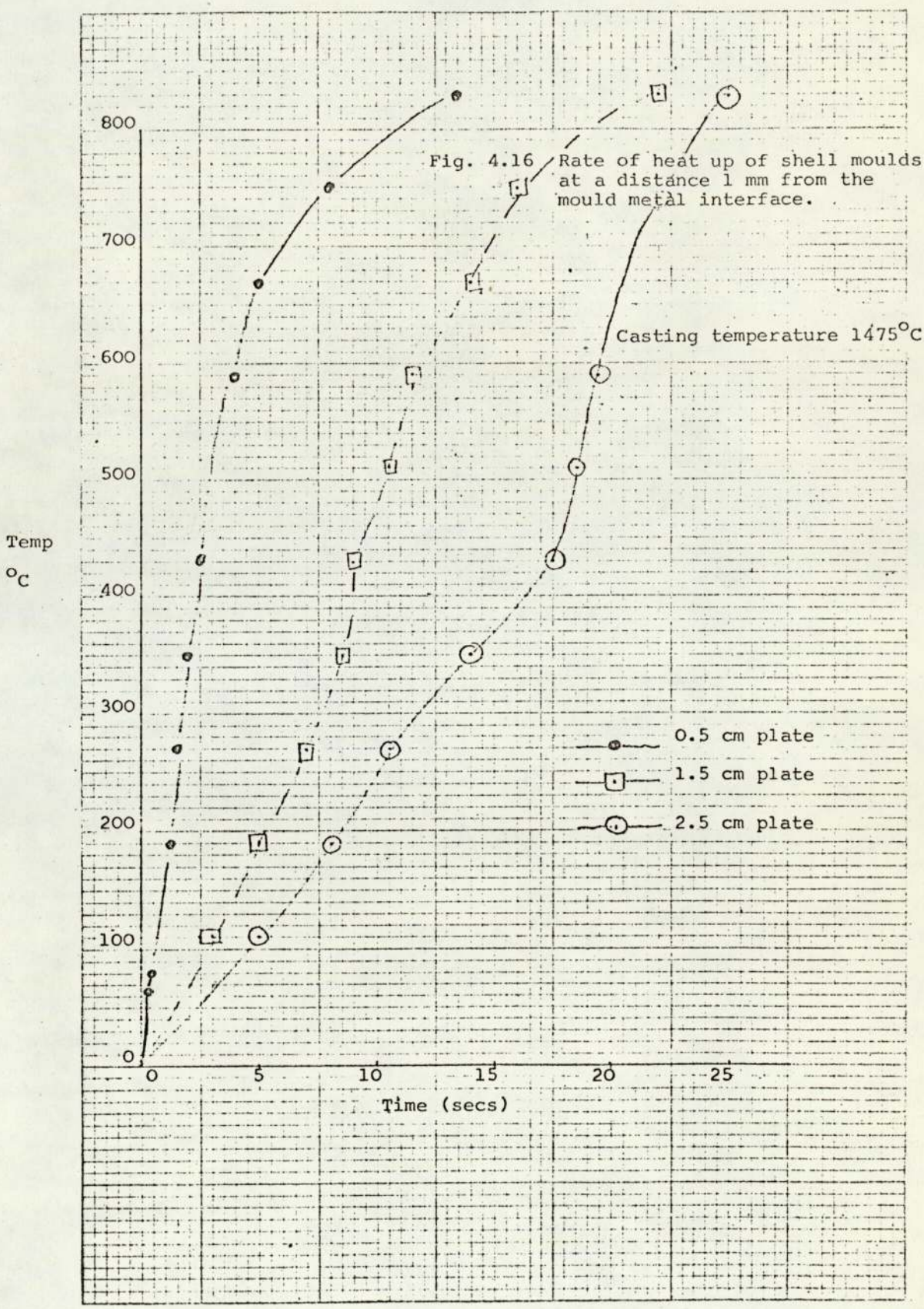
Fig. 4.16 Rate of heat up of shell moulds at a distance 1 mm from the mould metal interface.
Casting temperature 1475°C
Temp °C
800
700
600
500
400
300
200
100
0
0
5
10
15
20
25
Time (secs)
0.5 cm plate
1.5 cm plate
2.5 cm plate

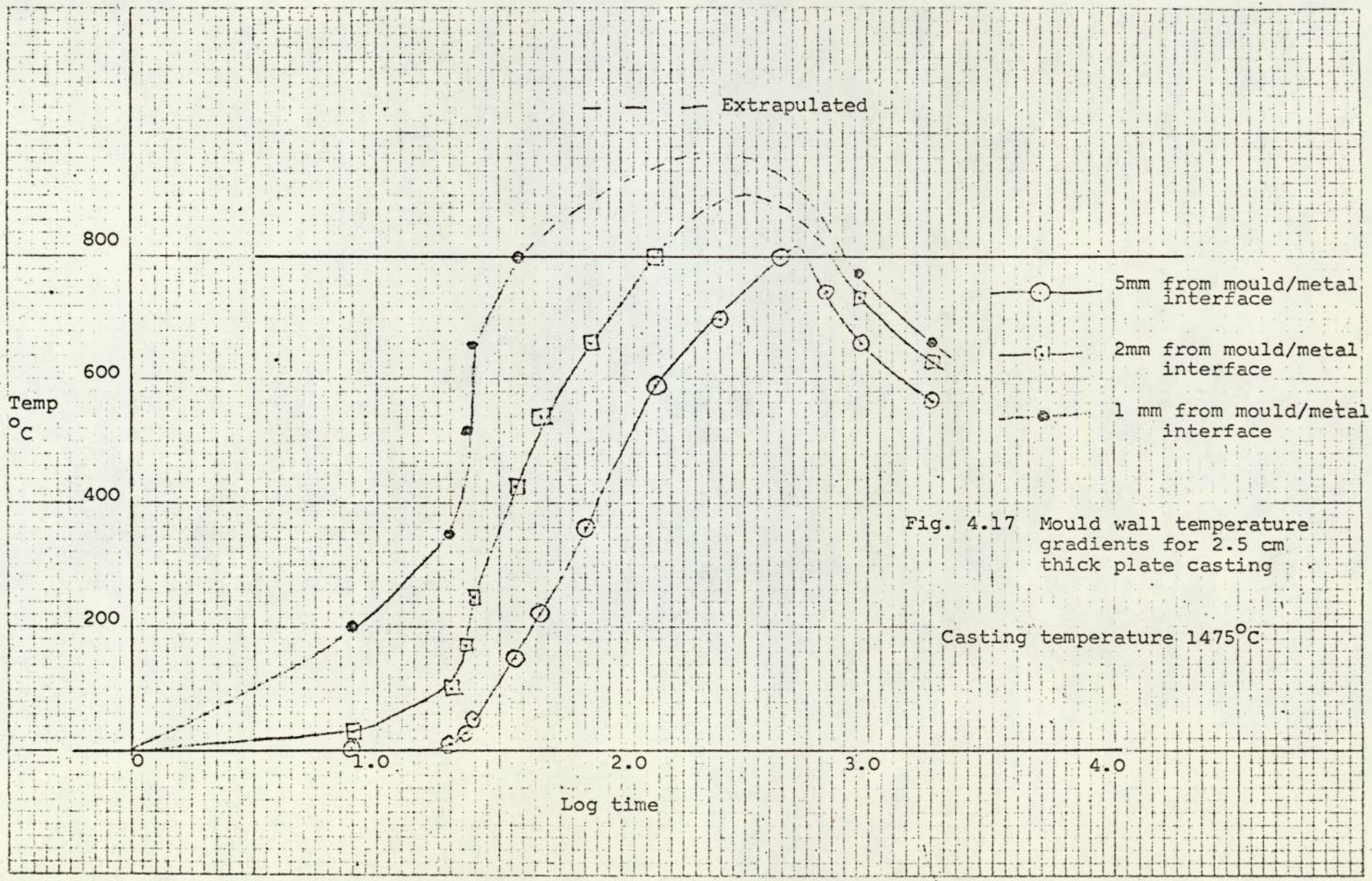

Fig. 4.17 Mould wall temperature gradients for 2.5 cm thick plate casting

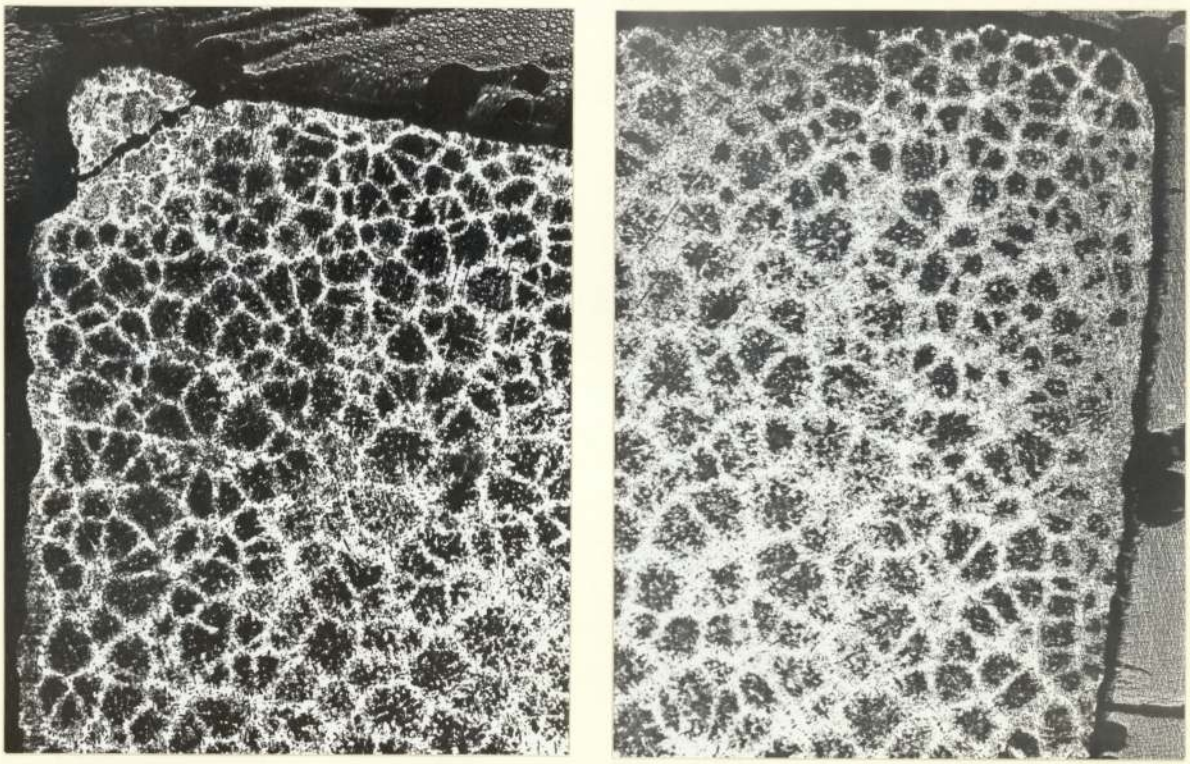

(a) Silica shell cast Wedge.

(b) Clay bonded green sand cast wedge

Fig. 4.18 Cell structures of chill test wedges. Etched Steads reagent. Magnification X15.

of 'A' type graphite and a matrix of pearlite for the green sand wedge but of a mixtrue of 'A' and 'D' graphite with a matrix of ferrite and pearlite for the shell cast wedge. The ferrite in thelatter was associated with the 'D' type graphite and amounted to approximately 30% of the total structure for a depth of 2mm. The structure on theimmediate surface was a band of 'A' graphite and 100% pearlite. The depth of this band was not greater than 0.2 mm.

4.3.5 Relationship of cooling rate and solid state transformation

The plate castings produced and described above were all removed from the mould after solidification but prior to the solid state transformation occurring, this being typical of normal casting production. The influence of cooling rates ranging from air cooling to oil quenching were examined. Micro-examination of the specimen shown in Fig. 4.8 showed that the matrix structure at theoil quenched end was 100% martensitic. At the air cooled end the specimen had a matrix structure which was 100% ferritic. The structures in the intermediate zone are illustrated in Figs. 4.19 and 4.20. Fig. 4.19 shows the matrix structure consisting of ferrite, pearlite and martensite. At no point was the matrix structure free from ferrite except where a large percentage of martensite existed. Fig. 4.20 shows the matrix structure of ferrite and pearlite, the pearlite existing only at the centre of the original austenite dendrites and at no point in contact with the graphite flakes.

Fig. 4.19 Microstructure of grey cast iron plate subjected to part oil quenching, illustrating co-existence of martensite and ferrite. Ferrite is present in areas associated with 'D' type graphite. Etched 2% nital. Magnification X1000

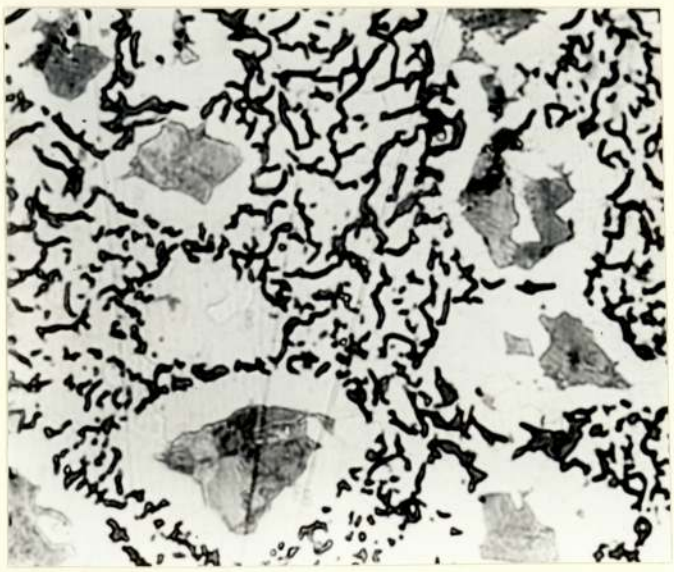

Fig. 4.20 Microstructure of grey cast iron plate subjected to part oil quenching, showing existence of pearlite at the centre of the original austenite dendrites and away from 'D' type graphite. Etched 2% nital. Magnification X1000.

The results indicate that for an iron of this composition, with 'D' type graphite present in the structure, suppression of ferrite in favour of 100% pearlite is not possible whatever the cooling rate employed.-

Cooling rates obtained on two 1.5 cm thick plates 1 mm from the mould interface and produced in a silica shell mould and the second in a green sand mould are shown in Table 4.6.

Table 4.6

Comparison of cooling times to the solid state transformation temperature for shell and clay bonded moulds

Mould material	Time from pouring to reach 720°C	Rate of cooling
Silica shell mould	46 mins	16.4°C min^{-1}
Clay bonded green sand mould	28 mins	27.0°C min^{-1}

CHAPTER 5

DISCUSSION

The solidification times determined illustrate only very small differences between a green sand mould and any type of shell mould for the 0.5 cm plate casting. The solidification time from the start of pouring was of the order of 60 seconds and varied by only7% from the shortest time for the olivine shell mould and clay bonded mould to the longest time for the silica shell mould. This difference is small enough to be disregarded since experimental error could account for such a difference. These results verify the indicated difference in solidification times for shell moulds and clay bonded moulds, produced by measurement of thermal properties using the Amitec technique. The results obtained were completely in accordance with the theoretical heat absorption characteristics for this solidification time, as shown in Fig. 3.8. The fact that little difference existed between silica, olivine and zircon shell moulds in relation to solidification time might have been unexpected due to the density differences which exist. However, heat absorption by the mould is a function of the chilling power which is a function of the heat diffusivity, e.g. $b = \sqrt{kc\rho}$. Values of

the heat diffusivity calculated from theoretical values of thermal conductivity and specific heat for olivine and zircon moulds are shown below, with the determined value for silica.

Material	Heat Diffusivity at 1350°C
Silica	.0188 c.g.s. units
Zircon	.0125 c.g.s. units
Olivine	.0118 c.g.s. units

Hence, it could be expected that the silica shell mould would give the fastest rate of solidification although this was not proved to be so. The higher density value of zircon sand is offset by the much lower value of specific heat. The solidification times for the 1.5 cm. thick castings were the same for both zircon and silica shell moulds confirming the results of the 0.5 cm plate castings. The clay bonded mould sand, however, had a solidification time for the 1.5 cm plate casting 16.0% shorter than for the silica shell mould. This difference verified the results suggested by the value of the chilling power for the two types of mould.

These results confirm the previous work carried out by Moray, Bishop and Pellini (10), Ames (9) and Glick (12) who indicated that solidification times for unbacked shell moulds were greater than for clay bonded moulds. The difference in solidification times indicated is substantially different, from one worker to another. Differences between green sand

and unbacked shell moulds of 40 - 70% were recorded by Moray et al for various alloys while Glick rationalised his results, to suggest that for gun metal and Al-Cu-Si alloys the silica shell mould required 20% longer solidification times. The spread of these results and the differences obtained in this work for the 0.5 and 1.5 cm plates is explained most satisfactorily, by examination of the specimens used in relation to differences determined in the mould constant. In the work of Moray et al, the test plate castings used varied from $\frac{1}{2}$" to $1\frac{1}{2}$" (12-36 mm) in thickness while Glick used a test specimen 1" (25 mm) thick. The difference in chilling power obtained in the present work at a casting temperature of 1420°C was 12.7% higher for the clay bonded material than for a silica shell mould. This difference would cause large variations in solidification time between the two mould materials where the total time was very large, i.e. a very thick specimen, but could result in virtually almost identical solidification times where the total heat removed was very small, i.e. very small section thickness castings. This is due to the parabolic form of the heat loss equation, i.e. $Q = \sqrt{t}$. Theoretical differences calculated from Fig. 3.8 are shown in Table 5.1.

Moray et al illustrated a number of cooling curves illustrating solidification times of 10 - 15 minutes, hence large differences between green sand moulds and shell moulds.

Table 5.1

Comparison of theoretical solidification times

Total heat loss for solidification to be completed	Theoretical solidification time for clay bonded specimen	Theoretical solidification time for silica shell mould	Increase % for shell mould
100 cal cm^{-1}	1.25 min	1.25 min	0
400 cal cm^{-1}	4.50 min	4.80 min	+ 6.7%
800 cal cm^{-1}	10.75 min.	13.50 min	+ 25.6%

were to be expected. The work of Glick in rationalising the rate of cooling and presenting a ratio of cooling for green sand moulds to silica shell moulds of 1.0:1.2 can only be true for a particular size of test specimen. For thin section specimens the ratio will approach unity and for thicker specimens will appear larger. The type of castings examined in this project would have very similar solidification rates whether produced in green sand moulds or in shell moulds. The range of solidification times into which these castings fall is important since shell moulding is usually used in the production of small castings. This is due to the fact that large castings where large amounts of heat have to be removed prior to solidification, can result in destruction of the resin binder and cohesion of the mould before solidification is complete. This is not of any significance where mould back-up materials are used, because these also influence the heat absorption characteristics of the mould.

The results illustrate, therefore, that a difference in mould constant exists between silica shell moulds and green sand moulds, when conventional mould thickness values are employed, but that this difference is not as large as the previous literature might suggest, and has no influence on the solidification rate or time for thin section grey iron castings, e.g. $\frac{1}{4}$" (6 mm). The reason for a variation in the value of $\mathcal{E}$ is almost certainly the

difference in mould thickness and hence total heat capacity. The shell mould as illustrated in Fig. 3.10 is quickly saturated with heat and hence the rate of heat absorption is quickly reduced. As the shell mould thickness is increased, conditions approaching those appertaining to a conventional green sand mould occur. This is in agreement with the findings of Moray et al who showed that solidification time increased with decreasing shell mould thickness.

The results of the wedge test provide further verification that solidification times for silica shell and clay bonded moulds are the same for thin section castings, since the depth of chill was the same for wedges produced in each type of mould. Any large difference in chilling power would have been expected to result in a variation in chill depth. It is of significance that due to the lower value of the chilling power and the rapid change in the value of $\frac{dQ}{dt}$ during cooling in shell moulds, the solidification times for thin sections (e.g. 6 mm) and thick sections (e.g. 25 mm) will differ more widely than for green sand castings. Therefore, the occurrence of hot tearing in materials liable to this defect, e.g. white cast iron, at the junction of a change in section will be more likely in shell moulds. This fact has been observed in the industrial production of malleable castings by shell moulding (47).

While the results enable a clearer insight into the solidification characteristics of shell moulds compared to green sand moulds, there is no evidence to explain the type of structures which arise in thin section shell mould castings. The shell cast test plate castings produced exhibited the same micro-structural differences as with the clay bonded test plates, as observed in industry and described by Thwaites (15) and Klaban (16). This is shown most clearly in Fig. 4.10 for a silica shellmould and Fig. 4.14 for a zircon shell mould. A correlation between the solidification time and the type of micro-structure obtained for a shell mould compared to a clay bonded mould does not exist. The occurrence of ferrite in themicro-structure has been shown to arise due to the existence of 'D' type graphite. While shell moulds undergo very rapid heating up and result in very slow cooling through the solid state transformation (Table 4.6) most industrial castings are removed from the mould at times well before that required to reach temperatures of 720^{o}C, and plate castings illustrating ferrite in the matrix structure in this work were also removed from the mould before the solid state transformation took place.

The variable cooling rates achieved by partly oil quenching a specimen of grey iron of the composition used for the experiments illustrated that with such short diffusion distances, cooling rates high enough to produce

martensite still do not completely suppress ferrite in the regions of 'D' type graphite. Evidence that diffusion distance is the crucial factor, was shown in Fig. 4.20 where pearlite only existed in areas furthest away from the graphite flakes. It may be concluded that in an iron of this particular composition it is impossible to obtain a completely pearlitic matrix when 'D' type graphite structures exist, under casting cooling conditions normally encountered.

The differences observed in macro and micro-structure were not restricted to the presence of ferrite co-existing with 'D' type graphite. The cell structures of the wedge test pieces and of 0.5 cm plate castings illustrate a difference between the shell mould and clay bonded mould. The shell moulded specimens illustrate a distinct skin effect at the surface, the cell boundaries ending at the skin and not continuing to the edge of the specimens. This structure was easily reproduced in all the shell moulds in which castings were produced. In the clay bonded specimens this is not the case, the cell boundaries extending to the edge of the castings. The micro-structures indicate the casting skin to containfine 'A' type graphite flakes in a matrix of pearlite.

The differences which exist in graphite form could be due to a variable degree of under cooling, and it has been shown (Fig. 4.19) that shell moulded castings did undergo

a greater degree of undercooling than green sand moulded castings. This variation, however, is independent of cooling rate, i.e. 0.5 cm silica shell moulded plate undercooled 20°C, while similar green sand moulded plate undercooled 10°C, total solidification times were 60 seconds and 56 seconds respectively.

The reactions which occur during the casting of a high melting point alloy e.g. cast iron into the two types of mould involved, are very different from each other. In shell moulds the pyrolysis of the resin shown in Fig. 4.15 results in the formation of large quantities of hydro-carbon gases, together with some small quantity of nitrogen and carbon dioxide. Decomposition of the gases results in the formation of a graphite film on the top surface and side walls of the mould cavity, which subsequently burns out by a secondary combustion process. The latter stage is shown in Fig. 4.15(b) where the existence of a carbonaceous deposit at the edges of the plate casting can also be seen. The film produced can remain on the casting if it is removed from the mould before combustion can take place. Such a graphite film obtained in the experiments carried out for a 2.5 cm plate produced from a shell mould has been shown in Fig. 5.1.

The occurrence of this type of graphite film gives rise to established defects in shell moulded iron castings, e.g. lap defects and the 'orange peel' effect. This mould reaction contrasts sharply with a green sand mould, where the surface

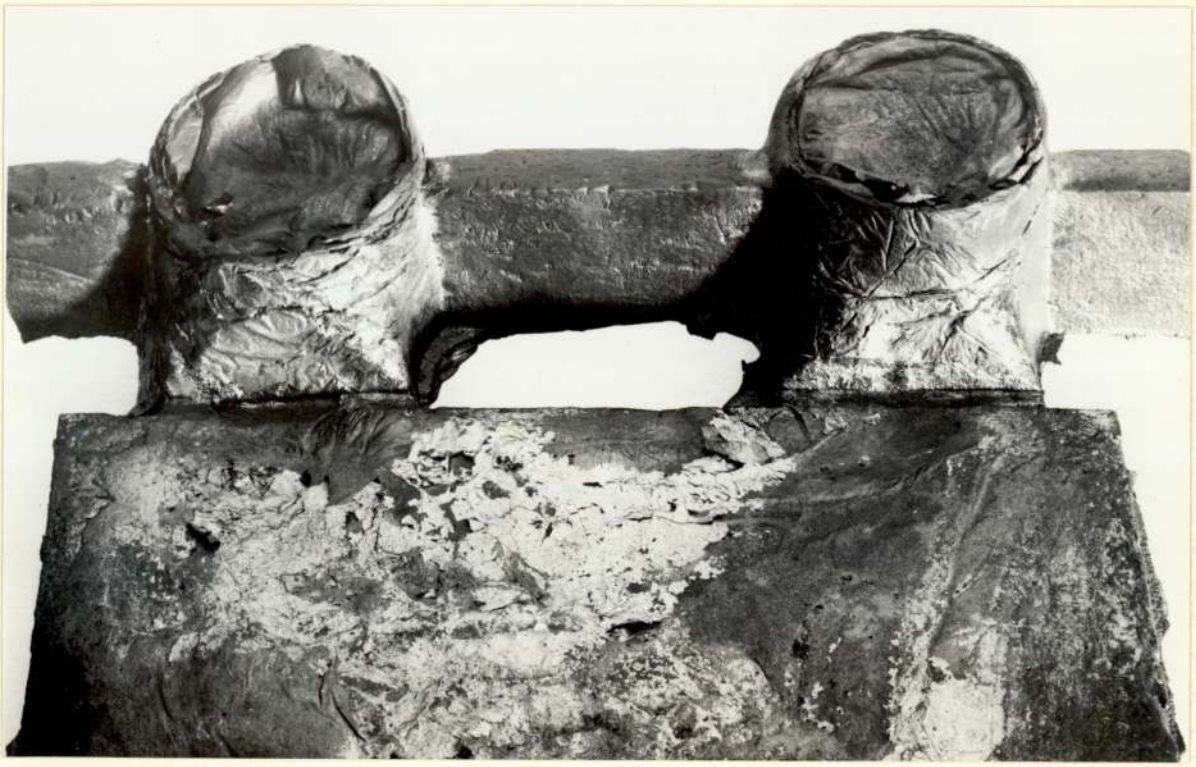

Fig. 5.1 2.5 cm plate casting produced from silica shell mould illustrating graphite film on top surface.

contains much smaller particles in the form of coaldust and clay, the principal gaseous product is steam arising from themoisture content.

The degree of undercooling enables a possible explanation for the 'D' type graphite formoccurring in shell moulded castings and hence the occurrence of ferrite surface structures. However, 'D' type graphite is not usually sensitive to the degree of undercooling but the reduction in eutectic temperature which may occur with undercooling. In the results obtained, the eutectic temperature for the shell cast plates was no lower than for the green sand moulded plate cast from the sameladle of metal. The increased degree of undercooling would not account for the deep casting skin which arises in shell castings,hence both occurrences must be a function of the mode of solidification.

Due to the differences which exist it is possible that the gaseous products of the shell mould can modify the form which the graphite takes on solidification, e.g. as obtained with titanium additions; alternatively, the steam generated in clay bonded moulds may have an influence on the graphite form and thus its absence may be of significance.

No evidence can be put forward from the results to suggest an increased tendency for the occurrence in carbides in shell moulded grey iron, due toincreased rates of solidification. However, it was noticed that it was possible to run much thinner sections in shell moulds than in green moulds, and hence flash occurred much more readily. Flash inevitably

chills and in some instances this chill may be carried into the actual casting. The increased fluidity is probably accounted for by the reduced grain size of the sand used and the hardness of the mould surface.

CHAPTER 6

CONCLUSIONS

The conclusions which can be deduced from the results may be summarised as below.

1. The Amitec technique enables values for the mould constant to be obtained at high temperatures which compare favourably with values of other workers obtained by calculation after measuring the thermal conductivity and specific heat.

2. The chilling power of a silica shell mould is 11.3% lower than a clay bonded mould at 1350°C. The difference is principally due to the difference in mould thickness.

3. The generally accepted view that shell moulds give increased solidification times requires qualification. The rate of heat extraction $\frac{dQ}{dt}$ and solidification rate for castings solidifying under 2 minutes is the same for silica shell, zircon shell and green sand moulds. Silica shell moulds show progressively increased solidification times over clay bonded moulds as the total time is increased. The freezing range of shell castings with large variations in section thickness is wider than for green sand castings, hence explaining thegreater tendency for hot tearing which exists.

4. Resin content does not influence the chilling power of shell moulds in the range 4 - 5%.

5. The mode of solidification in shell moulds is different in shell moulds giving rise to an extensive casting skin.

6. Shell moulds do not show any increase in chill depth measured by wedge testing.

7. For the same material and casting conditions, shell moulds cause, more frequently, the formation of 'D' type graphite at the surface of iron castings. The presence of this graphite form subsequently gives rise to the occurrence of a ferrite matrix in cast ironstypical of the composition employed.

8. An increased degree of undercooling without any decrease in the eutectic temperature was observed for shell moulds.

CHAPTER 7

SUGGESTIONS FOR FURTHER WORK

Further work is required to clarify the reasons for the formation of 'D' type graphite in shell moulds. It is suggested that investigations of the following points could produce further evidence to enable a complete explanation.

(a) Examination of the formation of the casting skin andits composition.

(b) Measurement of $\frac{dQ}{dt}$ at very short intervals of time, i.e. under 20 seconds.

(c) A study of the influence of the products of combustion of shell moulds on the form of the graphite phase.

REFERENCES

1. Physical & Engineering Properties of Cast Iron. H. T. Angus B.C.I.R.A. Birmingham 1960.
2. The Croning Process, Foundry Trade Journal 4th December, 1947.
3. W. Büchen. Giesserei 1956 43 pp 291-295.
4. B. J. Alexander. Schnectady Midland Ltd., private communication.
5. Research on Shell Moulding. Massachusetts Inst. Technology 1952.
6. A. D. Morgan, Modern Moulding and Coremaking Techniques using Resin Binders. B.C.I.R.A. 1970.
7. B. J. Alexander. Schnectady Midland Ltd., private communication.
8. B. N. Ames, S. B. Donner and N. A. Khan. American Foundryman, January 1952 pp 112-117 and pp 287-295.
9. B. N. Ames. Proc. I.B.F. 1953 46 p.A35.
10. R. E. Moray, F. Bishop and W. S. Pellini, Trans A.F.S. 1954 p.448.
11. R. A. Flinn et al. Trans. A.F.S. 1955 pp 143-156.
12. W. W. Glick. British Foundryman 53 p.1-10.
13. W. A. Pollard. Trans A.F.S. 1966 p.201.
14. Jamuszewicz and Harpula. Drace Instytuta Odlewnictwa 11 No. 1 1961 pp 1-20.
15. C. J. Thwaites. Iron and Steel June 1969 pp 201-208.
16. J. Klaban. Foundry Trade Journal November 23rd 1967. pp 745-750.

17. W. Jackson. Journal BSCRA 35 1957 June p.16-19.

18. A. Fuller and I. C. H. Hughes. B.C.I.R.A. Journal R & D 7 1959 p.288.

19. C. R. Loper and R. W. Heine. Trans. A.F.S. 69 1961 p.585.

20. J. V. Dawson and W. Oldfield, B.C.I.R.A. Journal 8 1960 p.221.

21. W. Oldfield. Report 532. B.C.I.R.A. Journal 8 1960 p.177.

22. I. C. H. Hughes. I.S.I. Reprint Joint Conference on solidification of metals, 1967.

23. M. Hillert. I.S.I. Reprint Joint Conference on solidification of metals, 1967.

24. I. C. H. Hughes. B.C.I.R.A. Journal R. & D. 1957 7 pp 10-22.

25. H. Morrogh. B.C.I.R.A. Journal R. & D. 1955 5 pp 655-673.

26. J. V. Dawson. B.C.I.R.A. Journal 9 1961 pp 199-236.

27. H. Morrogh and W. Oldfield. Iron and Steel 32 pp 431-434.

28. Russian Castings Production 1966 2 p.89.

29. A.Fuller. B.C.I.R.A. Journal R. & D. 1959 7 pp 725-733.

30. A. Boyles. The Structure of Cast Iron, Cleveland, A.S.M. 1947.

31. A. L. Norbury & E. W. Morgan. J.I.S.I. 1936 134 pp 327-346.

32. A. Fuller. B.C.I.R.A. Journal R.& D. 1959 7 pp 725-733.

33. V. Kondic et al. Foundry Trade Journal 1957 102 pp 267-277 and 311-314.

34. W. Oldfield. A.S.M. Symposium "Research in Cast Iron" 1964.

35. A. Boyles and C. H. Lorig. Trans. A.F.S. 1941 p.769-781.

36. R. W. Heine et al. Trans. A.F.S. 77 1969. p.185-191.

37. R. W. Heine et al. Trans. A.F.S. 78 1970 p.363.

38. R. W. Heine et al. Trans. A.F.S. 78 1970 p.187.

39. I. C. H. Hughes, unpublished work.

40. R. W. Ruddle 1957. The Solidification of Castings. 2nd ed. Institute of Metals Monograph and report No. 7.

41. F. A. Brandt, H. F. Bishop and W. S. Pellini. Trans. A.F.S. 62 1954 p.646.

42. R. P. Dunphy and W. S. Pellini. A.F.S. 1951 Preprint No. 51-22.

43. Solidification Rate of Cast Iron. Summary of report of sub-committee TS.33 I.B.F. Foundry Trade Journal Jan 16 1953.

44. J. Berry, V. Kondic and G. Martin. Trans. A.F.S. August 1959 p.449.

45. B. V. Atterton. J.I.S.I. 1953 174 p.201.

46. H. F. Bishop, F. A. Brandt and W. S. Pellini. Trans. A.F.S. 62 1954 p.646.

47. M. D. Bryant. B.C.I.R.A. private communication.

48. A. D. Morgan. B.C.I.R.A. Jnl. 15 Jan 1967 p.32.

49. British Industrial Sand. Private Communication.